ALMA MATER STUDIORUM
UNIVERSITÀ DI BOLOGNA

DEPARTMENT OF INDUSTRIAL ENGINEERING

SECOND CYCLE DEGREE IN MECHANICAL ENGINEERING FOR SUSTAINABILITY

……….

MODELING AND DESIGN OPTIMIZATION OF AN INDUSTRIAL VIBRATING DRYER THROUGH FINITE ELEMENT ANALYSIS

Dissertation in Mechanics and Dynamics of Machines

Supervisor

Prof. Alessandro Rivola

Co-Supervisor

Ing. Jean Edouard Lalanne

Defended by

Tommaso Lombardi

Graduation Session / July / 2026

Academic Year 2025/2026

Abstract

This thesis investigates the structural dynamic behavior of an industrial vibrating dryer used for the processing of organic natural acid crystals, in which fatigue cracks developed after approximately 150 operating hours. Experimental investigations revealed the occurrence of resonance phenomena. In fact, the operating excitation frequency generated by the vibrating masses coincided with the first natural frequency of the supporting structure. Despite the implementation of an initial structural modification, the dynamic problem was not completely resolved, motivating a deeper investigation of the machine's behavior.

This work addresses this problem by developing Finite Element models of two machine configurations and validates them against experimental evidence obtained from bump tests and forced vibration measurements. The modeling strategy combines engineering-based simplifications with experimental evidence to reproduce the structural dynamic response while maintaining computational efficiency. The models schematize parts excluded from the geometric domain through physically motivated equivalent formulations that preserve the essential dynamic characteristics of the system.

The validated numerical models provide information that experimental testing alone could not supply by identifying the deformation patterns associated with the measured natural frequencies. The analyses show that a coupled flexural–torsional vibration mode governs the resonance condition and demonstrate that the limited torsional stiffness of the supporting frame drives the fatigue damage.

Building upon these results, this work employs the validated computational model as a predictive design tool to evaluate alternative structural solutions. It compares retrofit interventions and a complete re-design of the supporting structure in terms of dynamic performance, structural efficiency, additional mass, manufacturability, and practical feasibility. The proposed solutions significantly increase the separation between the operating excitation frequency and the structural natural frequencies, thereby mitigating the resonance risk.

Overall, this work demonstrates that physically consistent engineering assumptions,

supported by experimental validation, enable Finite Element models to accurately reproduce the dynamic behavior of complex industrial machinery. Beyond explaining the origin of the observed failures, the developed numerical framework provides a reliable predictive tool for optimizing future structural modifications while reducing development time, experimental iterations, and material consumption.

Contents

Chapter 1

Introduction

1.1 Industrial Context and Scope of Work

In industrial engineering, resonance represents both an opportunity and a potential source of critical mechanical issues. Vibratory phenomena are intentionally exploited in many applications, such as conveying systems or screening machines, where controlled oscillations improve processing efficiency. However, when excitation frequencies approach the natural frequencies of the structure, vibrations significantly amplify and could compromise the reliability of the system: some consequences may be excessive stresses, fatigue damage and premature failures.

One of the most well-known examples of resonance-related structural failure is the collapse of the Tacoma Narrows Bridge, which highlighted the importance of understanding dynamic behavior in engineering design. Beyond safety considerations, these kinds of failures may also lead to economic consequences, including unexpected shutdowns, maintenance costs and production losses. For these reasons, the dynamic behavior of industrial machinery requires careful analysis during both design and operation. From this perspective, excessive vibrations may reduce the lifespan of a mechanical component or a machine, increasing maintenance requirements, causing unplanned interruptions and leading to material consumption and unavoidable energy losses. Therefore, in addition to an accurate design process, vibration monitoring is a fundamental tool in industrial diagnostics and predictive maintenance strategies, both contributing to sustainable goals.

The present thesis work originates from an industrial case involving a vibratory dryer used for organic natural acid crystals processing, which developed fatigue cracks after approximately 150 hours of operation. Once resonance issues were confirmed by experimental tests, which demonstrated the existence of the problem solely in terms of the coincidence between the natural frequency of the system and the excitation

frequency, the machine structure has been modified in an attempt to eliminate this behavior. New instrumental tests did not reveal substantial differences.
The scope of the present work is to develop a numerical model and validate it on collected experimental data in order to show the modal shape in correspondence of resonance conditions and serve as a useful tool for outlining effective solutions to definitively shift the natural frequency of the machine, thus solving the problem.

1.2 Machine History and Operating Conditions

The whole equipment is composed of a relatively stiffer basement, made of structural steel, and an upper tank, made of stainless steel, where the product processing occurs. Four vibration isolators support the system, while two synchronous vibrating masses, rotating at 12.5 Hz, provide vibrating motion to the package.
Preliminary experimental investigations, including bump tests and forced response measurements, revealed the presence of resonance phenomena close to the operating excitation frequency. Nevertheless, due to very extensive machine and instrumentation limitations, the collected results did not allow a complete identification of the corresponding mode shape.
Based on the available experimental evidence and the experience of the technicians, an initial structural modification of the machine basement has been implemented in an attempt to alter the dynamic response of the system, which means moving the natural frequency out of the critical frequency range. This intervention defines the transition between the original ("Version 0") and the modified ("Version 1") machine configurations, a notation adopted throughout the remainder of the thesis.
Subsequent tests, which followed the structural stiffening intervention, showed only a limited shift in natural frequency, highlighting the need for a more comprehensive dynamic interpretation of machine behavior.

1.3 Modeling Activity

Within this context, the investigation of the modal behavior of the structure and the identification of the modal shapes associated with the resonance condition require a Finite Element modeling approach. Compared to simplified analytical approaches, the Finite Element method allows for a more realistic representation of an extended geometry like the one under analysis, as well as a more precise mass

distribution and boundary conditions application. The preliminary activity focuses on the development of a model of both "Version 0" and "Version 1" machine configurations. Then, the correlation of the numerical results with the natural frequencies identified experimentally through the bump tests validates the model.
SimScale performs these modeling and numerical analyses; this software is cloud-based, so it does not need dedicated local hardware resources, rather it is a simulation platform that enables Finite Element analyses through a flexible and user-friendly computational environment.
The entire system has complex geometry and dynamic behavior that are difficult to reproduce exactly. Therefore, it is necessary to introduce simplifications and assumptions in the modeling activity, always defined according to engineering considerations. The objective is to maintain a balance between model reliability, computational efficiency, and physical representativeness of the system. For instance, the solid model includes only the stiffest part of the machine, since it should to mainly affect the overall dynamic behavior. A further aspect concerns the influence of the product, in particular the interaction between the product itself and the tank that contains it. Due to its morphological properties, impacts and friction phenomena characterize the motion of the product, thus introducing nonlinear behavior into the system. In the present work, a linear approximation of this interaction holds by considering the product and the structure as partially uncoupled.
Throughout the modeling activity, simplified analytical approaches based on the classical mechanics of vibrations theory support engineering decisions and validate modeling assumptions. In particular, equivalent One-, Two- and Three-Degree-of-Freedom systems, together with energy-based methods such as Rayleigh's Method, are employed to obtain preliminary estimations of natural frequencies and dynamic properties. These simplified calculations provided useful reference values for assessing the consistency of the numerical models and verifying that the adopted assumptions produced results within the expected order of magnitude.
Once the numerical model is sufficiently robust to represent the real system, it becomes the main tool for a deeper investigation of the machine vibrational behavior. For both versions of the system, the model allows modal shapes related with the natural frequencies to be identified, information that experimental tests were not able to determine.

1.4 Thesis Outline

This thesis develops through seven chapters. Together, they investigate the resonance problem, interpret the structural dynamic behavior of the machine and develop effective structural solutions.
Following this introductory section, Chapter 2 presents the vibrating dryer under investigation and describes its operating principles together with the main structural components governing its dynamics. Fundamental concepts of vibration mechanics explain how eccentric masses generate the excitation forces and how the vibration isolators dynamically uncouple the machine from its supporting frame. This background provides the engineering basis for the modeling assumptions adopted in the numerical analyses.
Chapter 3 introduces a chronological reconstruction of the events, from the appearance of the first fatigue cracks to the experimental investigations and the subsequent structural modifications introduced before the modal behavior of the machine was fully understood. Bump tests and forced vibration measurements confirm the presence of resonance by identifying the first natural frequency of the structure.
Chapter 4 is part of the core of the thesis and focuses on the development of Finite Element models for both machine configurations and on their validation against the available experimental evidence. The discussion targets the engineering assumptions, the adopted simplifications and the validation strategy required to obtain a reliable representation of the structural dynamic behavior despite the different operating and boundary conditions of the experimental campaigns.
Chapter 5 presents the results of the Finite Element analyses and complements the experimental investigation by identifying the modal shapes associated with the experimentally detected natural frequencies. The validated numerical models provide the physical interpretation that experimental tests alone could not deliver, allowing the investigation of the deformation mechanisms responsible for the observed resonance condition.
Chapter 6 exploits the validated numerical model as a predictive engineering tool to develop and compare alternative structural solutions. The proposed interventions increase the separation between the operating excitation frequency and the structural natural frequencies while accounting for structural efficiency, additional mass, manufacturing simplicity and practical implementation constraints.
Finally, Chapter 7 summarizes the main findings of the work, discusses their engineering implications and outlines possible future developments. A comparative assessment of the proposed solutions identifies the most effective engineering strat-

egy according to both dynamic performance and practical feasibility.

Chapter 2

System Description

The purpose of this chapter is to provide a comprehensive description of the vibrating dryer investigated throughout this work. After introducing the industrial process in which the machine operates, the chapter presents the main structural components of the vibrating assembly and illustrates the operating principles responsible for product transportation. Particular attention is devoted to the vibration generation mechanism and to the isolation system, since both play a fundamental role in the dynamic behavior of the machine. The engineering concepts introduced in this chapter establish the physical basis for the modeling assumptions and numerical analyses presented in the following chapters.

2.1 Industrial Process Overview

The investigated vibrating dryer operates within an industrial production line dedicated to the processing of natural organic acid crystals.
These crystals are commonly recovered from the processing of agri-food industrial by-products. The circular economy and sustainable issues are involved, as the recovery process allows the transformation of agri-food residues into a valuable industrial product and thereby minimizes the generation of waste. After extraction and purification stages, the natural organic acid undergoes drying processes to obtain a stable crystalline powder, that finds application in several sectors, ranging from its reintroduction into the food&beverage industry to pharma and cosmetics production.
As shown in Fig. 2.1, raw acid crystals enter the machine from the feeding section in the form of a moist particulate material, while dry crystalline powder exits the system after undergoing a controlled residence time and moisture removal. Hot air enters a chamber, the *plenum*, where it is distributed uniformly over the entire sur-

face to maximize the moisture removal efficiency.

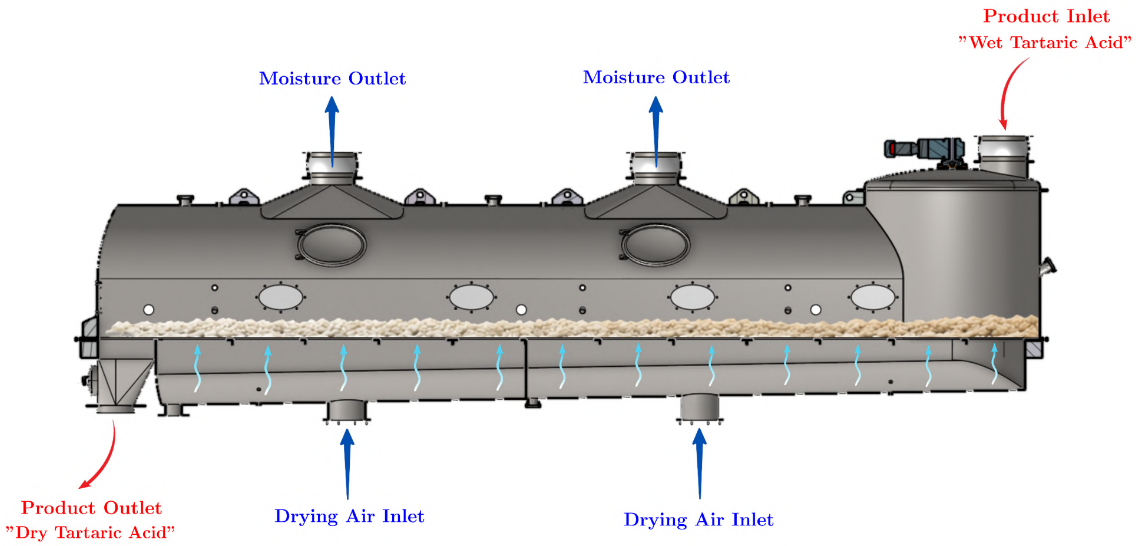

Figure 2.1: *Scheme of dryer working principle*

The product transportation mechanism relies on structural vibrations, which simultaneously promote product advancement and enhance the heat exchange mechanism. In fact, mechanical oscillation induces continuous rearrangement of product bed, increasing the surface exposed to the drying airflow. Oscillations are exploited by eccentric masses, whose rotation speed - and thus frequency - is a fundamental parameter to ensure process requirements and target product flow rate. In the investigated system, the rotating eccentric masses operate at an excitation frequency of *12.5 Hz*.

2.2 Mechanical System Architecture

The entire package consists of many subsystems, rigidly or flexibly connected to each other: four vibration isolators support the machine, while a rigid support frame, anchored to concrete foundations, supports in turn the vibration isolators.
The dryer assembly consists of a rigid basement made of structural steel, to which a stainless-steel trough containing the processed material is welded. A horizontal plane splits the trough longitudinally, dividing it into the *plenum*, permanently welded to the supporting frame, and an upper removable section that contains the product, mechanically connected through bolted joints. A perforated stainless-steel plate separates the lower plenum chamber from the upper conveying trough. The plate

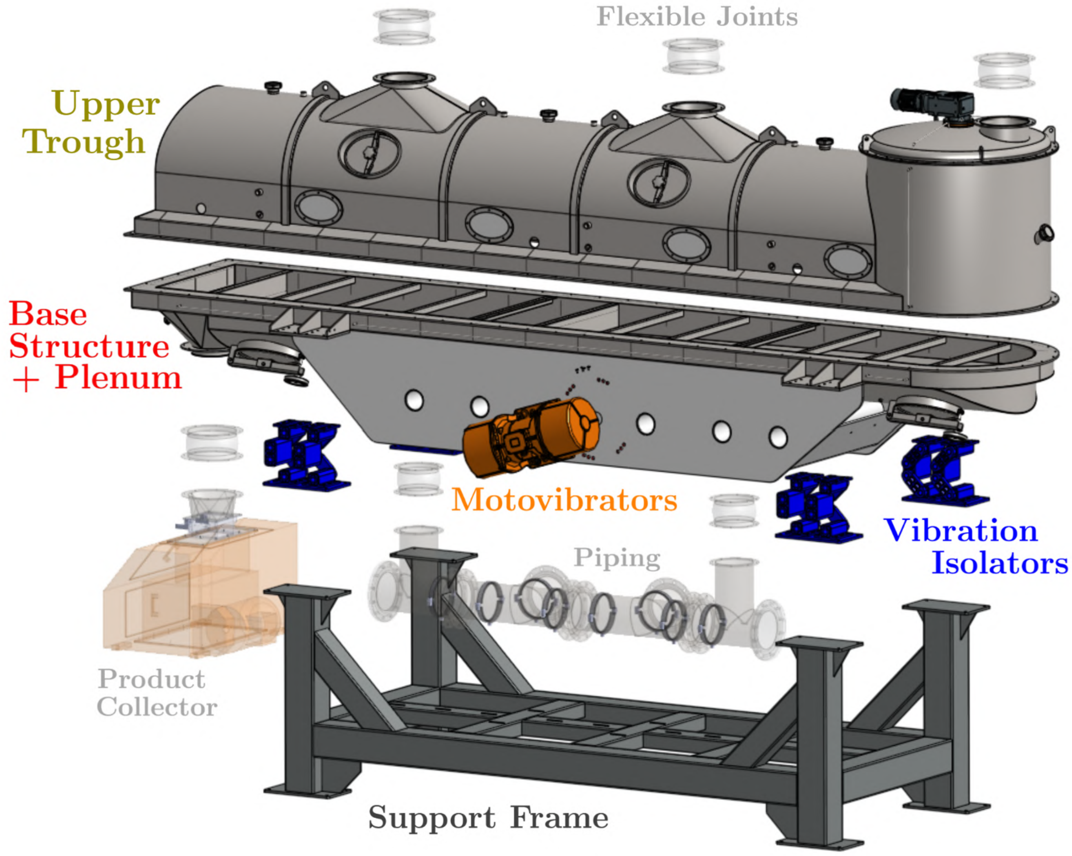

Figure 2.2: *Exploded view of dryer package*

supports and distributes the product bed while allowing hot air to pass through holes from the plenum below, ensuring uniform airflow distribution and effective moisture removal.

Additional secondary components, such as the process piping and the dried-product collector assembly, connect to the machine. Flexible joints isolate the vibrating assembly from the auxiliary equipment wherever the two interface, thereby avoiding dynamic coupling.

Vibrating masses connect to longitudinal plates on both sides of the dryer through bolted joints.

Table 2.1: *Main Components of Dryer Assembly*

Item	**Material**	**Weight [kg]**
Base Structure	Structural Steel	1065
Plenum	Stainless Steel	685
Upper Trough	Stainless Steel	900

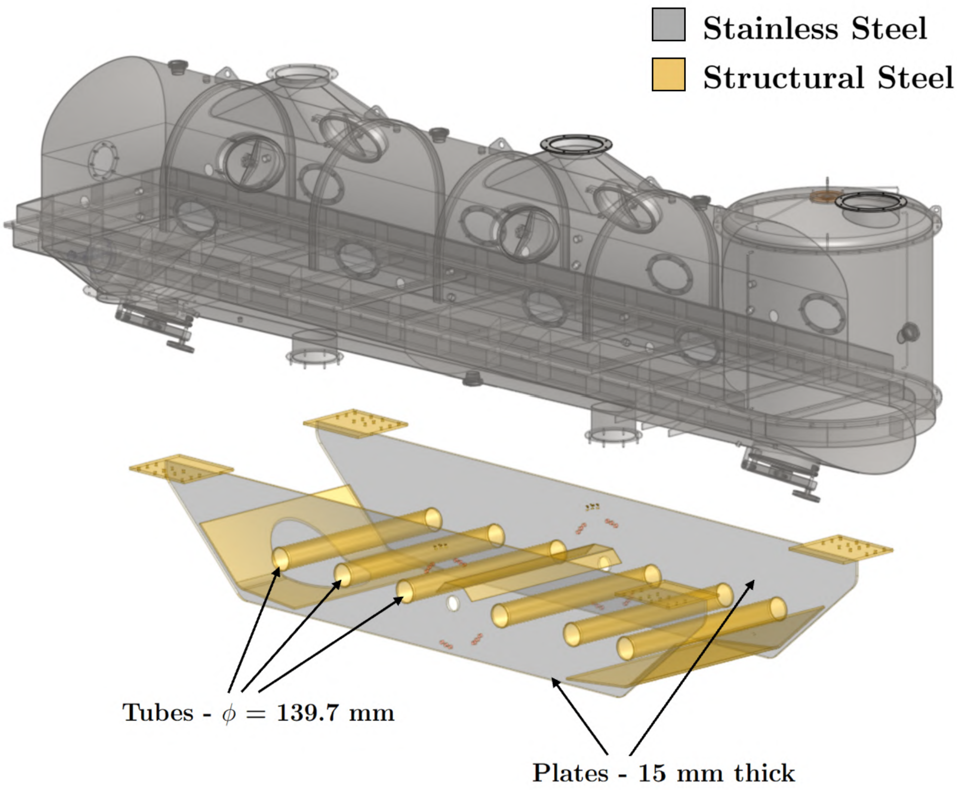

Figure 2.3: *Structural layout of dryer assembly*

The focus is now restricted to the vibrating assembly located above the vibration isolators. Fig. 2.3 reports the structural layout of the vibrating assembly, highlighting the main load-bearing elements of the dryer architecture. In fact, the machine design follows a stiffness hierarchy, where the supporting structure provides the required structural rigidity, while the conveying trough is designed according to process requirements and conveying needs. As a consequence, the trough shell is manufactured with stainless-steel plates with thicknesses ranging between 3 mm and 5 mm. In contrast, significantly thicker structural steel plates make up the supporting structure, with thicknesses ranging from 12 mm up to 15 mm.

From a constructive standpoint, two longitudinal vertical steel plates, each 15 mm thick, mainly constitute the basement. Transverse tubular members, characterized by an external diameter of 139.7 mm and a wall thickness of 5.74 mm, interconnect these plates.

This configuration provides considerable in-plane stiffness, while, as highlighted by the machine cross-sectional view in Fig. 2.4, the overall structural arrangement exhibits a predominantly open-section configuration, resulting in low torsional inertia.

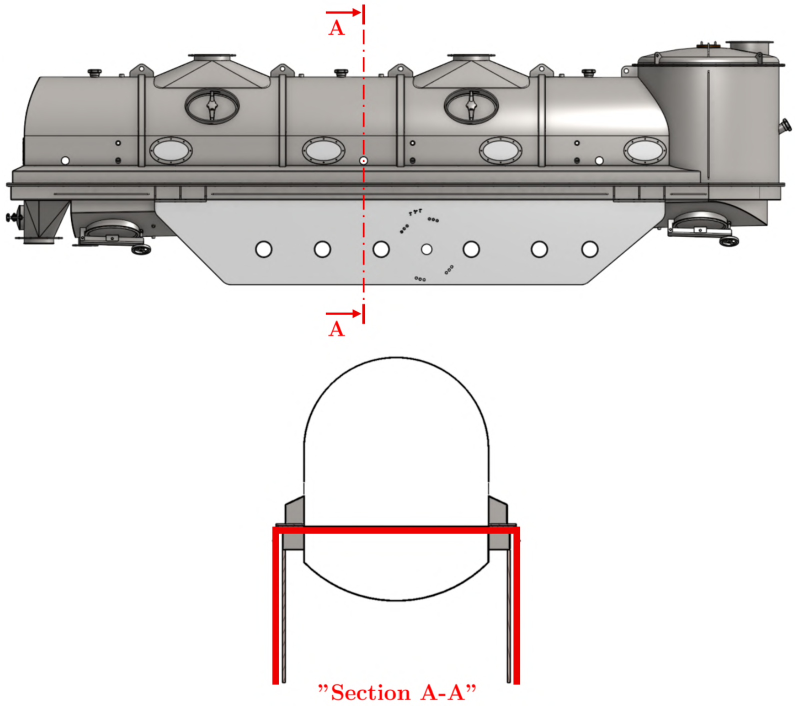

Figure 2.4: *Cross-sectional view*

2.3 Vibratory Motion Generation

Rotating eccentric masses mechanically generate the oscillatory motion of the structure, thereby transporting the product through the machine. The rotational motion of masses, rigidly and eccentrically connected to a motor crankshaft, generates centrifugal inertial forces that the machine structure transmits as vibration. Depending on the eccentric mass arrangement and relative angular positioning, the system generates excitation forces along specific structural directions.

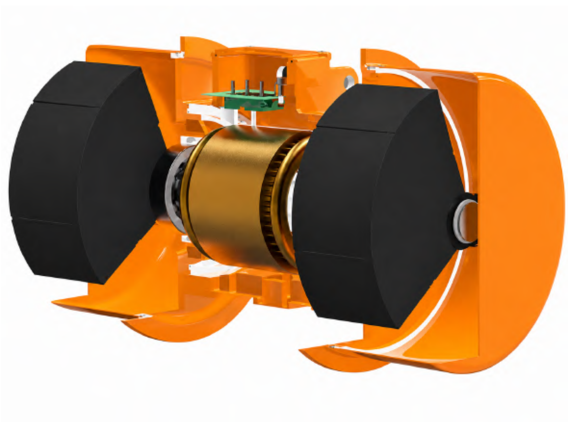

Figure 2.5: *Motovibrator assembly*

Fig. 2.6 schematizes the operating principle and Eq. (2.1) holds.

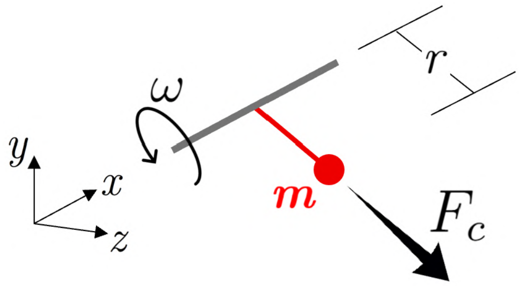

Figure 2.6: *Working principle of motovibrators*

$$F_c = mr\omega^2 \tag{2.1}$$

where F_c is the resulting *centrifugal force*, m is the *eccentric mass*, r is the *eccentricity* between mass center of gravity and shaft axis, and ω is the *rotating speed*. If $x - axis$ is consistent with shaft axis, centrifugal force always lies on $y - z$ plane and decomposes into its vector components accordingly.
In the particular case under study, two motovibrators are mounted on lateral plates of the machine and rotate synchronously in opposite directions. In this configuration, the force components that lie in the vertical plane add together, while the horizontal components cancel each other out.
Now, let x-y-z denote the local coordinate system attached to the vibration motor, where the $x - axis$ coincides with the motor shaft axis, and let X-Y-Z represent the global coordinate system of the machine, where X is aligned with the machine longitudinal direction, Z is transverse, and Y points upward, as shown in Fig. 2.7 (where axes z and Z coincide).

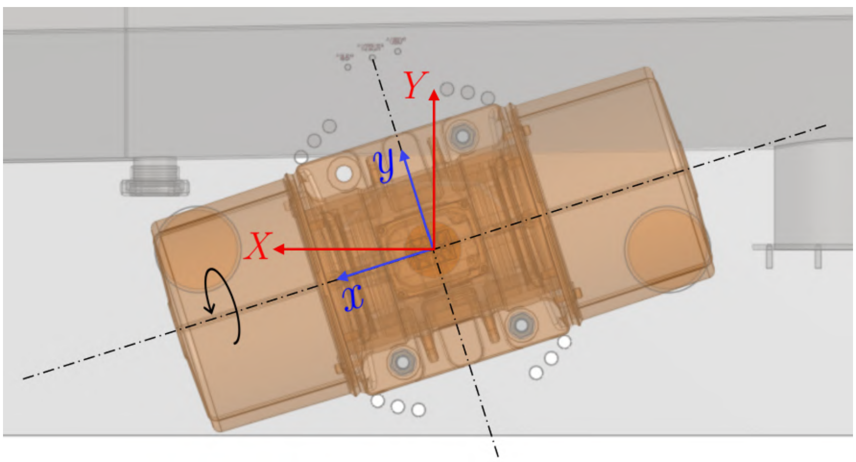

Figure 2.7: Local and global reference systems

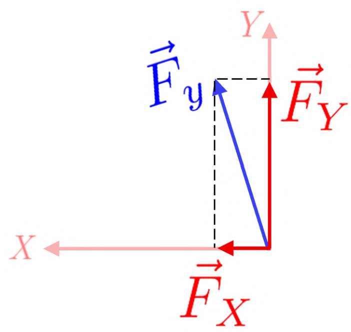

Figure 2.8: Vector F_y decomposition in global reference system

Due to eccentric rotating masses, the motor generates a harmonic excitation force lying in the local $y-z$ plane and rotating around the $x-axis$ at the motor angular speed. The motor axis is tilted relative to the horizontal plane, such that the only remaining force, which lies on the $y-axis$, decomposes in the global coordinate system into the X component $\vec{F}_X$, responsible for the forward transport of the product, and a vertical component $\vec{F}_Y$ along the $Y-direction$, which promotes detachment and upward motion of the material bed.
As previously stated, the actual excitation system adopted in the investigated machine consists of two identical motor vibrators installed symmetrically on the dryer supporting structure. Operating conditions are design parameters selected according to process requirements in order to guarantee the target product flow rate. The main characteristics of the installed motor vibrators are summarized in Tab. 2.2.

Table 2.2: *Operating Parameters of Installed Motovibrators*

Parameter	**Value**
Number of motor vibrators	2
Motovibrator mass	315 kg
Rotational speed	**750 rpm**
Excitation frequency	**12.5 Hz**
Installation configuration	Counter-rotating

The selected excitation frequency plays a key role in the dynamic response of the vibrating assembly, so it is a fundamental parameter in this thesis work.

2.4 Vibration Isolation System

Four vibration isolators support the dryer by connecting the vibrating assembly to the support frame, which anchors to the concrete foundations. The isolation system preserves the oscillatory motion required for product transport. At the same time, it minimizes the dynamic stresses transmitted to the foundations and supporting structure and limits vibration propagation to adjacent equipment and piping systems.
The degree of uncoupling η provided by the selected vibration isolation system is evaluated with reference to Appendix A. In particular, given the exciting pulsation ω of the harmonic force acting on the dryer, the scope is to calculate the natural frequency, so natural pulsation ω_n of the isolation system, intended as the first natural frequency of the Single-Degree-of-Freedom system, where the machine is thought to be infinitely rigid as a concentrated mass, in order to achieve a degree of the uncoupling of 80-90%.
Degree of decoupling η and transmissibility T_f are complementary according to Eq. (2.2).

$$\eta = (1 - T_f) \cdot 100 \tag{2.2}$$

Given $r = \omega/\omega_n$ and η, it is possible to compute the value of natural frequency that must be required from Eq. (A.8).

$$r = \sqrt{1 + \frac{1}{T_f}} \tag{2.3}$$

and

$$\omega_n = \frac{\omega}{r}, \qquad therefore \qquad f_n = \frac{f}{r} \tag{2.4}$$

Assuming an uncoupling efficiency of $\eta = 80 \div 90\%$, the isolation criterion yields a natural frequency range of $3.8 \div 5.1\ Hz$.
The abacus shown in Fig. 2.9 confirms the same result graphically.
It should be noted that the oblique lines shown in Fig. 2.9 do not directly represent η. Rather, they correspond to constant values of the frequency ratio $r = f/f_n$, which, in logarithmic coordinates, generates a family of straight and parallel lines according to the relation $f_n = f/r$. Since the transmissibility factor T_f, and consequently the degree of uncoupling η, are uniquely determined by the frequency ratio r from Eq. (2.3) and Eq. (2.2), each line corresponds directly with a specific attenuation level. For this reason, the chart labels the constant-R lines with the corresponding

attenuation percentage.

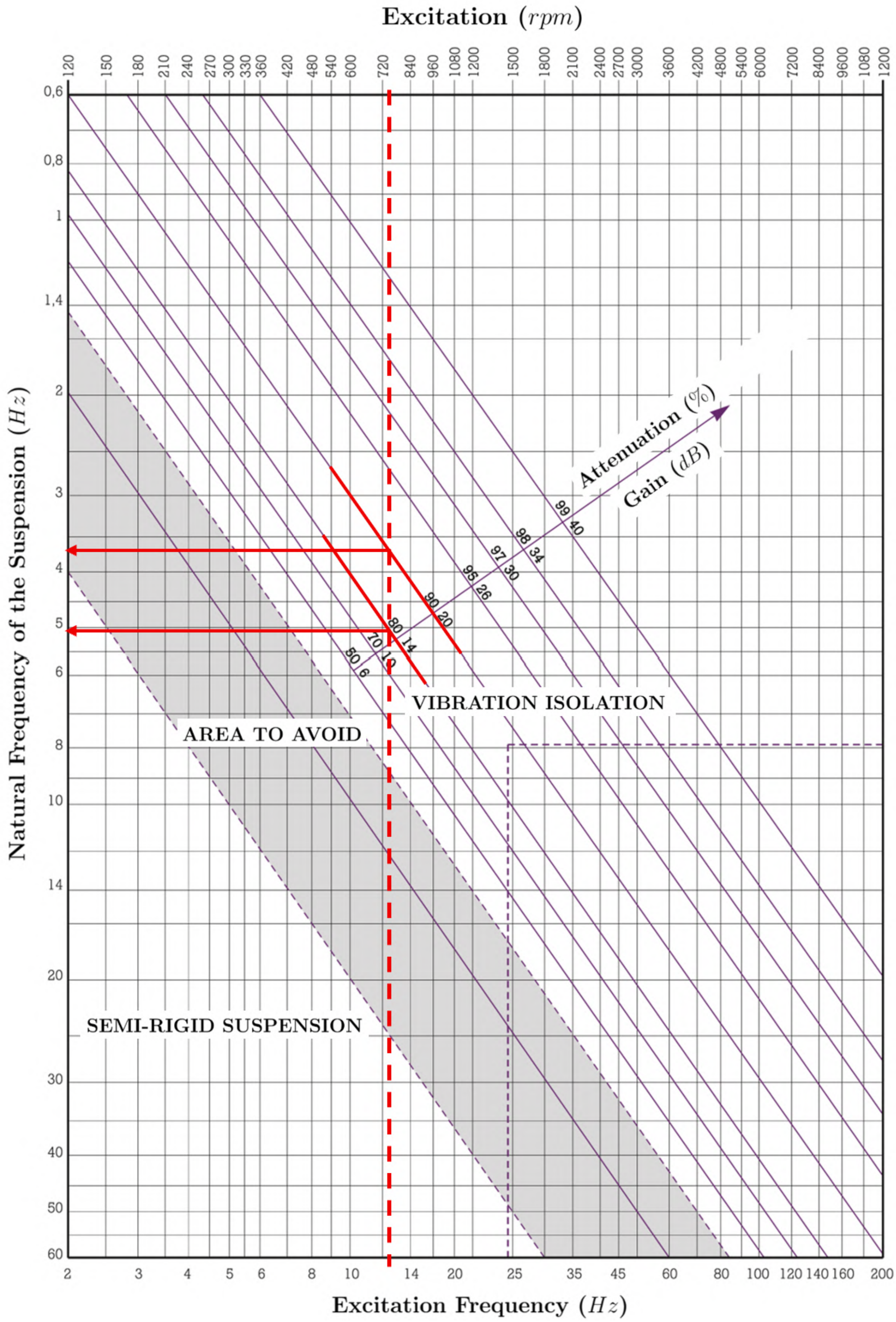

Figure 2.9: *Attenuation as a function of natural frequency and excitation frequency (Theoretical chart for an undamped suspension) [27]*

As discussed in the following chapters, the frequency range predicted by the above vibration isolation design procedure is consistent with the rigid-body modes identified through modal analysis of the numerical model. This result provides an independent validation of the selected suspension characteristics.
Tab. 2.3 summarizes the main elastic properties of the adopted vibration isolators. Reported stiffness values refer to a single support point and account for the parallel contribution of the two isolator elements installed at each location.

Table 2.3: *Main Stiffness Properties of Vibration Isolators*

Horizontal	**Vertical**
[N/mm]	**[N/mm]**
280	640

Chapter 3

Chronology of Events and Experimental Tests

The purpose of this chapter is to present a chronological overview of the events that led to the identification of the structural problem affecting the vibrating dryer, from machine commissioning to crack appearance, machine modification and instrumental tests.
The implementation of the structural modification marks the boundary between two different machine configurations. To simplify the discussion presented in the following chapters, the original configuration will be identified as "*Version 0*" and the modified configuration as "*Version 1*".

3.1 "*Version 0*": Original Configuration

3.1.1 Machine configuration

The initial configuration of the vibrating dryer corresponds to the structural arrangement described in Chapter 2.
The machine was designed to convey and dry organic natural acid crystals, a by-product of the winery industry. Eccentric masses rotating at 750 rpm (12.5 Hz) generate the controlled mechanical vibrations that transport the product through the machine.
The trough that contains the product is welded to a supporting structure, which in turn rests on a bed of vibration isolators.
The "Version 0" layout of the machine is shown in Fig. 2.2.

3.1.2 Appearance of fatigue cracks

After approximately 150 hours of operation, fatigue cracks developed in several regions of the supporting structure. Visual inspection revealed crack patterns characteristic of fatigue failure induced by cyclic loading, with crack propagation occurring around the circumference of the tubular welded junction with longitudinal 15 mm thick plates, as shown in the figures below.

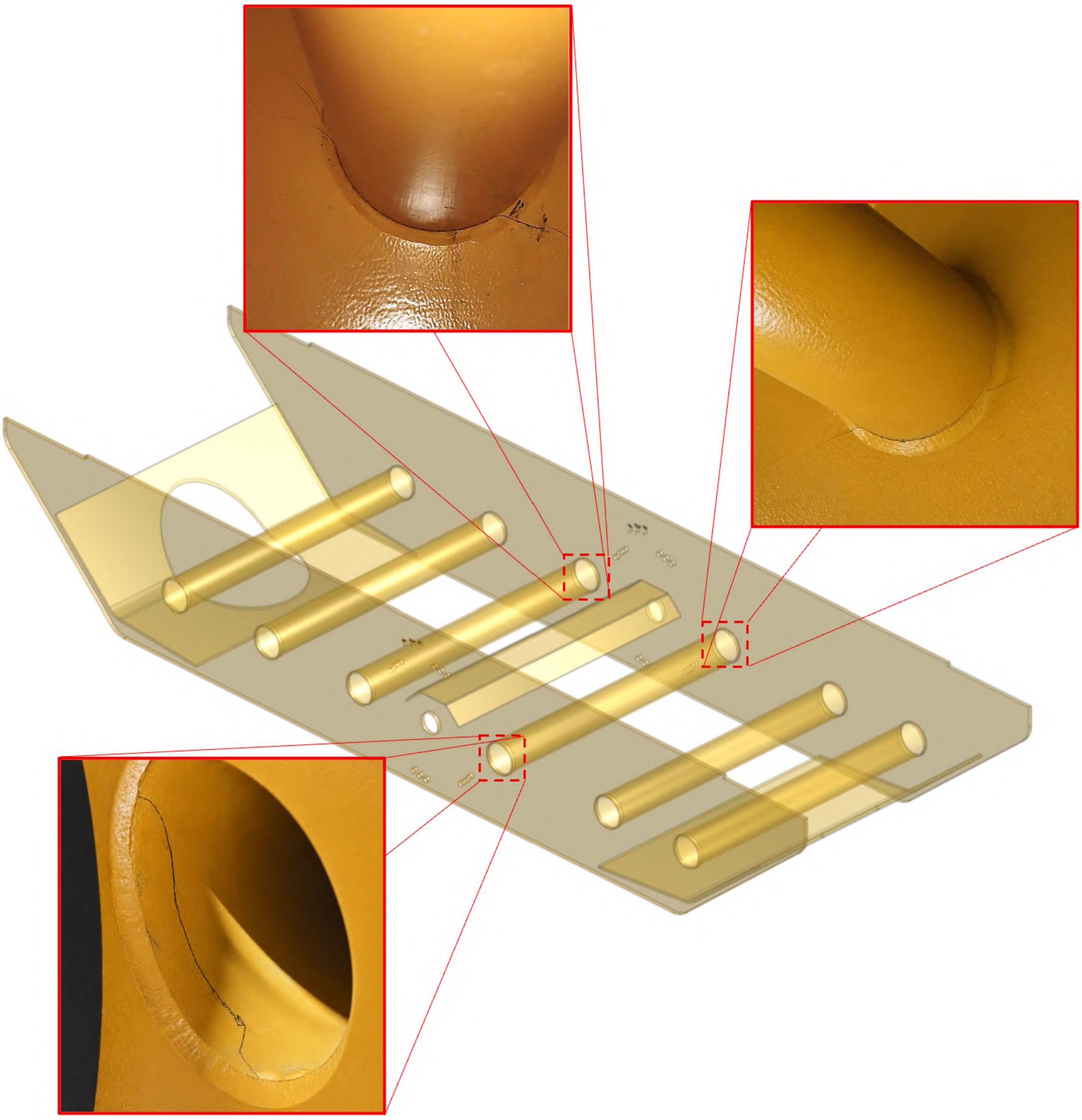

Figure 3.1: *Zoom on appeared cracks*

As an immediate corrective action, drilling stop-holes at the crack tips arrested the crack propagation, thereby increasing the local radius of curvature and reducing the stress concentration. Subsequently, machining and repairing of the cracked regions by means of full-penetration welding restored the "Version 0" structural integrity of the machine.

Figure 3.2: *Crack repair example with full-penetration weld*

Despite these repairs, crack re-initiation occurred, indicating that the root cause of the problem had not been removed and that significant cyclic stresses were still present during operation.

3.1.3 Experimental investigation

A campaign of experimental dynamic tests was carried out on the machine in order to investigate the origin of fatigue damage. The objective of these tests was to identify the natural frequencies of the structure and to assess the possibility of resonance phenomena occurring within the operating speed. The measurements considered the machine under empty conditions: this aspect provides fundamental information for the modeling activity presented in the following chapter.

Bump test

The experimental campaign conducted a bump test by exciting the structure with a hammer in a specific point and recording the response using an accelerometer, positioned at a strategic point and direction.
In the specific case of the vibrating dryer, the measurement locations were selected at the mid-span of the main longitudinal beams, with the accelerometer oriented

along the vertical direction, as shown in Fig. 3.3.

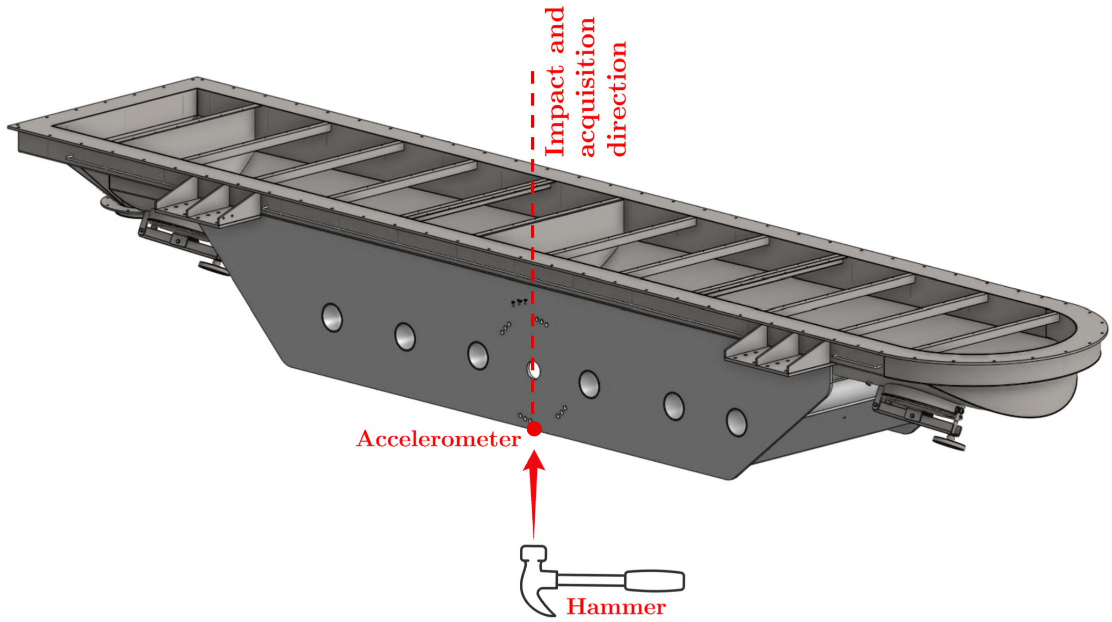

Figure 3.3: Impact hammer testing setup

The measurements adopted a *drive-point* configuration, in which the impact point and the point where acceleration response is recorded coincide.
Some limitations affected the experimental:

- not instrumented impact hammer: input force cannot be directly measured, thus the quality and repeatability of excitation relied on experience of the technician performing the test;

- only one accelerometer used: impact hammer would not provide sufficient energy to far points due to large extension of the machine. As a result, measurements could only be acquired sequentially, and it was not possible to simultaneously record the response at multiple locations.

The acquired signals were processed in the frequency domain in order to identify the dominant resonance frequencies of the structure. For clarity, the acquired FRFs are classified as *left-side* and *right-side* measurements. The adopted convention refers to the direction of product flow inside the dryer.

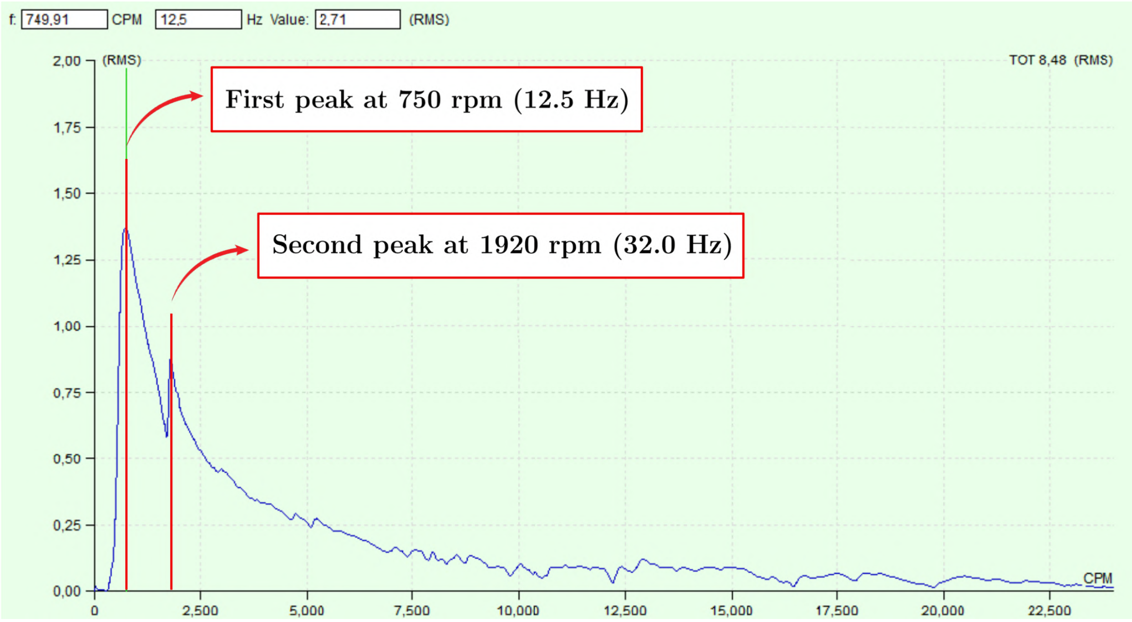

Figure 3.4: *"Version 0" - Result of bump test on right-side structure*

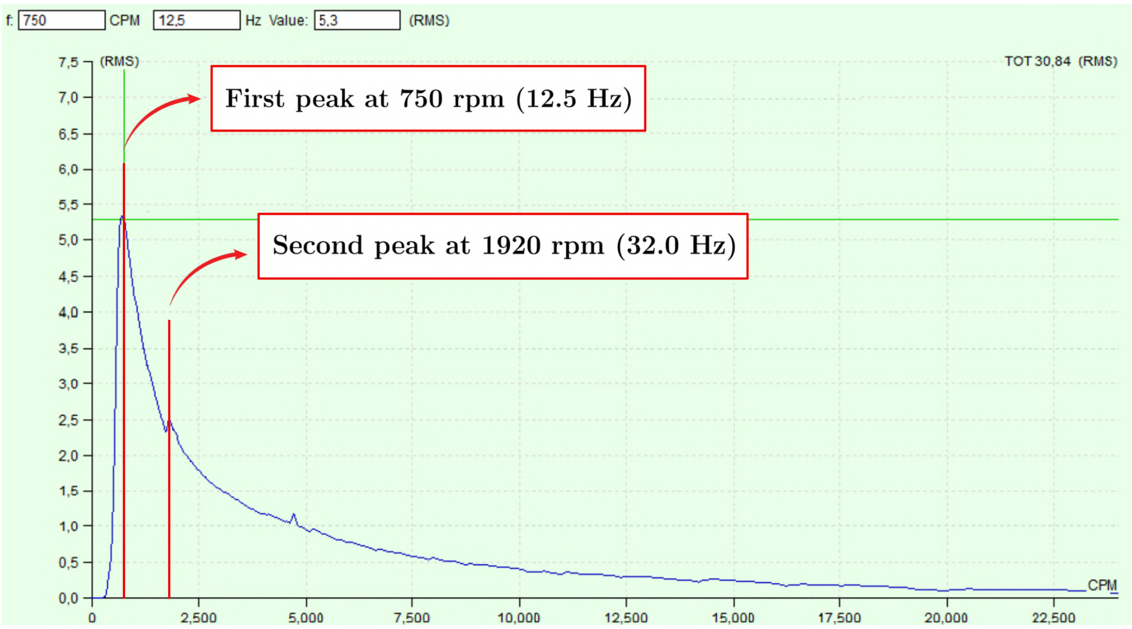

Figure 3.5: *"Version 0" - Result of bump test on left-side structure*

The results obtained show a high degree of consistency between right-side and left-side measurements. In both cases, two dominant resonance peaks can be clearly identified at approximately 12.5 Hz (750 rpm) and 32.0 Hz (1920 rpm), indicating the presence of two main structural vibration modes. Given the close agreement between measurements, they are likely to be representative of global dynamic behavior rather than local effects. These natural frequencies identified experimentally constitute

the primary reference for the validation of the numerical model developed in the following chapters.
A particularly significant observation is that the first resonance peak coincides with the operating excitation frequency generated by the rotating eccentric masses. This frequency matching condition is characteristic of resonance.

Forced vibrations measurement

Forced vibration measurements performed during normal machine operation (motovibrators rotating at 750 rpm) allowed for the assessment of the actual vibration levels throughout the machine. Particular attention was given to the dynamic behavior of the supporting structure and to the effectiveness of the vibration isolation system.

Table 3.1: *"Version 0" - Measurement points and acquisition directions*

Label No.	**Description**	**Acquisition Direction**
1	Above vibration isolator - Load side - Left side	Vertical - y
2	Under vibration isolator - Load side - Left side	Vertical - y
3	Support frame - Load side - Left side	Horizontal - z
4	Near vibrating masses - Left side	Horizontal - z
5	Transverse plate - Load side	Horizontal - x
6	Transverse plate - Discharge side	Horizontal - x
7	Transverse beam	Vertical - y
8	Transverse beam	Horizontal - z
9	Longitudinal plate - Mid-span	Vertical - y

The experimental campaign measured the dynamic response using an accelerometer placed at several locations on the structure. Fig. 3.6 and Tab. 3.1 show the selected measurement points and the corresponding acquisition directions. The analysis selected these locations to capture the dynamic response of both the dryer and the supporting frame below the vibration isolators.
The following frequency spectra summarize the vibration response measured at the selected locations during normal machine operation.

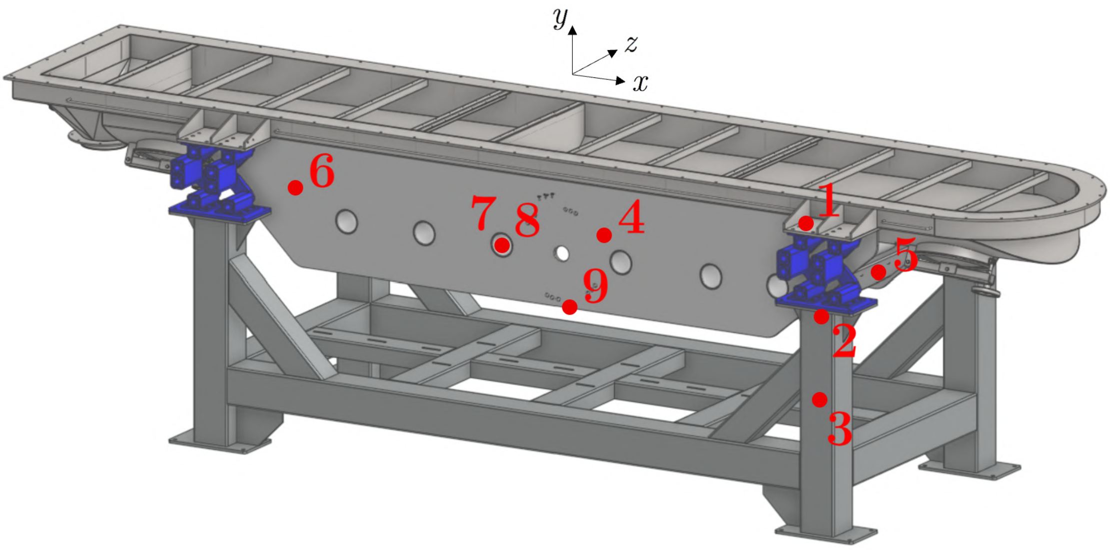

Figure 3.6: *"Version 0" - Accelerometers positioning labels*

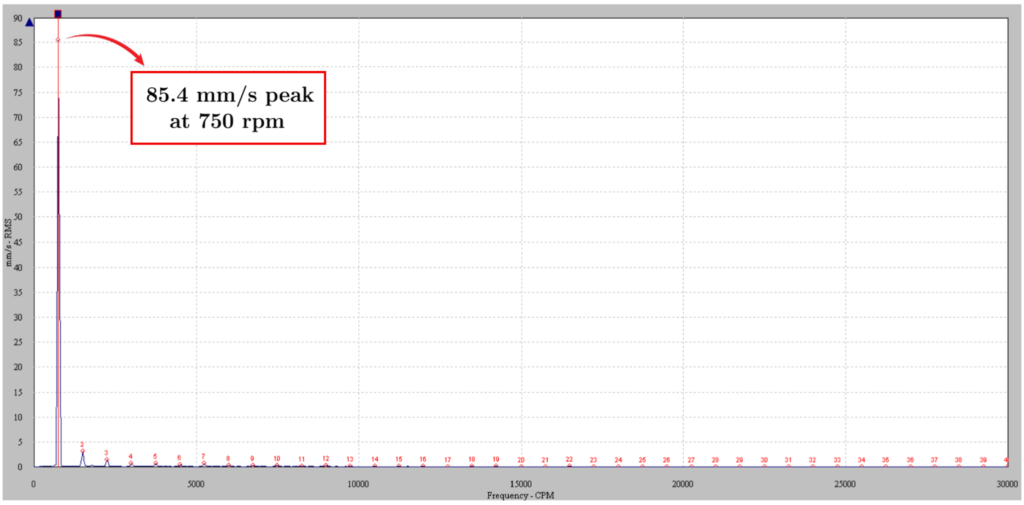

Figure 3.7: *Position 1 - RMS velocity spectrum*

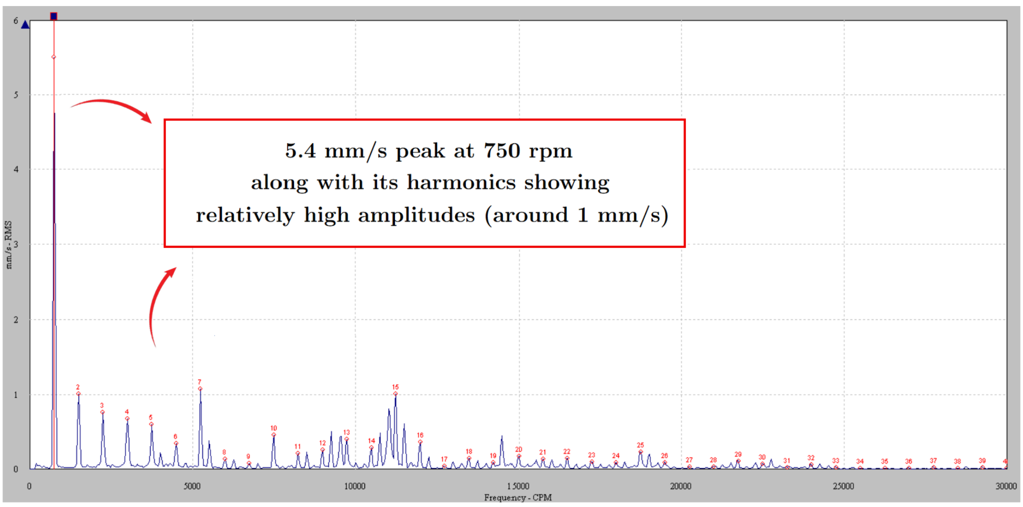

Figure 3.10: *Position 4 - RMS velocity spectrum*

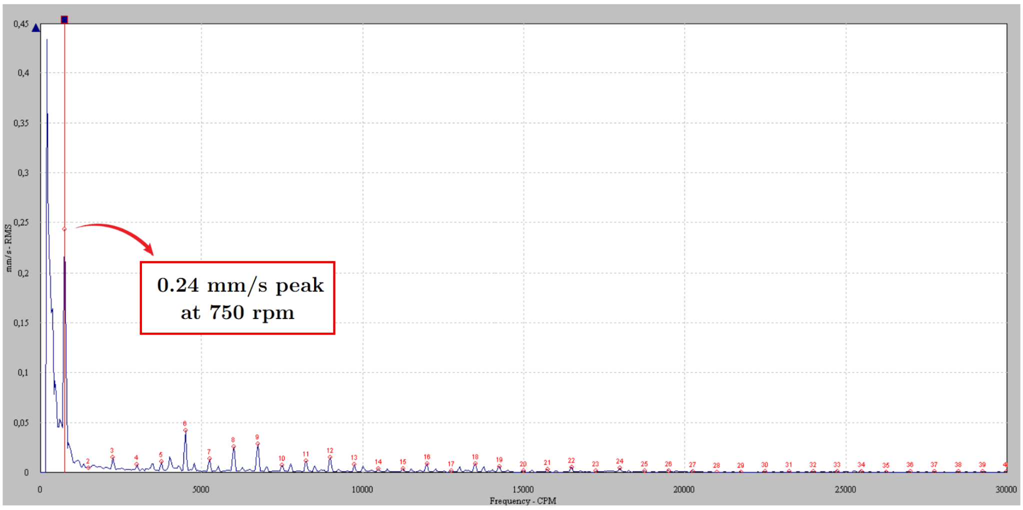

Figure 3.8: *Position 2 - RMS velocity spectrum*

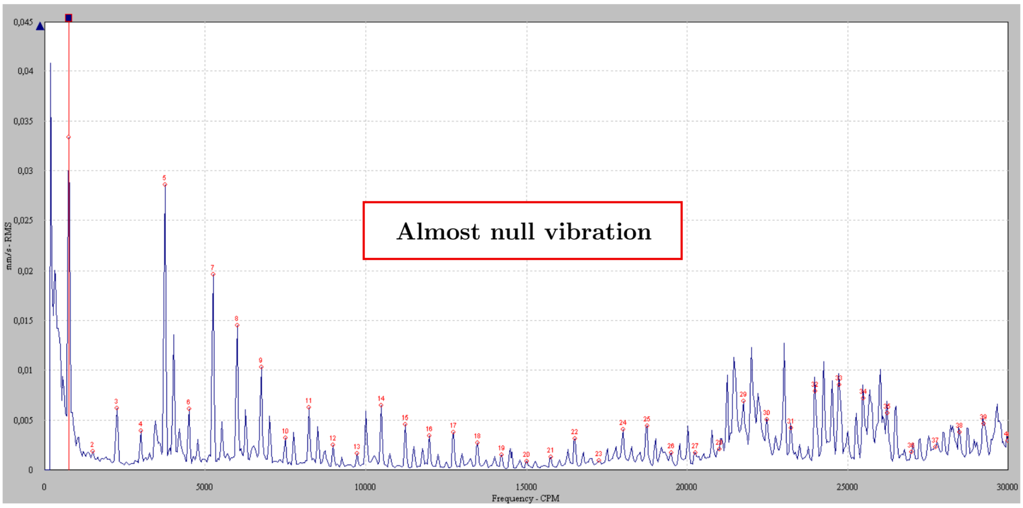

Figure 3.9: *Position 3 - RMS velocity spectrum*

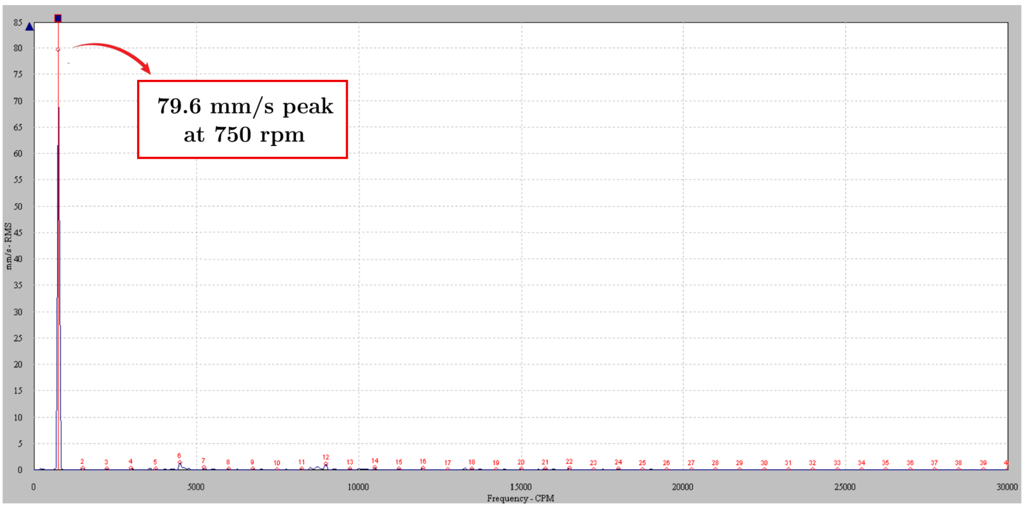

Figure 3.11: *Position 5 - RMS velocity spectrum*

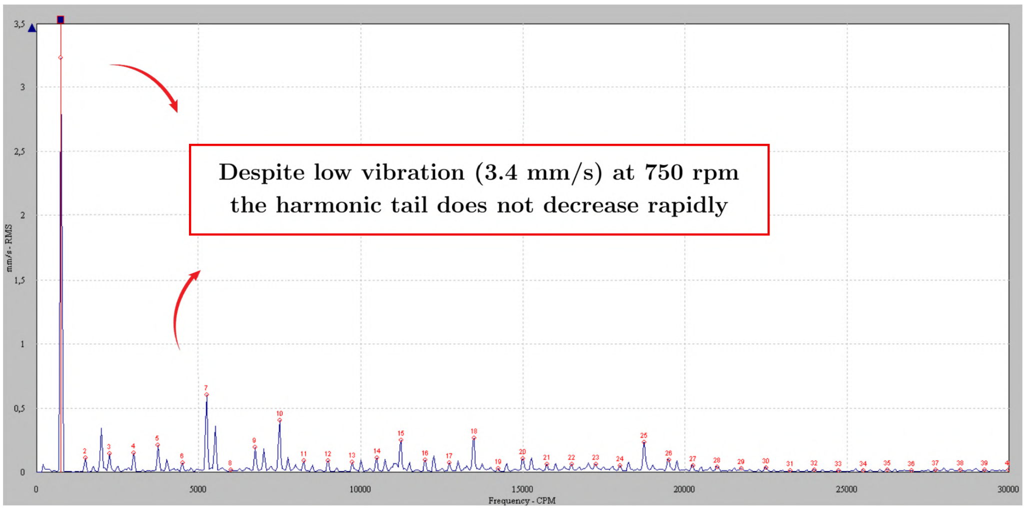

Figure 3.12: *Position 6 - RMS velocity spectrum*

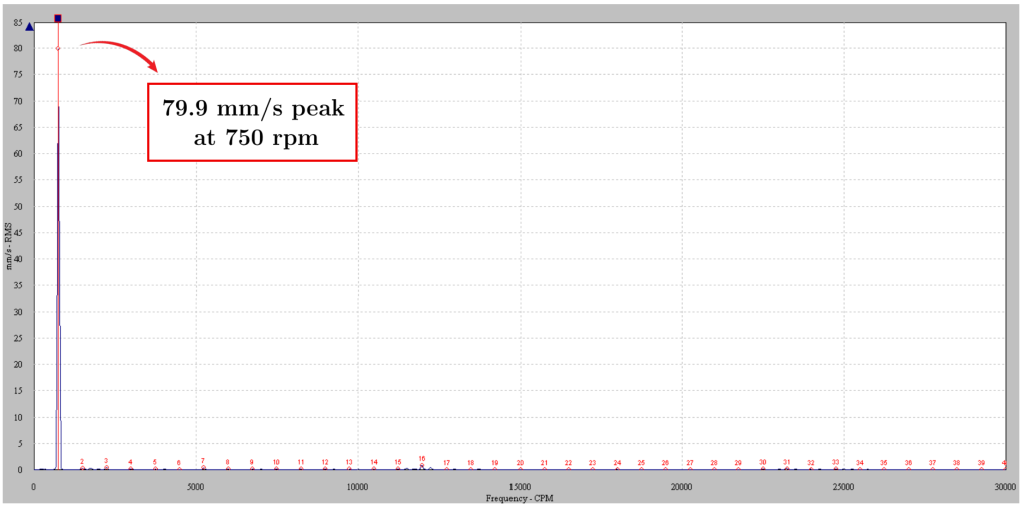

Figure 3.13: *Position 7 - RMS velocity spectrum*

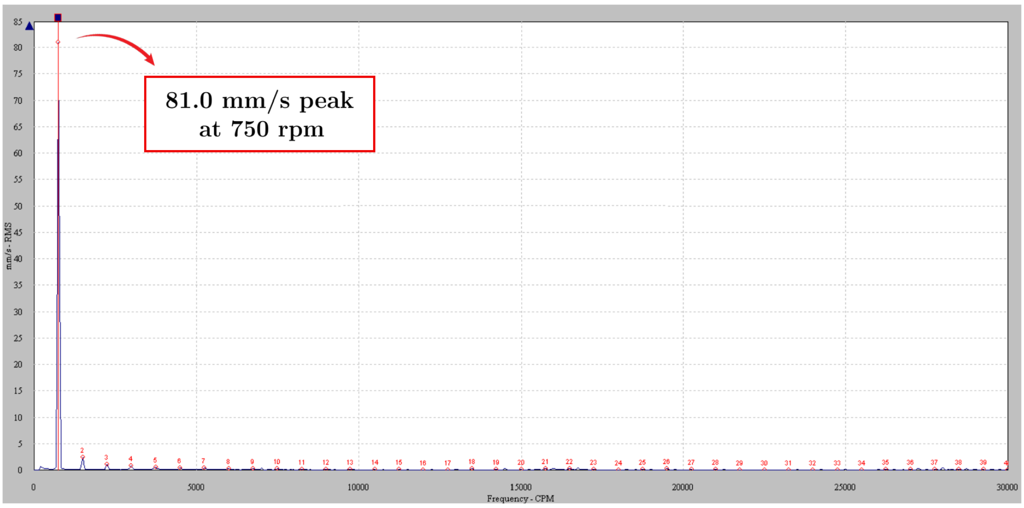

Figure 3.14: *Position 8 - RMS velocity spectrum*

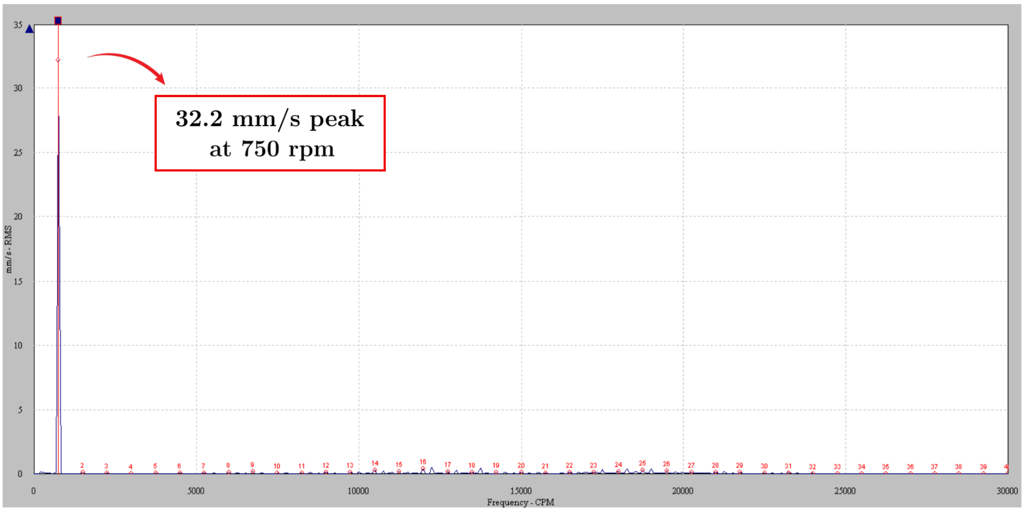

Figure 3.15: *Position 9 - RMS velocity spectrum*

Observing previous graphs, the following conclusions emerge:

- Comparing dynamic responses above and below the vibration isolator, respectively Fig. 3.7 and Fig. 3.8, the vibration reduces significantly;
- With reference to Fig. 3.10 and Fig. 3.12, and based on technician experience, the presence of an irregular harmonic tail with a slow decay rate may indicate excessive structural flexibility. Such compliance can lead to non-linear behaviors, including large deformations and friction-induced effects, thereby altering the dynamic response of the structure.

The combined evidence of good uncoupling of vibration isolators and structural weakness problems supports the hypothesis that resonance phenomena occur.

3.1.4 Conclusions and design choices

The experimental results provided strong evidence of resonance and valuable information about the structural weaknesses. Although the available instrumentation allowed for the identification of the dominant natural frequencies, the experimental setup included only a single accelerometer. Consequently, it was not possible to reconstruct the corresponding mode shapes or perform phase-based modal identification.
The absence of modal shape information limited the possibility of identifying the most effective locations for structural reinforcement. Therefore, the subsequent modification strategy was developed primarily on the basis of engineering judgment.

Based on these observations, the machine supplier proposed a structural modification aimed at increasing the transverse stiffness of the supporting frame and shifting the first natural frequency away from the operating excitation frequency.

3.2 "*Version 1*": Modified Configuration

3.2.1 Machine configuration

The conclusions drawn from the first experimental campaign led to a substantial modification of the machine structure. The intervention affected only the supporting structure of the vibrating assembly. The re-design activity replaced the original support structure after cutting and removing it.

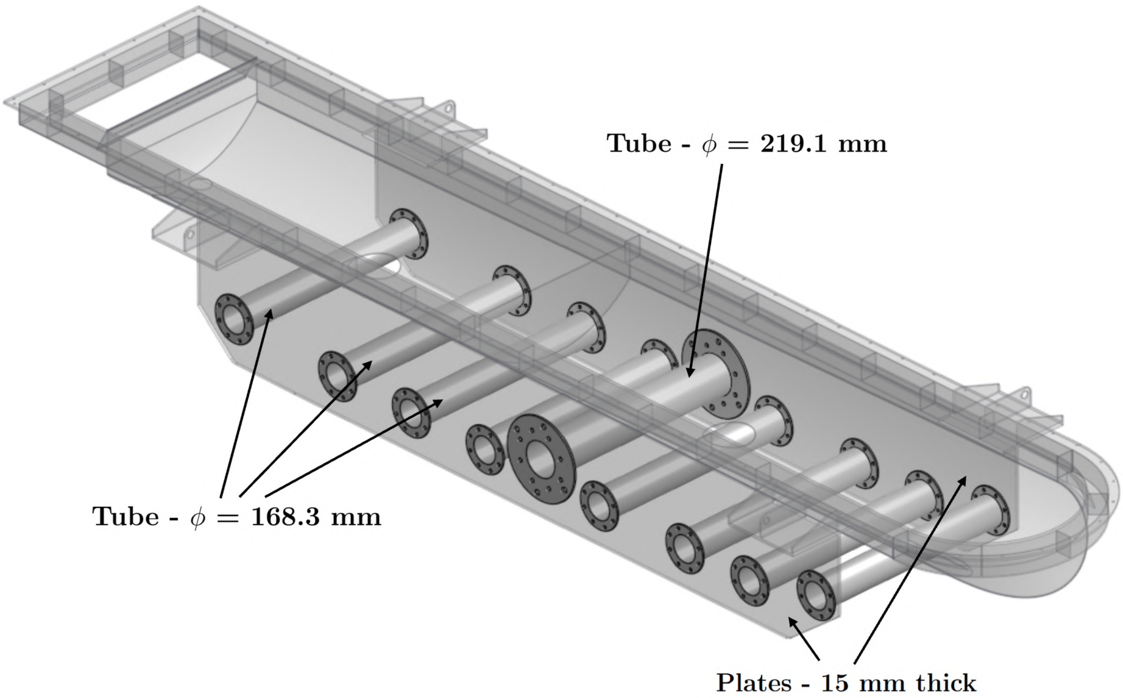

Figure 3.16: "Version 1" structure layout

The most significant difference between the two configurations concerns the tubular cross-members connecting the longitudinal side plates. In the "Version 0" configuration, these members consisted of tubes with an outer diameter of 139.7 mm and a wall thickness of 5.74 mm. In the "Version 1" configuration, they were replaced by larger tubular members with an outer diameter of 168.3 mm and a wall thickness of 10.95 mm. Furthermore, an additional heavy-duty central cross-member was

introduced between the two vibrator motors. This element consists of a tube with an outer diameter of 219.1 mm and a wall thickness of 12.7 mm, providing a direct structural connection between the motor supports and significantly increasing the local stiffness of the frame. All transverse beams are now joined to longitudinal plates by means of bolted connections instead of welded ones.
Fig. 3.16 shows a view of the "Version 1" machine configuration.
Since the modification did not affect the trough, the following table summarizes the structural weights.

Table 3.2: *Main Components of "Version 1" Dryer Assembly*

Item	**Material**	**Weight [kg]**
Base Structure	Structural Steel	1290
Plenum	Stainless Steel	685
Upper Trough	Stainless Steel	900

3.2.2 Experimental tests

Immediately after installing the "Version 1" structure, the experimental campaign carried out a second series of tests.
The operating and boundary conditions during these tests differed from those adopted for the "Version 0" investigation. In particular, the machine contained approximately 1000 kg of product, and the eccentric masses also operated at slightly different rotational speeds.
The comparison between the two experimental campaigns must account for these differences, since changes in mass distribution and operating conditions may influence the measured dynamic behavior.

Bump test

The experimental campaign repeated the bump test on the "Version 1" configuration using the same measurement layout adopted for "Version 0". Consequently, the analysis kept the excitation points, acquisition locations, and measurement directions unchanged to allow a direct comparison between the two experimental campaigns, apart from the differences described above.
The following figures report the resulting Frequency Response Functions.

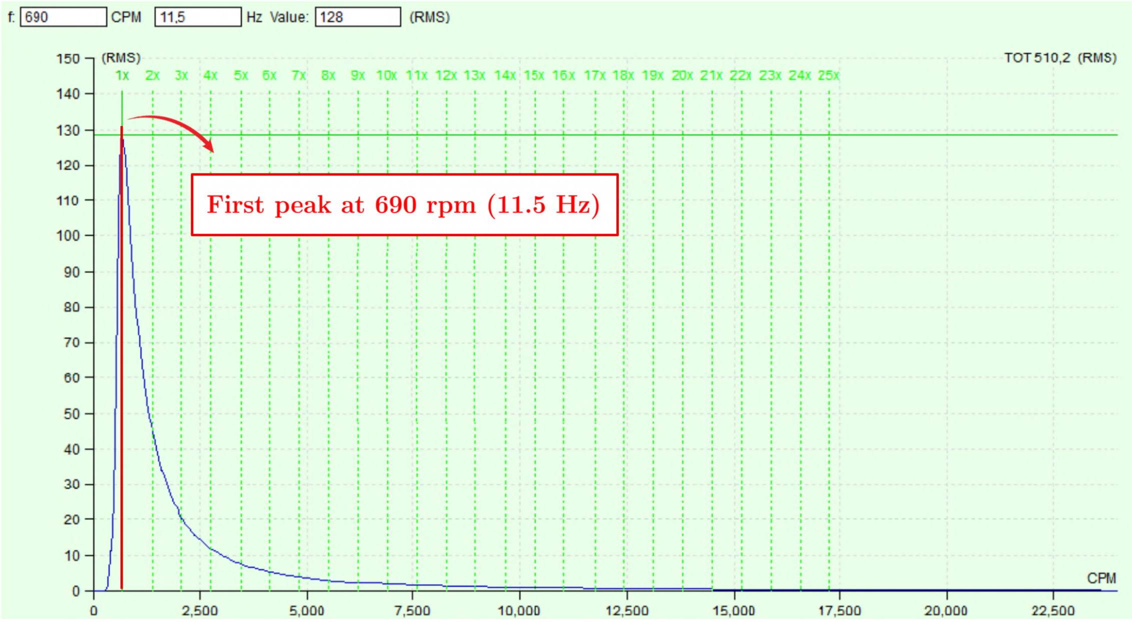

Figure 3.17: *"Version 1" - Result of bump test on left-side structure*

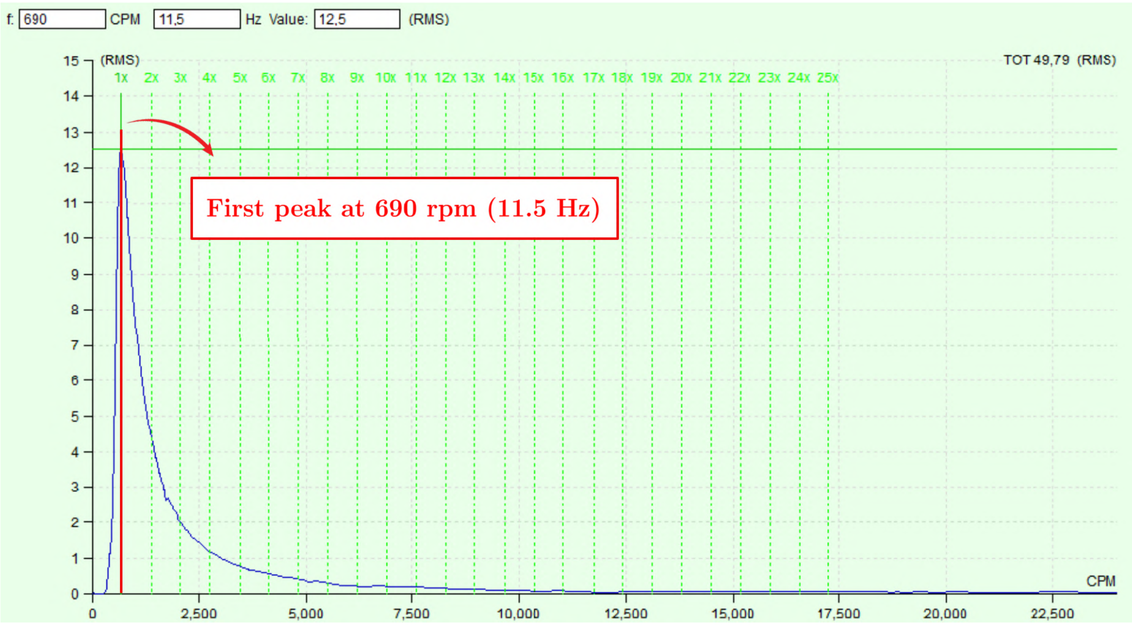

Figure 3.18: *"Version 1" - Result of bump test on right-side structure*

The measured *FRFs* show that the first natural frequency shifted from approximately 12.5 Hz in "Version 0" to approximately 11.5 Hz in "Version 1". Although the structural modification aimed to increase the stiffness of the supporting frame, the experimental results indicate a slight reduction of the first natural frequency. According to the fundamental relation $\omega_n = \sqrt{(k/m)}$ and considering that the product load represents a significant increase in the total mass of the vibrating system,

it is reasonable to assume that the additional mass contributed to the observed frequency reduction. In fact, the introduction of approximately 1000 kg of product increased the total vibrating mass by about 25–30%, while the first natural frequency decreased by approximately 8% (from 12.5 Hz to 11.5 Hz). According to the relationship between natural frequency and mass, this reduction corresponds to an increase in effective vibrating mass of approximately 18%, which is of the same order of magnitude as the actual mass increase.
An additional observation emerges from the comparison between the FRFs of the two configurations. Although the first resonance peak remains clearly identifiable, the second natural frequency observed at approximately 32 Hz in "Version 0" is no longer evident in the measurements performed on "Version 1". This observation suggests that the structural intervention altered the dynamic behavior of the machine, but not in the critical frequency range. As a consequence, the resonance condition associated with the first vibration mode was not effectively eliminated, despite the significant modification of the supporting structure.

Forced vibrations measurement

The forced vibration measurements performed on "Version 1" followed the same methodology adopted for the "Version 0" machine configuration described in Section 3.1.3. As in the previous experimental campaign, the analysis acquired vibration velocity spectra at several locations on the machine structure and the supporting frame. However, the revised experimental layout introduced a partially different measurement configuration. Tab. 3.3 summarizes the selected acquisition points and the corresponding measurement directions, while Fig. 3.19 illustrates their locations.

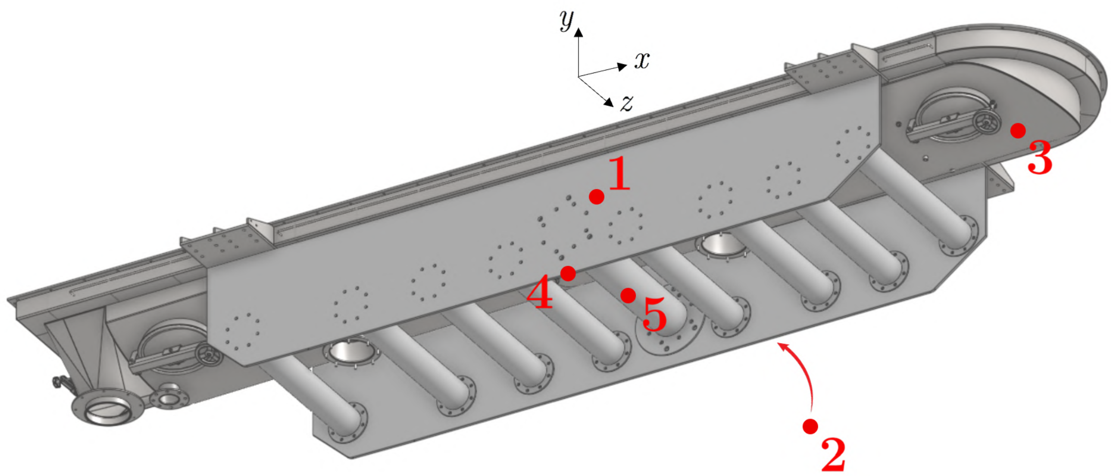

Figure 3.19: *"Version 1" - Accelerometers positioning labels*

Table 3.3: *"Version 1" - Measurement points and acquisition directions*

Label No.	**Description**	**Acquisition Direction**
1	Near vibrating masses - Left side	Horizontal - z
2	Near vibrating masses - Right side	Horizontal - z
3	Dryer bottom - Load side	Horizontal - x
4	Longitudinal plate - Mid-span	Vertical - y
5	Transverse beam	Vertical - y

The machine operated at approximately 788 rpm, a rotational speed slightly different from that adopted during the tests on "Version 0".
The analysis processed the acquired signals in the frequency domain. The following figures present the resulting spectra.

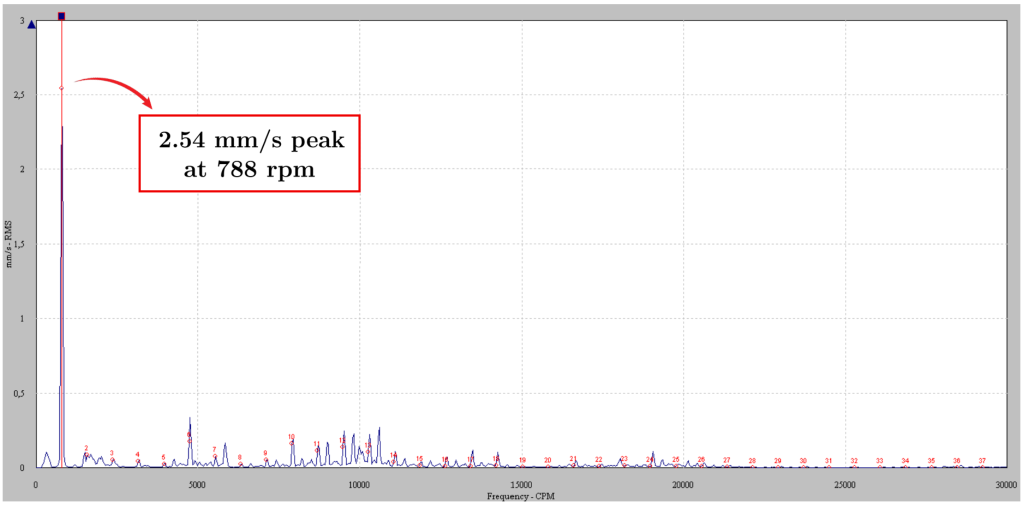

Figure 3.20: *Position 1 - RMS velocity spectrum*

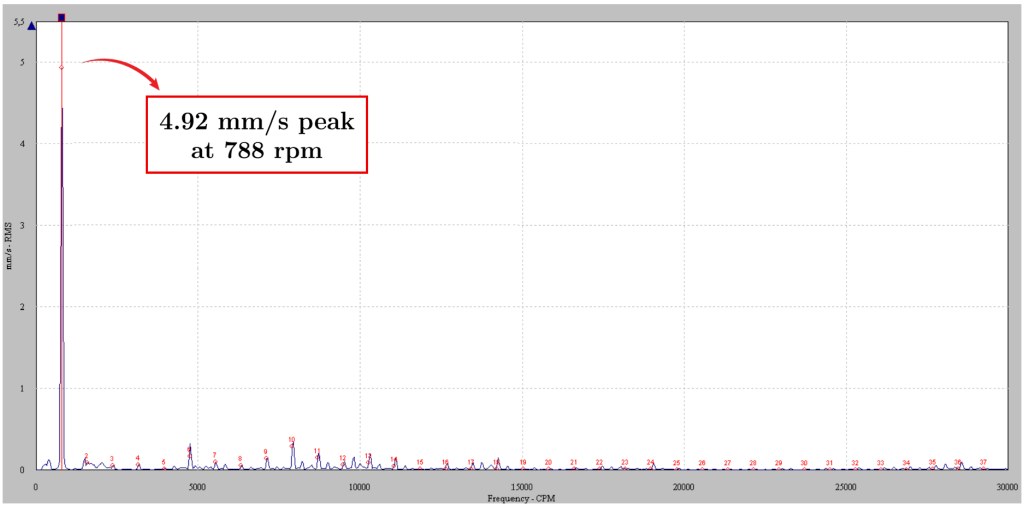

Figure 3.21: *Position 2 - RMS velocity spectrum*

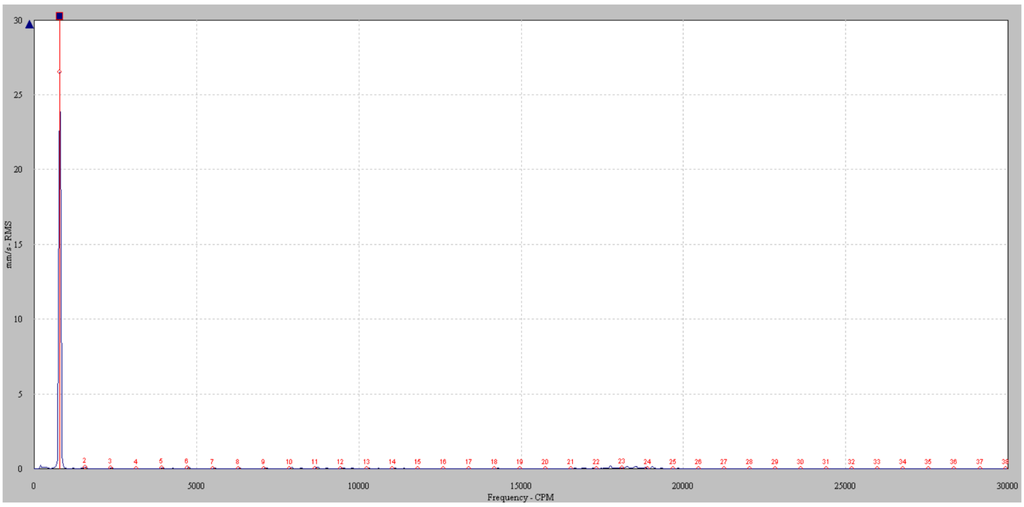

Figure 3.22: *Position 3 - RMS velocity spectrum*

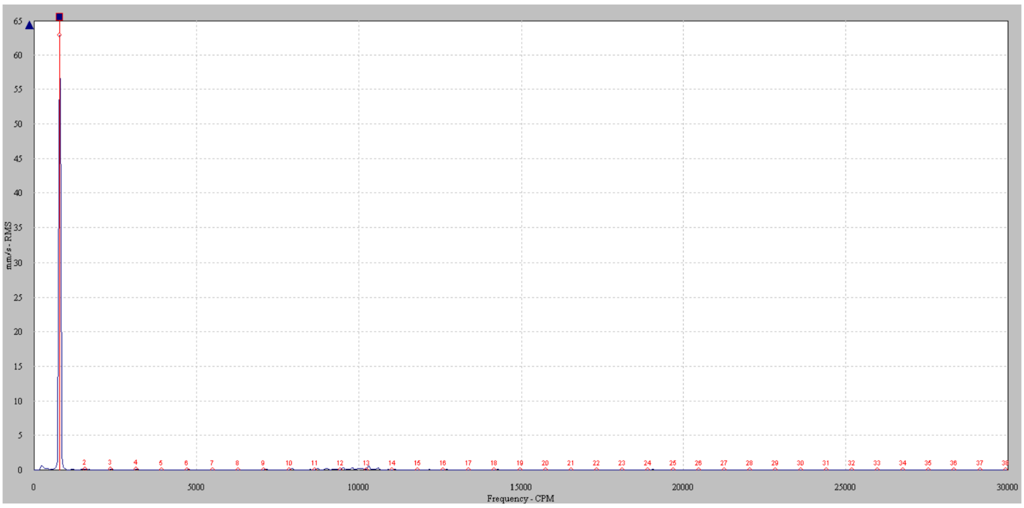

Figure 3.23: *Position 4 - RMS velocity spectrum*

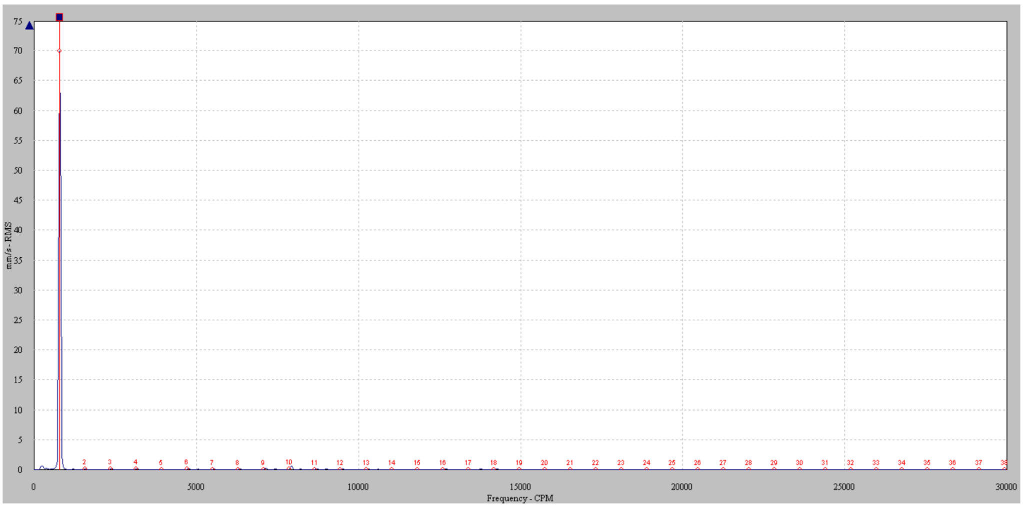

Figure 3.24: *Position 5 - RMS velocity spectrum*

Nevertheless, a qualitative comparison still provides useful insights. In particular, Fig. 3.20 and Fig. 3.21 show that the harmonic components associated with the excitation frequency remain clearly visible after the structural modification. However, their amplitude and overall energy content appear lower than those measured for the "Version 0" configuration. This observation suggests that the implemented structural intervention improved the dynamic response of the machine by reducing the vibration levels at the investigated location. Nevertheless, the persistence of the harmonic components indicates that the underlying dynamic issue persists.

3.2.3 Conclusions and operating choices

For "Version 1" of the machine, the hammer impact test alone does not isolate the effect of the structural modification from the influence of the added product mass. A more detailed assessment requires a numerical model that separately evaluates the contribution of stiffness and mass to the dynamic behavior of the machine. The forced vibration measurements lead to similar conclusions. Although the different boundary conditions prevent a direct comparison with the spectra acquired for "Version 0", the results suggest only a partial improvement in the structural dynamics of the machine.
Based on the available experimental evidence, the implemented modification does not completely separate the operating excitation frequency from the natural frequency of the machine.
As a consequence of these findings, the machine operators temporarily reduced the rotational speed of the eccentric masses to move the excitation frequency away from

the critical frequency range identified experimentally. However, this solution inevitably reduces the achievable production capacity.
At the time of writing this thesis, the machine still operates under these reduced-speed conditions. The operators have maintained this precautionary operating strategy while further investigations continue to identify and validate structural modifications capable of providing a definitive solution to the observed resonance phenomenon.

Chapter 4

Development of Numerical Model

This chapter describes the development of the Finite Element models adopted throughout the thesis and the methodology followed to reproduce the dynamic behavior of the investigated machine. The chapter progressively presents the modeling process, discussing the engineering assumptions, simplifications, and validation strategy adopted for both machine configurations. It focuses particularly on the representation of the non-modeled components and on the influence of the different operating and boundary conditions adopted during the experimental campaigns. The objective is to develop reliable numerical models whose predictions consistently correlate with the available experimental evidence before interpreting the structural dynamics.

4.1 Modeling Strategy and Validation Approach

The experimental investigations presented in Chapter 3 confirmed the occurrence of resonance phenomena within the operating frequency range of the vibrating dryer. However, they did not provide sufficient information to identify the corresponding mode shapes. The experimental setup relied on a single accelerometer, which prevented the simultaneous acquisition of responses at multiple locations. As a result, the investigation could not completely identify the modal properties, and the experimental data alone could not fully explain the dynamic behavior responsible for the observed fatigue damage.
For this reason, this work adopts a Finite Element modeling approach. The numerical model aims not only to reproduce the experimentally identified natural frequencies but also to identify the corresponding mode shapes. This additional information provides a deeper understanding of the structural mechanisms governing resonance

and fatigue crack initiation.
The computational model follows a progressive validation strategy based on an iterative correlation between numerical predictions and experimental evidence. The modeling procedure first identifies the structural features expected to dominate the global dynamic behavior of the system. It then introduces engineering assumptions and simplifications to achieve a suitable balance between model fidelity and computational efficiency.
In particular, the model development process uses the natural frequencies identified through the bump tests as reference values. The model progressively refines its parameters, assumptions, and simplifications until the numerical results satisfactorily agree with the experimental evidence. Engineering considerations guide every modeling choice and adjustment, from the physical interpretation of the structural behavior to preliminary analytical estimates.
The first stage of the work focuses on the development and validation of a numerical model representative of the original machine configuration, referred to as "Version 0". The main challenge consists of representing the components excluded from the geometric model while preserving their contribution to the overall mass, stiffness, and dynamic response of the system. After the numerical model reproduces the experimental results with satisfactory accuracy, the analysis freezes these assumptions because the excluded components remain unchanged after the structural modification.
The second stage addresses the "Version 1" configuration. At this stage, the analysis shifts its attention from the structural components to the processed material, whose mass was absent during the first experimental campaign.
An interesting opportunity offered by this modeling approach is the possibility of removing the material mass contribution from the "Version 0" model, allowing a direct comparison between the two structural configurations. In this way, the analysis directly assesses the actual increase in structural stiffness introduced by the modification, an outcome that the experimental campaign alone could not provide.
Another aspect that strengthens the robustness of the modeling approach concerns the higher-order natural frequencies. Although the calibration process primarily relies on the first experimentally identified natural frequency, the numerical model should also reproduce the subsequent natural frequencies. Consequently, the analysis does not use the second natural frequency of "Version 0" as an independent calibration target, but, instead uses this frequency as an additional validation parameter. The ability of the model to reproduce both natural frequencies with satisfactory accuracy provides strong evidence that the adopted assumptions and simplifications

capture the actual structural behavior, thereby increasing the overall reliability of the FE model and its suitability for subsequent predictive analyses.
Finally, the validated numerical models serve as a tool to identify modal shapes associated with natural frequencies for analyzing structural weaknesses responsible for resonance phenomena.

4.2 Geometry and Boundary Conditions

4.2.1 Geometry idealization

The development of a reliable computational model requires a preliminary idealization of the real system. The primary objective of the numerical analysis is the investigation of the structural portion of the machine where fatigue cracks appeared. Although the vibrating dryer consists of several interconnected components, the Finite Element geometry explicitly includes only the portion of the structure that provides the main contribution to the global stiffness of the vibrating assembly.

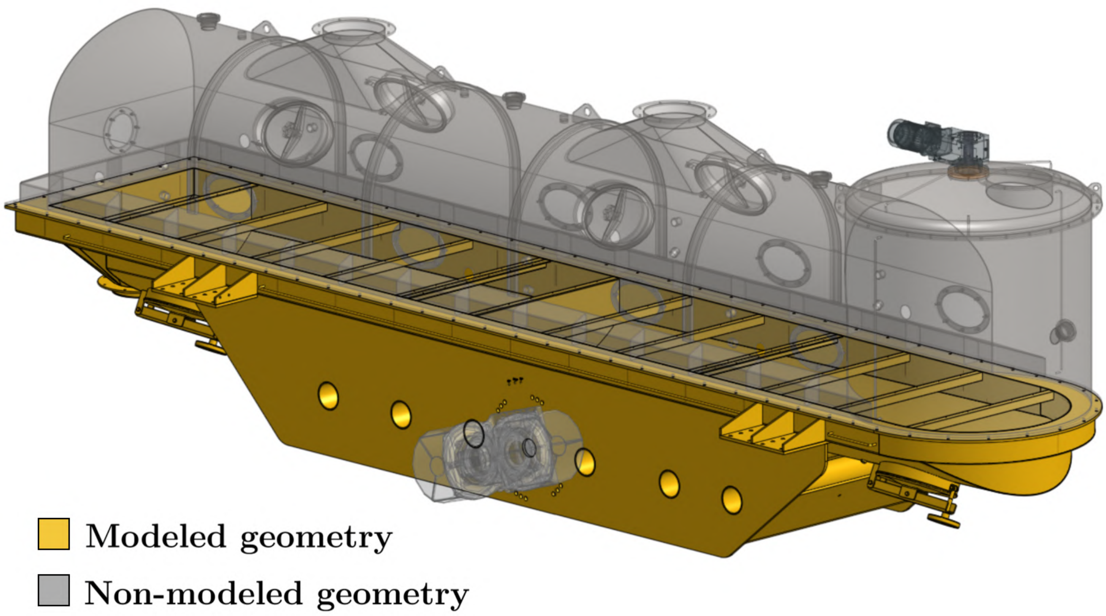

Figure 4.1: *Distinction between modeled and non-modeled portions*

Thin metal sheets and the motovibrators contribute negligibly to the global structural stiffness compared with the modeled supporting structure. Consequently, the model does not represent these components explicitly. Instead, equivalent mass

representations preserve their contribution to the overall mass distribution while avoiding unnecessary geometric complexity. This modeling choice is not merely computationally convenient; it reflects the engineering objective of retaining only the physical features that govern the global dynamic response while eliminating unnecessary numerical complexity.
Fig. 4.1 represents the modeling philosophy adopted for the dryer structure in "Version 0", but the same approach holds for the "Version 1" configuration. The only differences between the two models concern the structural modifications introduced on the supporting structure after the first experimental campaign and, subsequently, the representation of the processed material, as previously stated introduced only for "Version 1".

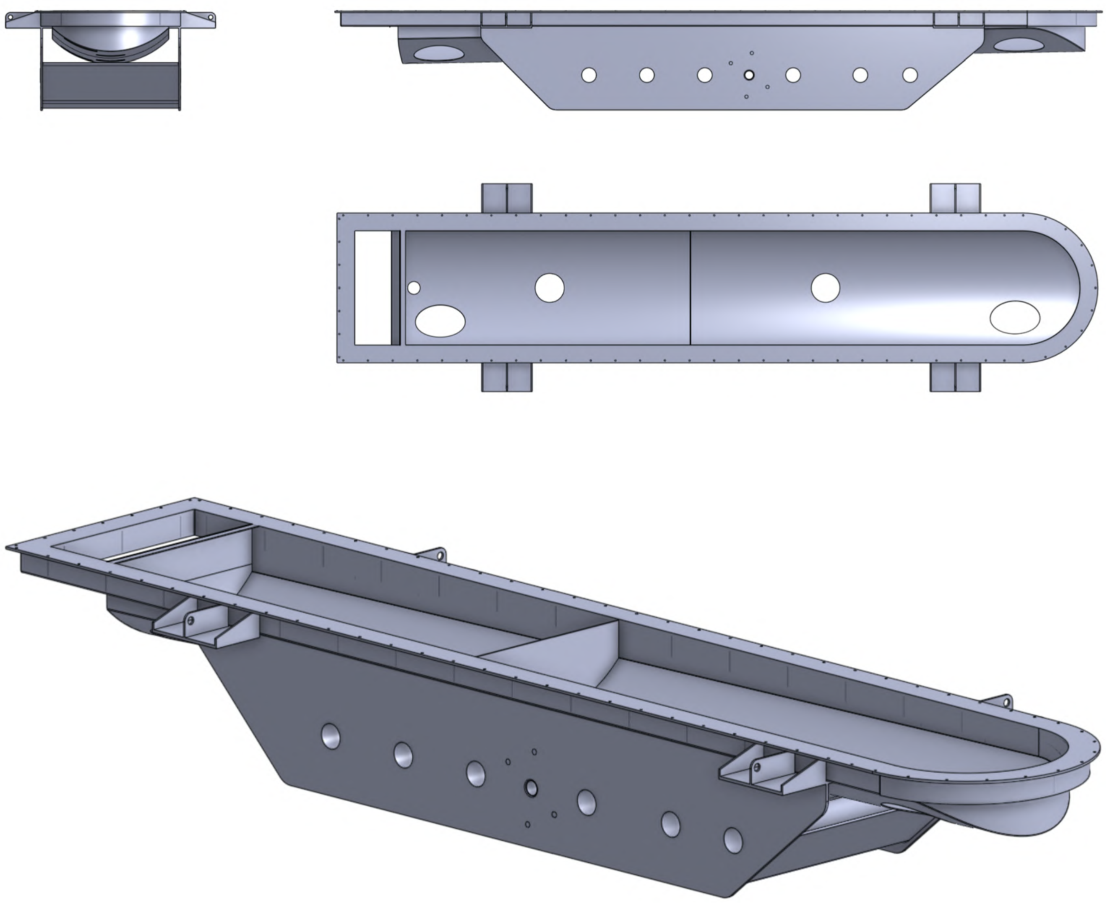

Figure 4.2: *Simplified geometry of the vibrating assembly adopted for the Finite Element model of "Version 0"*

The model further simplifies the geometry by removing local details that do not influence the global modal response, such as small holes, flanges, doors, and minor manufacturing features. These features would require local mesh refinements and significantly increase the computational effort. Their removal improves computational efficiency while preserving the accuracy required to reproduce the global dynamic behavior.

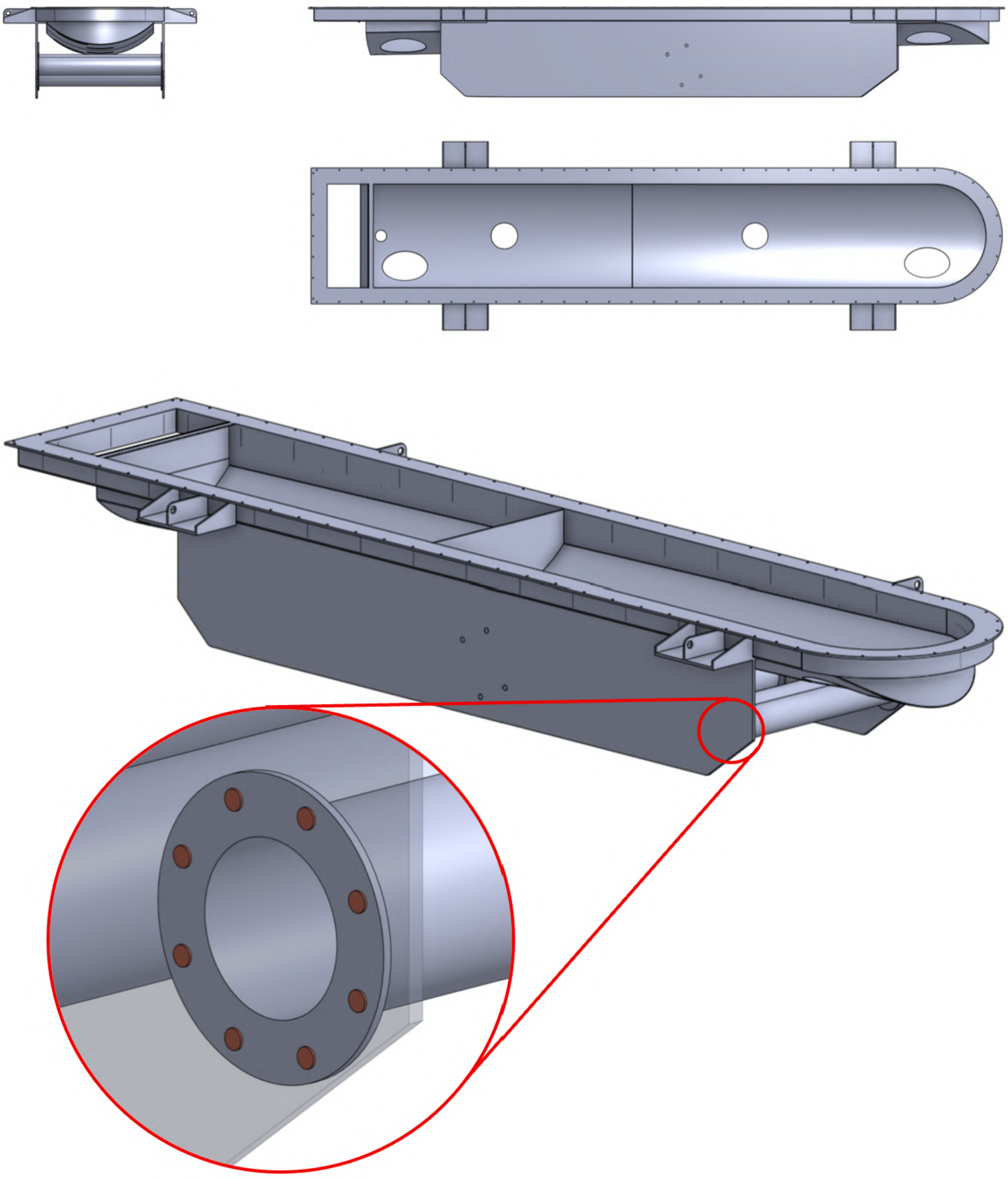

Figure 4.3: *Simplified geometry of the vibrating assembly adopted for the Finite Element model of "Version 1"; focusing lens on bolts modeling*

The representation of the bolted connections introduced in "Version 1" requires particular attention. Unlike the "Version 0" configuration, which connected the transverse tubular members to the longitudinal plates through continuous welds,

the "Version 1" structure relies on larger tubular members assembled with bolted joints. The model intentionally avoids representing the bolted assemblies through multiple bonded contacts because this approach artificially constrains the relative deformation of the connected plates and introduces fictitious stiffness that alters the computed modal response.
Instead, the model represents each bolt as a simplified cylindrical solid that connects the assembled components only at the actual fastening locations, as shown in Fig. 4.3. This strategy preserves the compliance of the real joint while keeping the model computationally efficient.
The geometric simplifications introduced during the idealization process inevitably modify the total mass of the modeled assembly. The modeling process intentionally removes several secondary components and local geometric details. Consequently, the actual density of structural steel no longer reproduces the nominal mass of the machine. To preserve the correct total mass, the model assigns an equivalent material density to the remaining geometry so that its overall mass matches the reference value reported in Chapter 2. This correction preserves the global inertial properties of the modeled structure while maintaining the simplified geometric representation adopted for the Finite Element Analysis.

4.2.2 Boundary conditions

The objective of the model is the identification of the natural frequencies and mode shapes of the vibrating dryer through modal analysis. Unlike conventional Finite Element structural analyses, no external loads, imposed displacements or particular boundary conditions are applied to the FE model, since the solution of the eigenvalue problem depends exclusively on the mass and stiffness distribution of the system. Consequently, the present work considers only the boundary conditions associated with the representation of the support system.
The analysis adopts different support configurations according to its specific objective. It uses free-free boundary conditions to identify and validate the structural modes, whereas it uses an equivalent spring-supported model to assess the actual degree of uncoupling provided by the vibration isolation system.
Since the stiffness of the vibration isolators is significantly lower than the structural stiffness of the vibrating assembly, they influence only the low-frequency rigid-body modes, whereas the deformable structural modes remain substantially unaffected. This assumption is consistent with common practice in experimental and numerical modal analysis, which widely adopts free-free boundary conditions to characterize

the intrinsic dynamic properties of structures independently of their support conditions.

Free-free condition

The primary objective of the analysis is to identify the natural frequencies and corresponding mode shapes of the structure, which primarily depend on its intrinsic stiffness. Consequently, the analysis performs the modal calculations under free-free boundary conditions, leaving all six degrees of freedom unconstrained.
From a theoretical standpoint, a structure analyzed under free-free conditions exhibits six rigid-body modes associated with three translational and three rotational motions, all occurring at zero frequency. These modes do not involve structural deformation and therefore do not provide information about the elastic behavior of the system. Conversely, the first deformable mode appears immediately after the six rigid-body modes and depends exclusively on the mass and stiffness distribution of the structure.

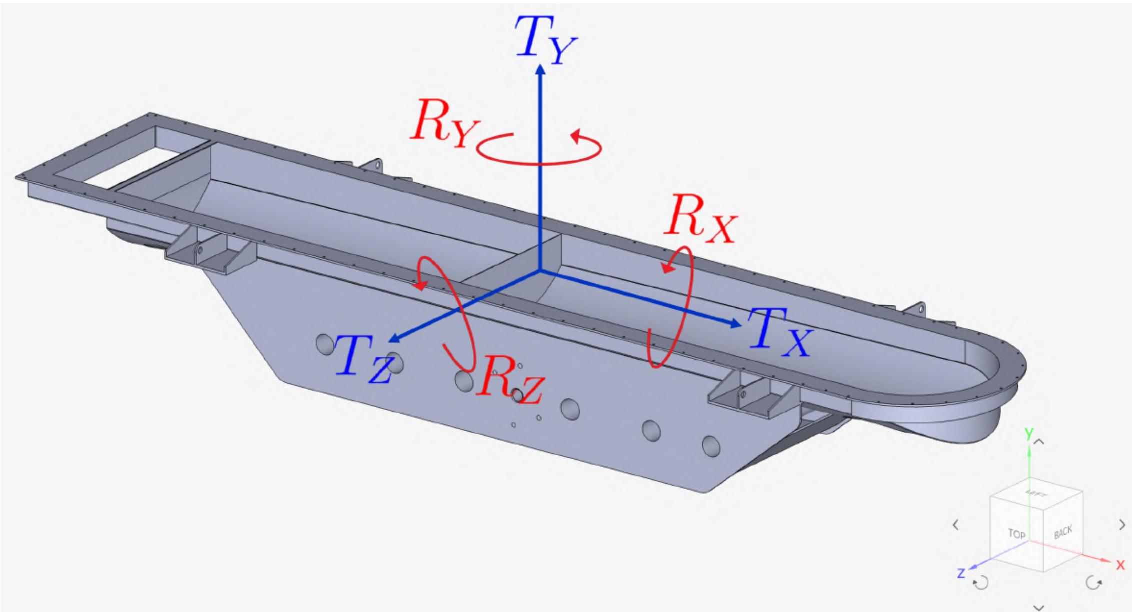

Figure 4.4: *Unconstrained Finite Element model.*
Source: author's elaboration using SimScale

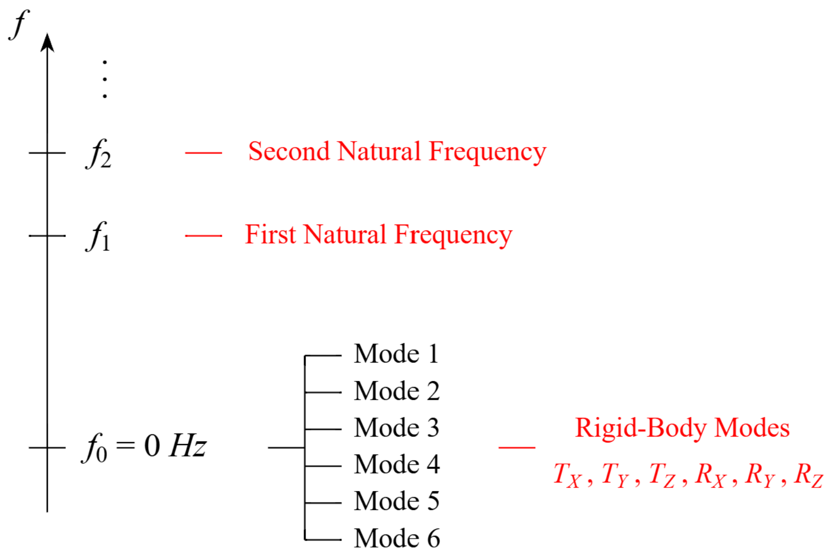

Figure 4.5: *Expected frequency sequence in free-free conditions*

Free-free boundary conditions remove the influence of the vibration isolators from the modal identification process. As a result, the analysis directly correlates the experimentally identified natural frequencies with the structural properties of the vibrating assembly. This approach considerably simplifies the interpretation of the results and provides a robust basis for validating the Finite Elements model.

Springs bed condition

In this case, equivalent linear springs located at the actual support positions represent the vibration isolators and reproduce the elastic interaction between the vibrating assembly and the supporting frame. The assigned stiffness values correspond to the characteristics of the installed vibration isolators reported in Tab. 2.3. This representation preserves the actual compliance of the suspension system and accurately captures its influence on the global dynamic response. At the same time, it avoids unnecessary geometric modeling and therefore limits the computational effort.
Unlike the free-free analysis, the presence of the elastic supports removes the rigid-body singularity of the system. The first six modes no longer correspond to null value of frequency, but become low-frequency rigid oscillation modes governed by the overall mass of the machine and the stiffness of the suspension system.

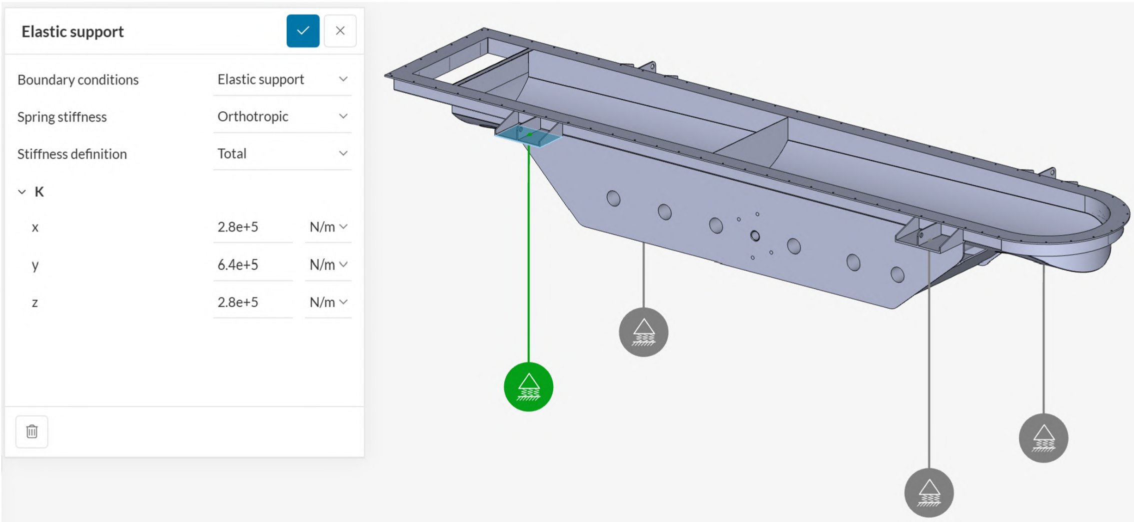

Figure 4.6: *Constrained Finite Element model by elastic supports. Source: author's elaboration using SimScale*

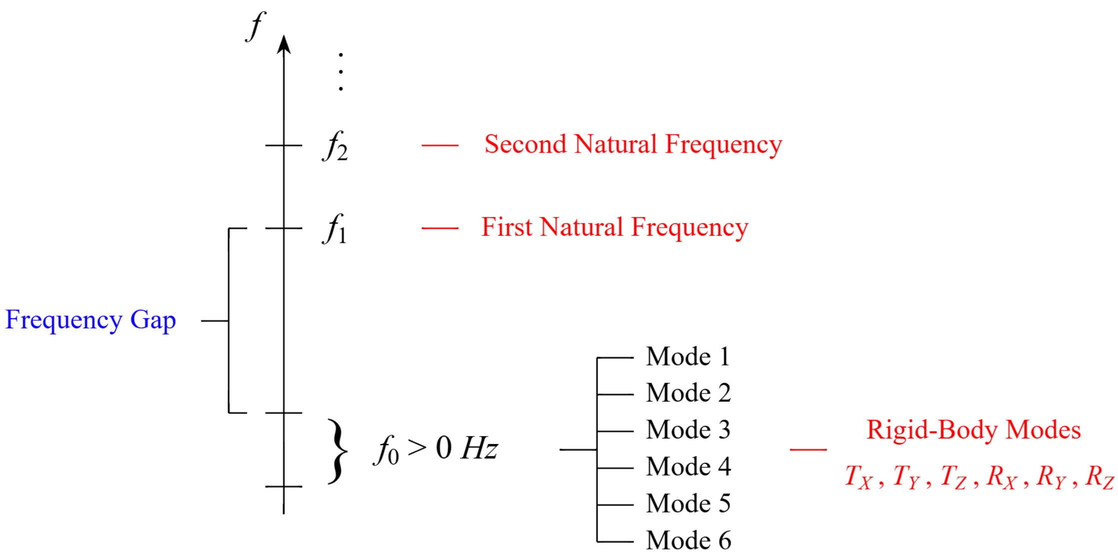

Figure 4.7: *Expected frequency sequence in constrained conditions*

The spring-supported model addresses two main objectives. The first is to verify that the rigid-body modes of the suspended system lie within the theoretical frequency range predicted by the analytical design of the vibration isolation system. The second is to assess the frequency separation between the suspension modes and the first deformable structural mode, providing an indication of whether the free-free assumption adopted for the model validation is appropriate.

4.3 Element Formulation Parameters

In order to compute the solution for a given simulation, the simulation domain needs to undergo a discretization process. Essentially, it means splitting up one large problem into multiple smaller mathematical problems.

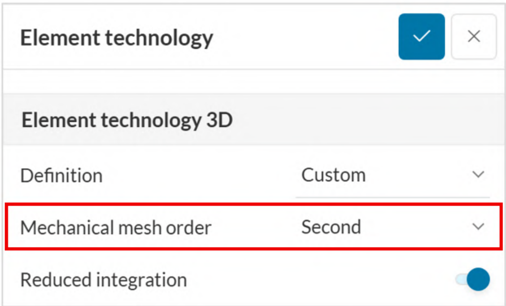

Figure 4.8: *Element technology.*
Source: author's elaboration using SimScale

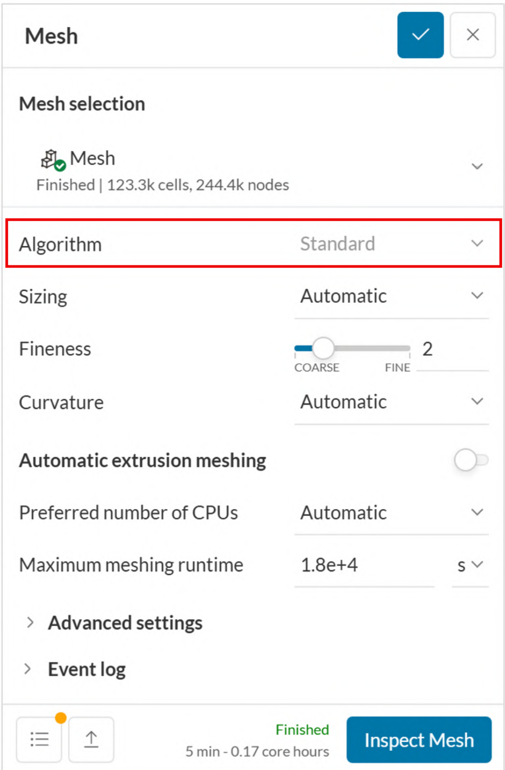

Figure 4.9: *Meshing algorithm.*
Source: author's elaboration using SimScale

The element formulation adopted throughout the present work follows the guidelines provided in the SimScale documentation. In particular, the modal analysis uses

second-order solid elements, consistently with the element order suggested by the software for this analysis type, as reported in "*Table 1: Mesh order automatically assigned depending on the Analysis Type and global settings*" [15].
The software generates the mesh using the *Standard meshing algorithm* recommended by SimScale for complex three-dimensional geometries. This algorithm produces an unstructured volume mesh based on tetrahedral elements, optimizing the automatic discretization of geometries characterized by curved surfaces, variable thicknesses, and multiple intersecting structural members without requiring extensive manual partitioning of the model. The adopted meshing strategy provides a robust and computationally efficient representation of the investigated structure while preserving the geometric fidelity required for the modal analysis [19].
The numerical model intentionally adopts a relatively coarse mesh, consistently with its objectives, for two main reasons. First, the investigation focuses exclusively on identifying the global structural dynamics of the vibrating assembly through modal analysis rather than on evaluating local stress concentrations. Consequently, the model does not require local mesh refinement around geometric discontinuities, such as holes or regions with small radii of curvature, where steep stress gradients would otherwise justify a finer discretization. Second, the analyses focus on the first structural modes of the system. These modes involve smooth global deformations, allowing the model to reproduce them accurately even with relatively large finite elements.

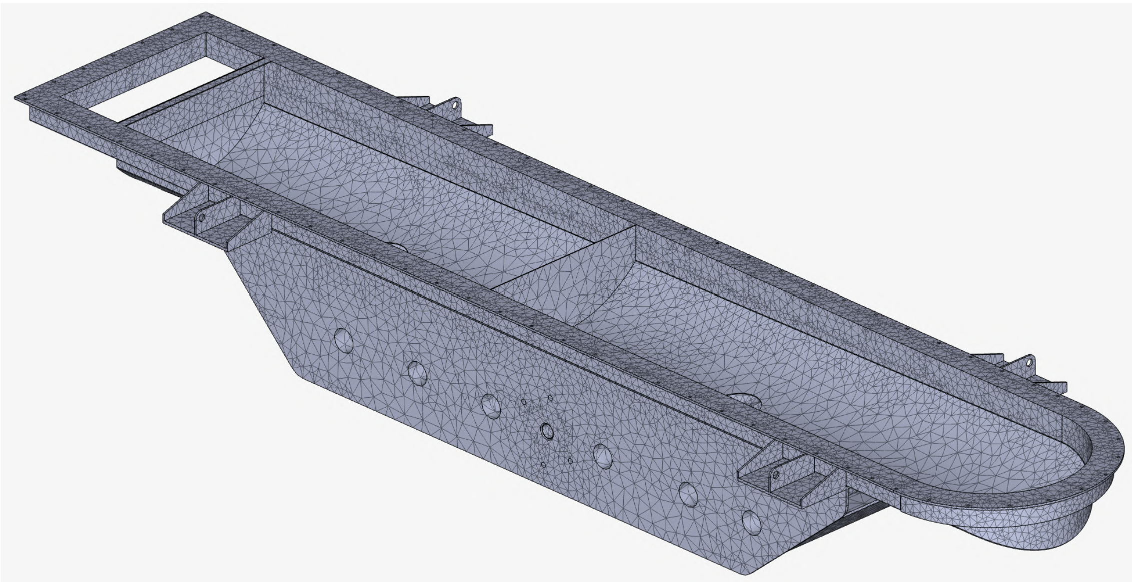

Figure 4.10: *Computed mesh.*
Source: author's elaboration using SimScale

Fig. 4.10 shows the adopted mesh, which provides an appropriate compromise between computational efficiency and numerical accuracy. The selected mesh accurately reproduces the first global structural modes without introducing significant artificial stiffness.
Fig. 4.10 shows the "Version 0" machine case, but the same mesh setup holds for "Version 1".

4.4 "*Version 0*": Modeling and Validation

4.4.1 Objectives of the modeling

Since the previous sections defined the model domain, boundary conditions, and finite element parameters, this chapter focuses on representing the upper portion of the vibrating assembly and the motovibrators excluded from the model geometry. The omitted portion accounts for a significant fraction of the total machine mass. However, the model cannot represent it solely through an equivalent weight. Its mass distribution and the way it interacts with the modeled structure also influence the global dynamic response of the system and therefore require appropriate representation.
To account for these effects, the model follows an iterative development procedure guided by engineering considerations and by the physical behavior of the excluded components. At each stage, the study introduces a specific assumption and evaluates its influence on the predicted modal response. The observations obtained from each analysis guide the subsequent refinement of the equivalent representation, progressively improving the agreement between the numerical predictions and the experimental results presented in Chapter 3.
The adopted procedure does not rely on empirical trial-and-error calibration. Instead, each refinement step investigates a specific hypothesis regarding the flexibility and mass distribution of the non-modeled assembly. Engineering reasoning, supported by numerical evidence, guides every modeling decision and ultimately leads to the final equivalent representation.

4.4.2 Equivalent representation of non-modeled parts

The Finite Element geometry does not explicitly include the upper portion of the vibrating assembly or the vibrating masses. Nevertheless, the model cannot neglect their contribution to the global dynamic response because these components account for a substantial fraction of the total mass of the system and connect mechanically to the modeled structure through bolted joints.

The computational model therefore requires an equivalent representation that accounts for the inertial effects of the omitted components while preserving reasonable computational efficiency. However, the equivalent representation must reproduce not only the total mass of the excluded components but also their mass distribution and their mechanical interaction with the supporting structure. Consequently, the adopted strategy preserves the distributed dynamic effect of the omitted components on the supporting structure, rather than merely reproducing their overall inertial contribution.

The model represents the vibrating motors as single remote masses located at their respective centers of gravity and assigned the corresponding inertia tensors. Their compact, monolithic construction justifies this assumption, since it allows the analysis to reasonably neglect internal compliance.

The upper tank of the vibrating assembly requires a different representation. This component mainly consists of thin-walled stainless-steel plates with thicknesses of only a few millimeters, resulting in a relatively flexible structure whose deformation contributes to the overall dynamic behavior of the machine. Consequently, its equivalent representation plays a fundamental role in the present work, and Section 4.4.3 discusses it in detail.

The adopted Finite Element formulation allows remote masses to connect to the structural model through either an *RBE2* or an *RBE3* scheme. Although both approaches allow the transfer of inertial effects between the remote point and the Finite Element model, they establish different kinematic constraints. Consequently, they influence the structural stiffness in substantially different ways. Appendix B provides a detailed description of the two formulations and their theoretical background.

For the purposes of the present work, the *RBE3* formulation better represents the actual behavior of the non-modeled assembly. This choice is consistent with the thin-walled construction of the upper tank and with the objective of preserving its global flexibility while accounting for its inertial contribution. The equivalent mass model developed in the following sections therefore relies on flexible remote masses connected to the Finite Element model through *RBE3* interpolation.

4.4.3 Development of remote mass distribution

The main challenge consists in determining how to represent the mass of the non-modeled upper tank within the numerical model. Although the machine specifications readily provide the total mass, several equivalent representations are possible. The model therefore follows a progressive development procedure in which each refinement step investigates a specific physical hypothesis. The numerical results obtained at each stage guide the subsequent modeling choices, ultimately leading to the final representation adopted in the present work.

Hypothesis 1 - Single remote mass

The simplest representation consists of concentrating the entire mass of the upper tank into a single remote mass, equal to 900 kg from Tab. 2.1, located at its center of gravity.

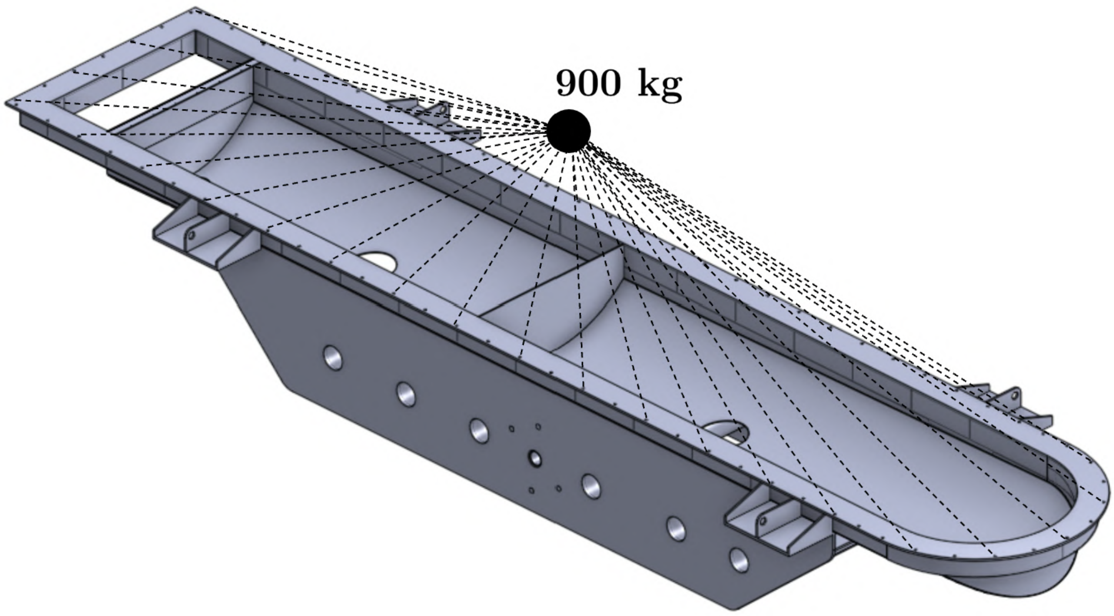

Figure 4.11: *Representation of the non-modeled upper tank as a single remote mass located at its center of gravity through RBE3 interpolation scheme*

Although an *RBE3* (deformable) interpolation scheme connects the equivalent mass to the Finite Element model, the equivalent mass itself behaves as a monolith, that is, as a single body with infinite intrinsic stiffness. Consequently, the model implicitly assumes a rigid connection between every point of the omitted assembly, thereby neglecting the internal flexibility of the upper trough.

Since this assumption is physically inconsistent with the actual thin-walled construction of the component, the resulting numerical model overestimates the global structural stiffness. Consequently, the first natural frequency predicted by the modal analysis should be higher than the experimentally identified value.
The numerical results confirm this expectation, yielding a first natural frequency of this system approximately 24 Hz, almost twice the target value of 12.5 Hz.

Hypothesis 2 - Longitudinal split of remote masses

Since the upper tank mainly extends along the longitudinal direction, the first refinement subdivides its equivalent mass into five independent longitudinal sections of equal length, as shown in Fig. 4.12.

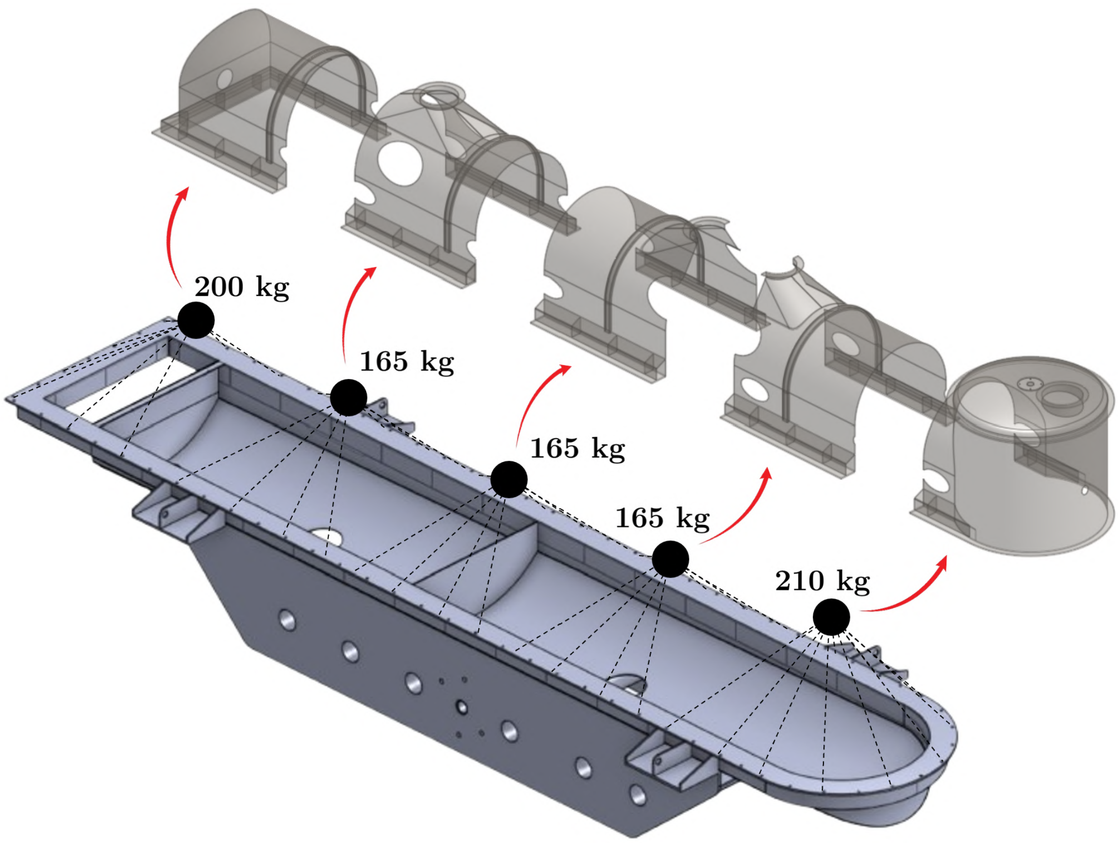

Figure 4.12: *Representation of the non-modeled upper tank as five remote masses located at their center of gravity through RBE3 interpolation scheme*

The original CAD model provides the mass properties of each section, including its mass and inertia tensor. These properties are then assigned to independent remote masses. Each remote mass connects independently to the corresponding influence area of the Finite Element model, allowing relative motion between adjacent sections

and introducing a first approximation of the longitudinal flexibility. This approach preserves the actual mass distribution of the omitted assembly while providing a more realistic representation of its dynamic behavior.
The overall stiffness of the numerical model should decrease with respect to the previous hypothesis, leading to a reduction of the first natural frequency and improving the agreement with the experimental results.
The predicted first natural frequency reduces from 24 Hz to approximately 15 Hz, representing a significant improvement with respect to the single remote mass representation. This result demonstrates that the longitudinal compliance of the upper tank plays a fundamental role in the global dynamics of the dryer assembly.

Hypothesis 3 - Further longitudinal split of remote masses

Although the five independent longitudinal remote masses significantly improve the agreement with the experimental results, the model still exhibits a residual discrepancy with respect to the target natural frequency. At this stage, it is necessary to determine whether this discrepancy originates from an insufficient longitudinal discretization or from a different aspect of the equivalent representation.
To investigate this aspect, the model further increases the number of longitudinal segments from five to nine while preserving the same modeling approach. If the previous discretization still failed to represent the longitudinal flexibility adequately, this refinement would further reduce the predicted natural frequency. Conversely, a negligible variation would indicate that the previous discretization already captures the longitudinal flexibility with sufficient accuracy and that other features of the equivalent model are responsible for the remaining discrepancy.
Since the modal analysis shows that the additional longitudinal subdivision produces only a marginal variation of the first natural frequency, the five-segment representation is considered to provide an adequate description of the longitudinal flexibility, and therefore the focus moves in the transverse direction.

Hypothesis 4 - Introduction of transverse split of remote masses

Since further refinement along the longitudinal direction produces only negligible improvements, the remaining discrepancy with the experimental results suggests that the model must also represent the transverse flexibility of the upper trough. To account for this effect, the model subdivides each longitudinal segment into two independent remote masses, resulting in a total of ten equivalent masses distributed over the geometric domain of the omitted component, as shown in Fig. 4.13.

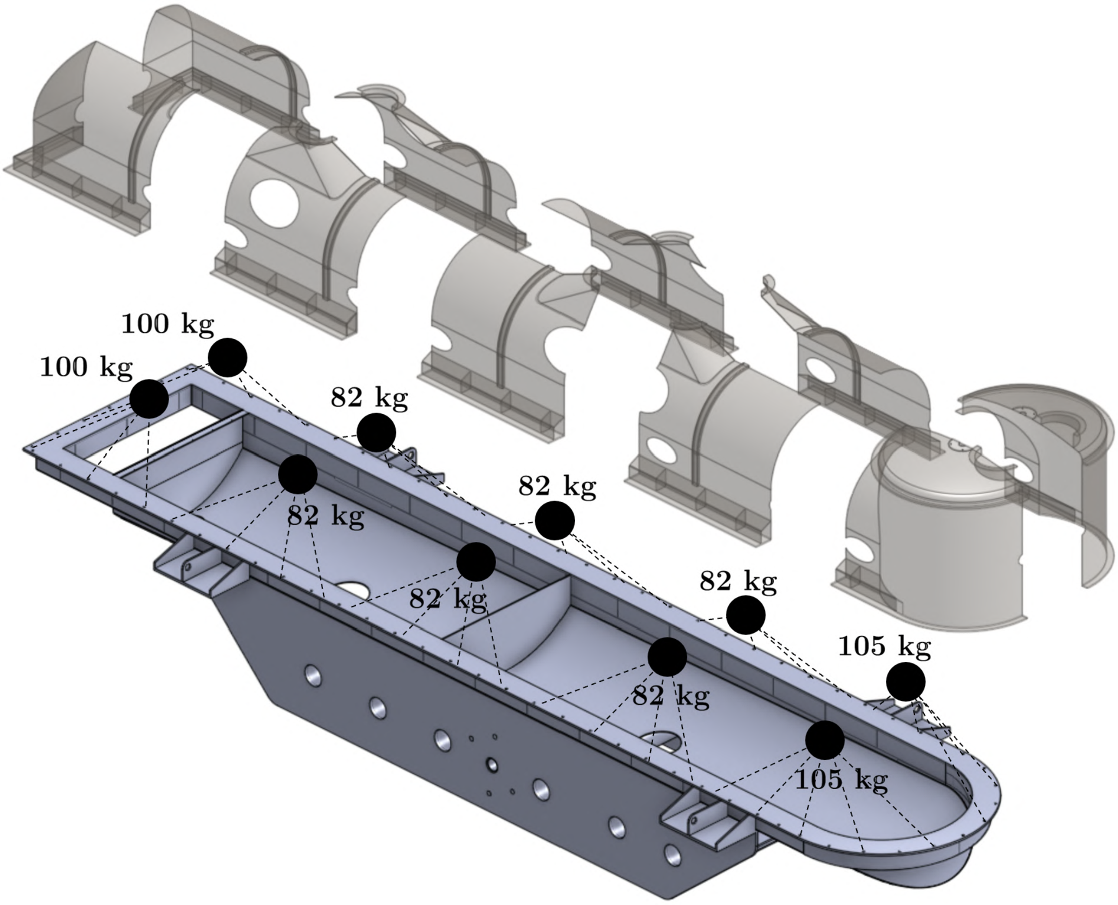

Figure 4.13: *Representation of the non-modeled upper tank as five remote masses located at their center of gravity through RBE3 interpolation scheme*

The model connects each remote mass to the Finite Element model through a "Deformable" scheme. It does not establish kinematic constraints among adjacent masses. Consequently, the adopted representation preserves the distributed flexibility of the non-modeled component while properly accounting for its inertial contribution.

From a physical standpoint, the transverse subdivision should further reduce the equivalent stiffness of the non-modeled assembly. It allows relative motion not only along the longitudinal direction but also across the width of the upper tank.

As expected, the final equivalent representation predicts a first natural frequency of approximately 12.4 Hz, in excellent agreement with the value identified during the experimental characterization. This result demonstrates that the adopted mass distribution reliably reproduces the dynamics of the system.

Although the first natural frequency represents the primary validation parameter adopted during the model development process, the modal analysis also shows a second natural frequency, which is strongly relatable to the one identified through

the bump test. Chapter 5 discusses this result, but provides feedback about the robustness of the modeling.
The following section describes the complete setup of the "Version 0" numerical model, including the equivalent representation of the upper trough and the vibrating motors.
The present configuration constitutes the final reference model adopted for all subsequent analyses. Furthermore, since the upper tank remains unchanged after the structural modifications, the equivalent representation and its experimental validation remain fully applicable to the simulation model of the machine in "Version 1".

4.4.4 Final model setup

Once the equivalent representation of the non-modeled components has reached its final form, the analysis defines the final numerical model of "Version 0". The previous sections have already described the geometric domain, element type, and mesh generation strategy. This section therefore presents the final implementation of the model, including the adopted material properties, the equivalent remote masses, and the simulation parameters used for the modal analysis.

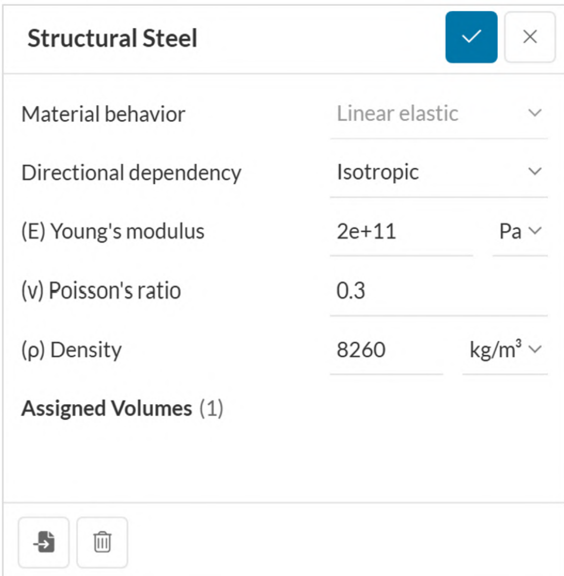

Figure 4.14: *Structural steel properties assigned to the model.*
Source: author's elaboration using SimScale

The model represents the structure as linear elastic isotropic steel. Figure 4.14 summarizes the adopted material properties. As discussed previously, the model assigns an equivalent density to compensate for the geometric simplifications introduced during the idealization process, thereby ensuring that the total mass of the Finite Element model matches the nominal value of 1750 kg. The original CAD model provides the inertia properties of each omitted component, which are then assigned to the corresponding remote masses.

As already discussed, the final model represents the upper tank through multiple distributed remote masses. This representation preserves not only the inertial contribution of the omitted assembly but also its distributed flexibility, allowing the Finite Element model to capture its influence on the global vibration behavior while minimizing computational effort. Remote masses model the motors and the upper trough and connect to the Finite Element model through "Deformable" behavior. The following figures show the implementation of these masses into the SimScale simulation setup.

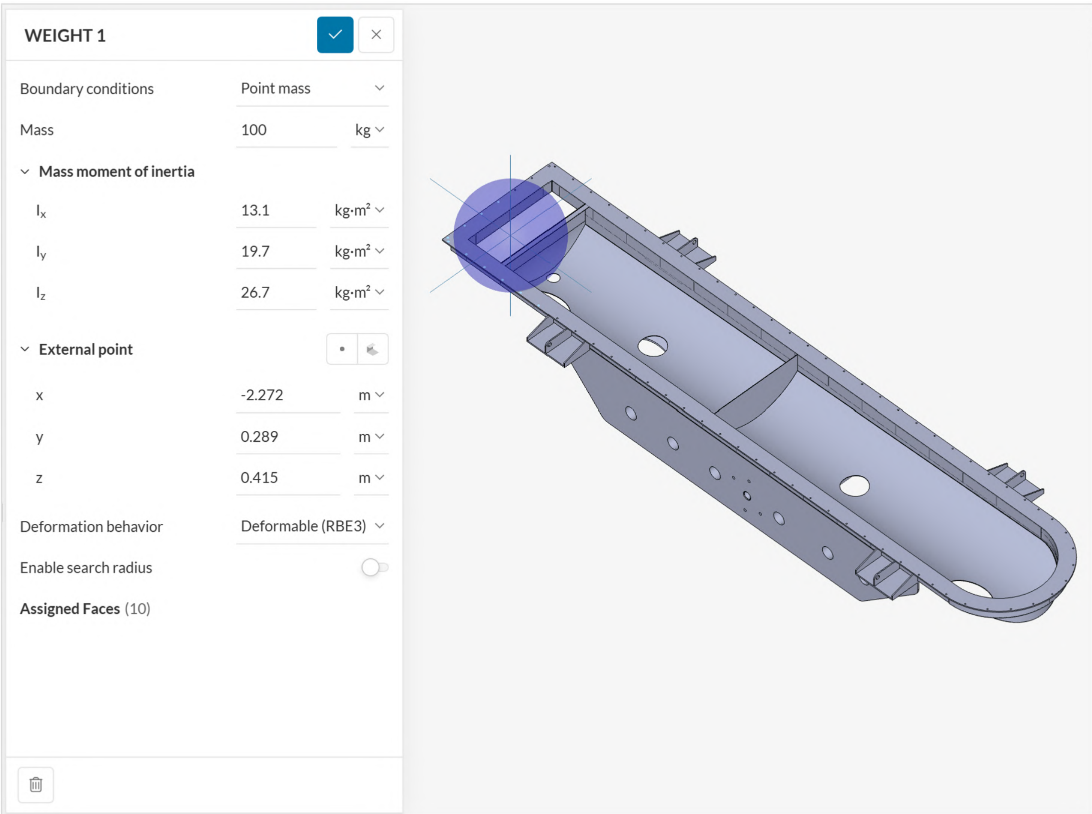

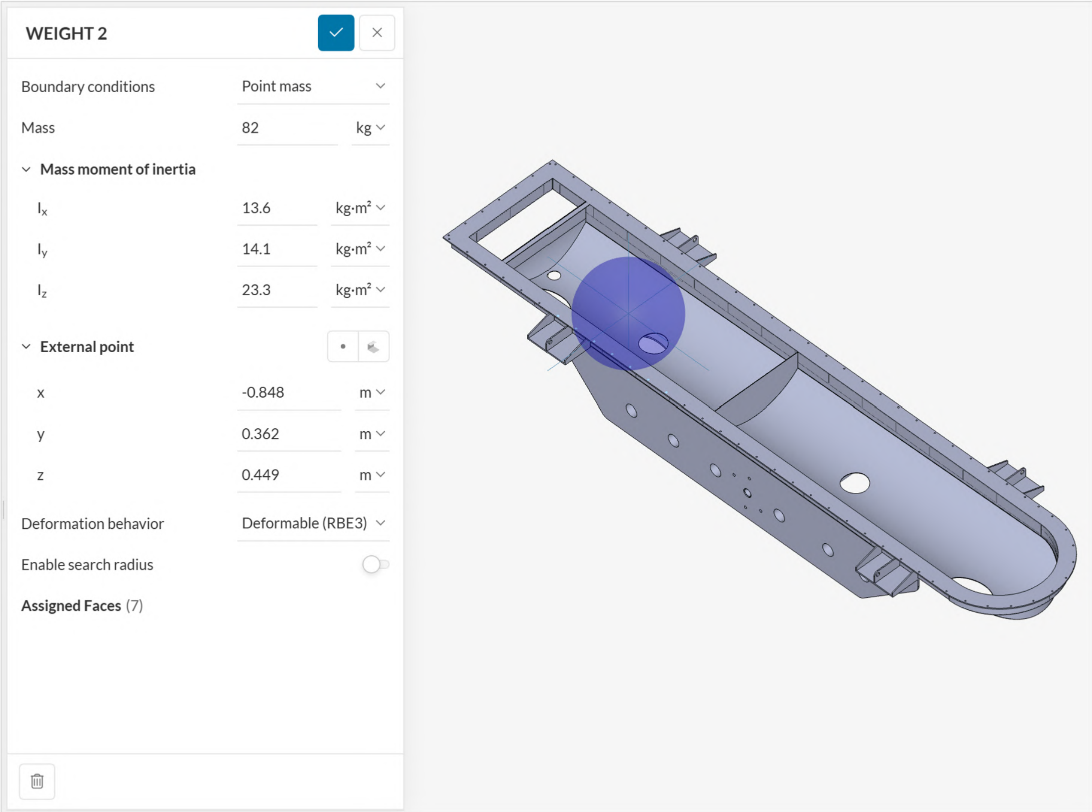
WEIGHT 2
Boundary conditions
Point mass
Mass
82
kg
Mass moment of inertia
Ix
13.6
kg·m²
Iy
14.1
kg·m²
Iz
23.3
kg·m²
External point
x
-0.848
m
y
0.362
m
z
0.449
m
Deformation behavior
Deformable (RBE3)
Enable search radius
Assigned Faces (7)

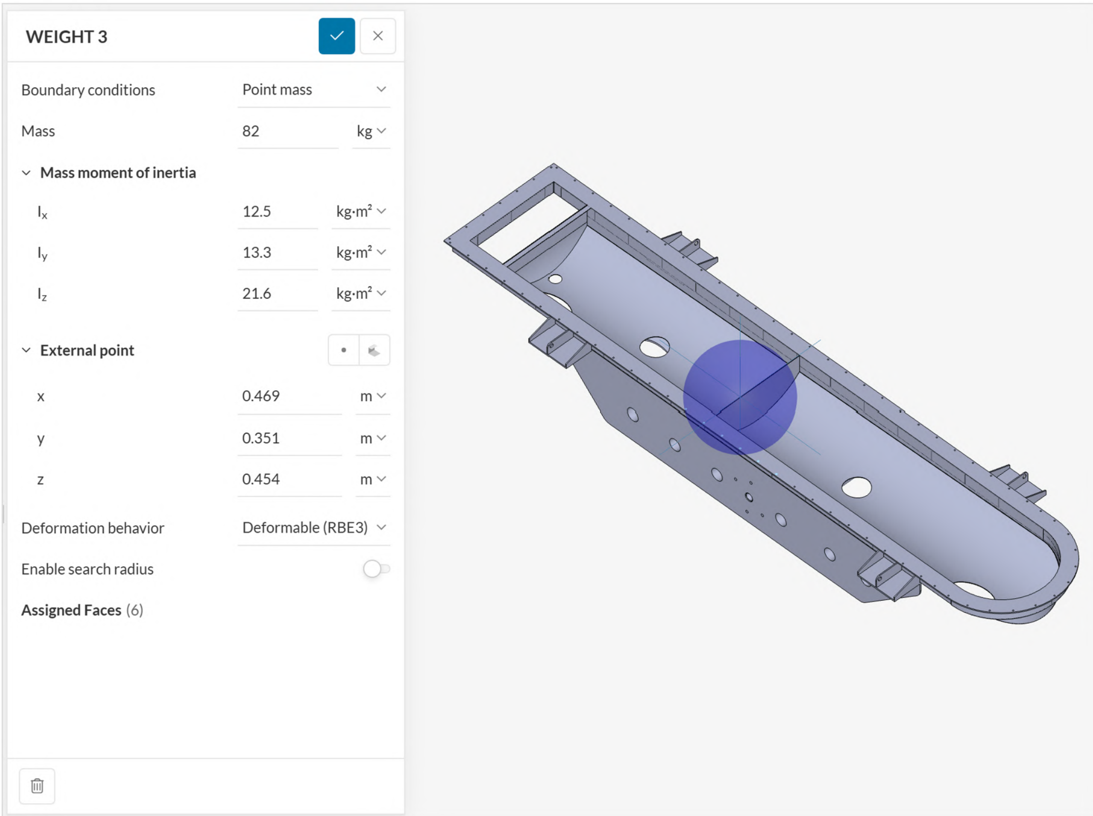
WEIGHT 3
Boundary conditions
Point mass
Mass
82
kg
Mass moment of inertia
Ix
12.5
kg·m²
Iy
13.3
kg·m²
Iz
21.6
kg·m²
External point
x
0.469
m
y
0.351
m
z
0.454
m
Deformation behavior
Deformable (RBE3)
Enable search radius
Assigned Faces (6)

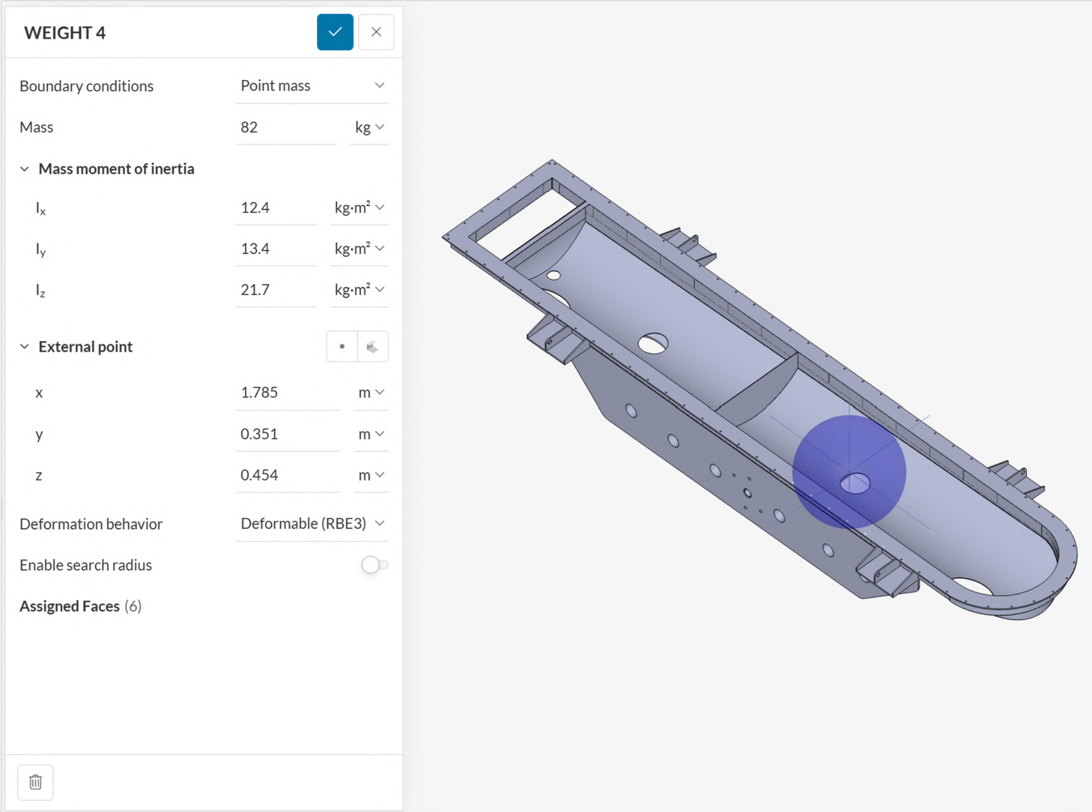
WEIGHT 4
Boundary conditions
Point mass
Mass
82
kg
Mass moment of inertia
I_x
12.4
kg·m²
I_y
13.4
kg·m²
I_z
21.7
kg·m²
External point
x
1.785
m
y
0.351
m
z
0.454
m
Deformation behavior
Deformable (RBE3)
Enable search radius
Assigned Faces (6)

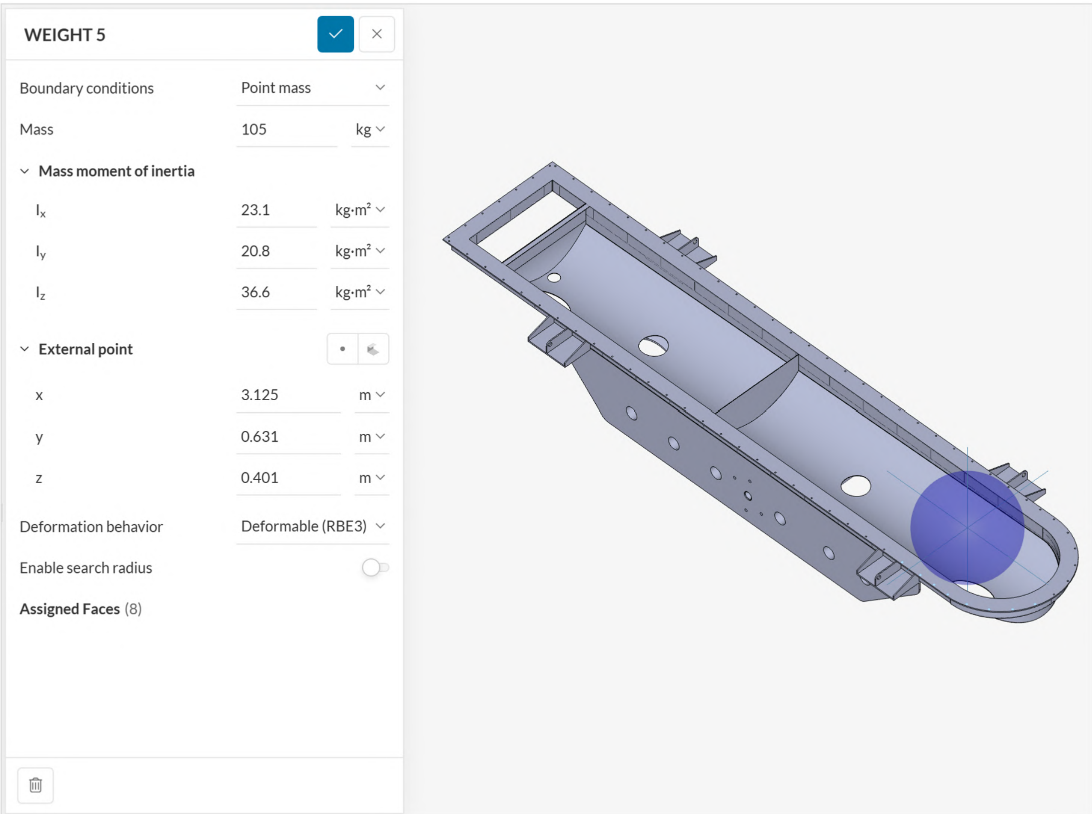
WEIGHT 5
Boundary conditions
Point mass
Mass
105
kg
Mass moment of inertia
I_x
23.1
kg·m²
I_y
20.8
kg·m²
I_z
36.6
kg·m²
External point
x
3.125
m
y
0.631
m
z
0.401
m
Deformation behavior
Deformable (RBE3)
Enable search radius
Assigned Faces (8)

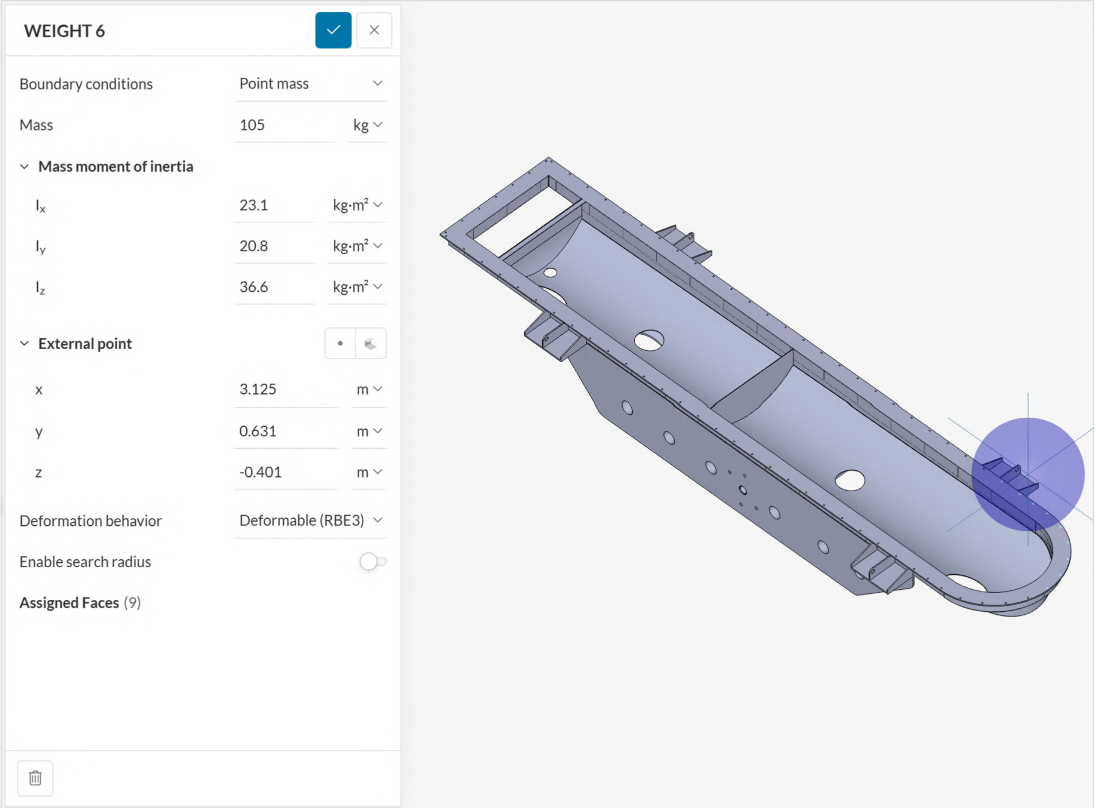
WEIGHT 6
Boundary conditions
Point mass
Mass
105
kg
Mass moment of inertia
I_x
23.1
kg·m²
I_y
20.8
kg·m²
I_z
36.6
kg·m²
External point
x
3.125
m
y
0.631
m
z
-0.401
m
Deformation behavior
Deformable (RBE3)
Enable search radius
Assigned Faces (9)

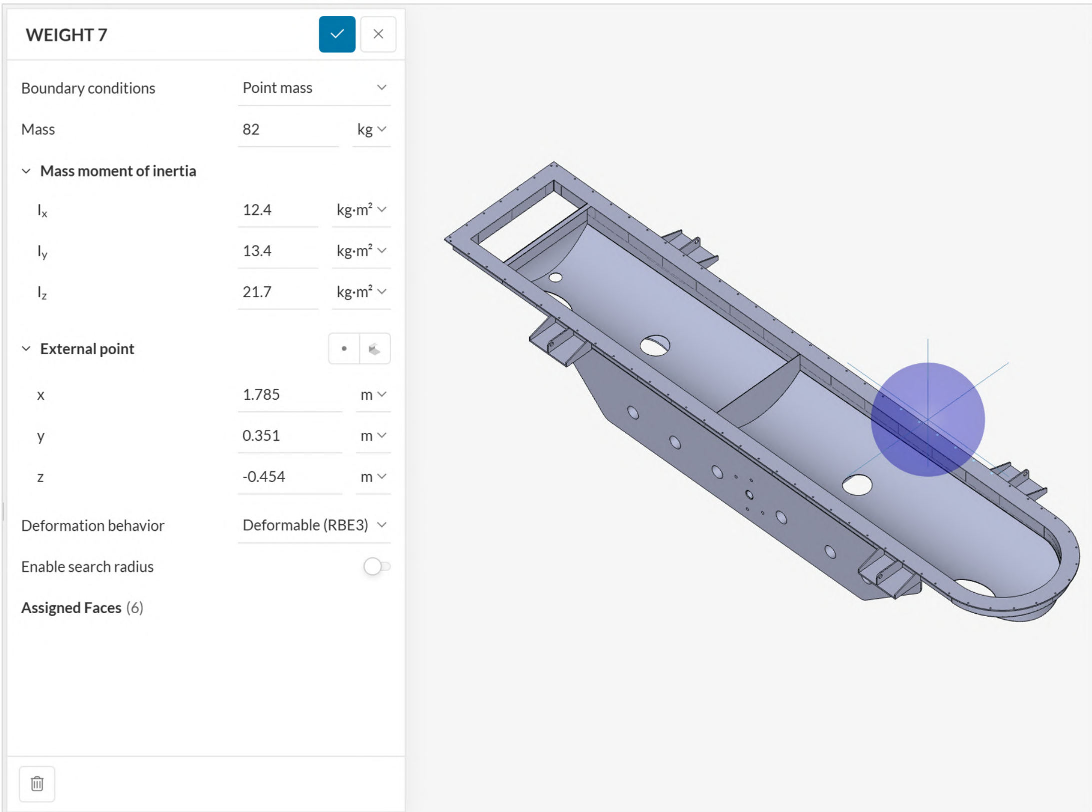
WEIGHT 7
Boundary conditions
Point mass
Mass
82
kg
Mass moment of inertia
I_x
12.4
kg·m²
I_y
13.4
kg·m²
I_z
21.7
kg·m²
External point
x
1.785
m
y
0.351
m
z
-0.454
m
Deformation behavior
Deformable (RBE3)
Enable search radius
Assigned Faces (6)

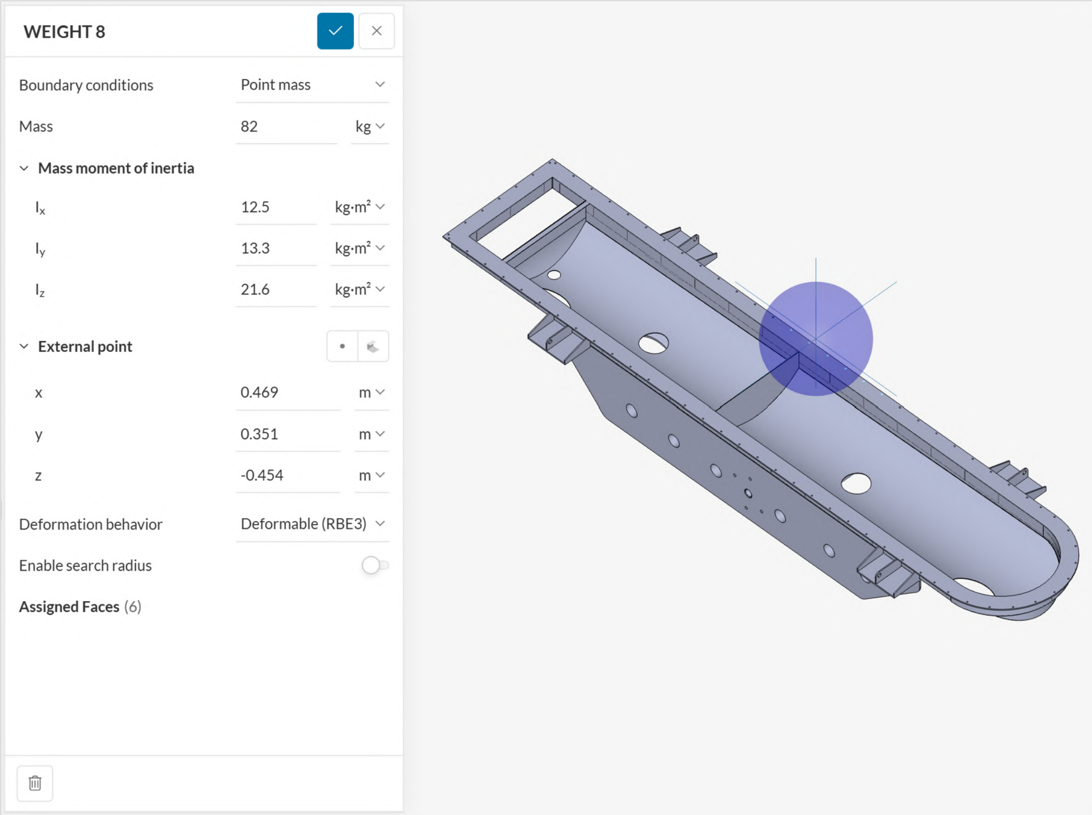
WEIGHT 8
Boundary conditions
Point mass
Mass
82
kg
Mass moment of inertia
I_x
12.5
kg·m²
I_y
13.3
kg·m²
I_z
21.6
kg·m²
External point
x
0.469
m
y
0.351
m
z
-0.454
m
Deformation behavior
Deformable (RBE3)
Enable search radius
Assigned Faces (6)

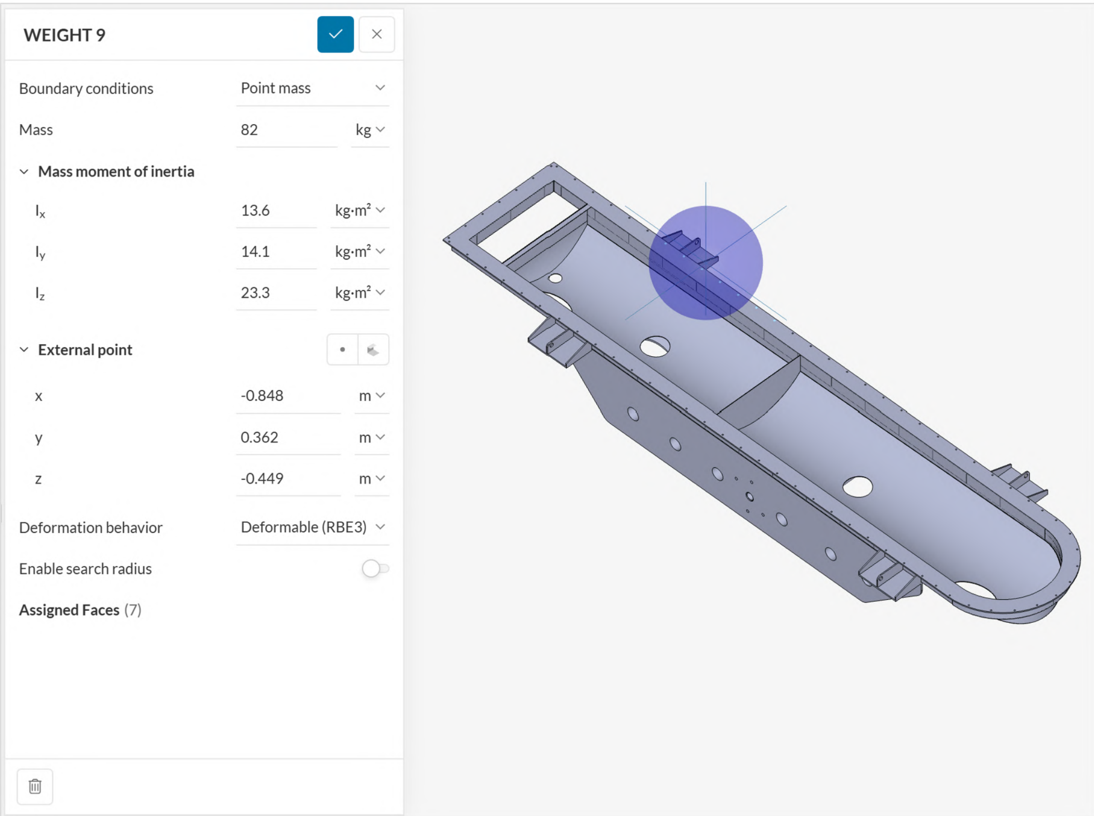
WEIGHT 9
Boundary conditions
Point mass
Mass
82
kg
Mass moment of inertia
I_x
13.6
kg·m²
I_y
14.1
kg·m²
I_z
23.3
kg·m²
External point
x
-0.848
m
y
0.362
m
z
-0.449
m
Deformation behavior
Deformable (RBE3)
Enable search radius
Assigned Faces (7)

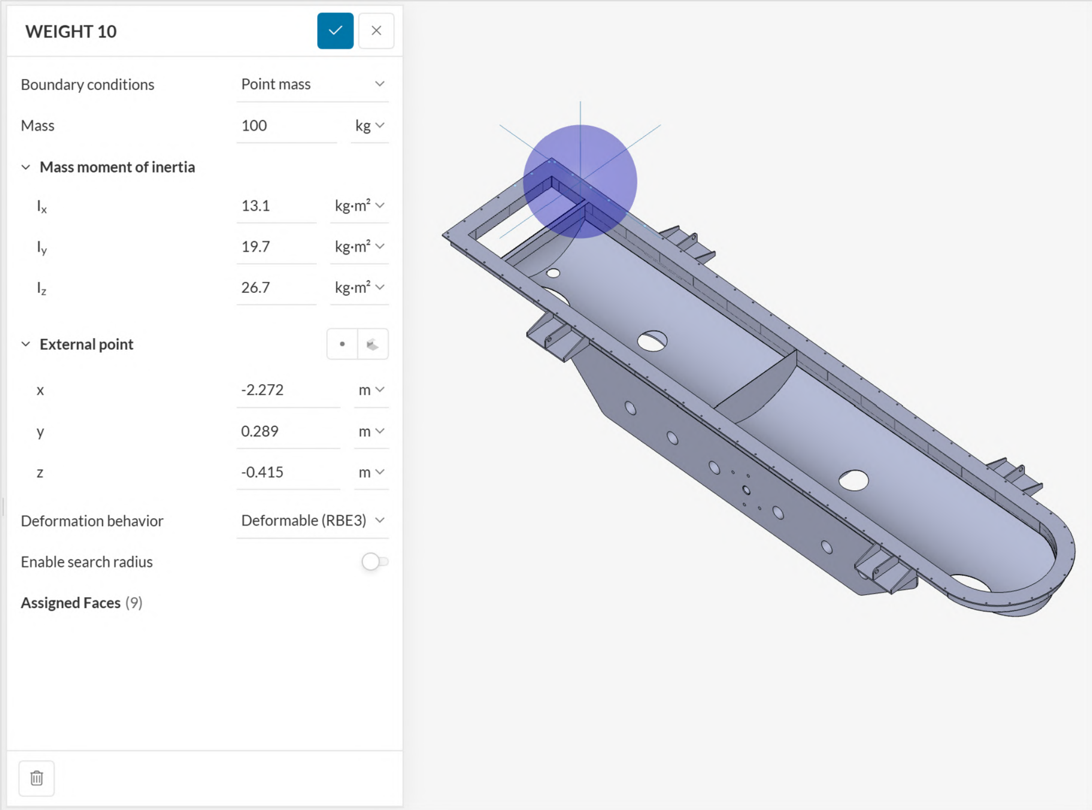

Figure 4.15: *Remote masses setup for upper trough representation. Source: author's elaboration using SimScale*

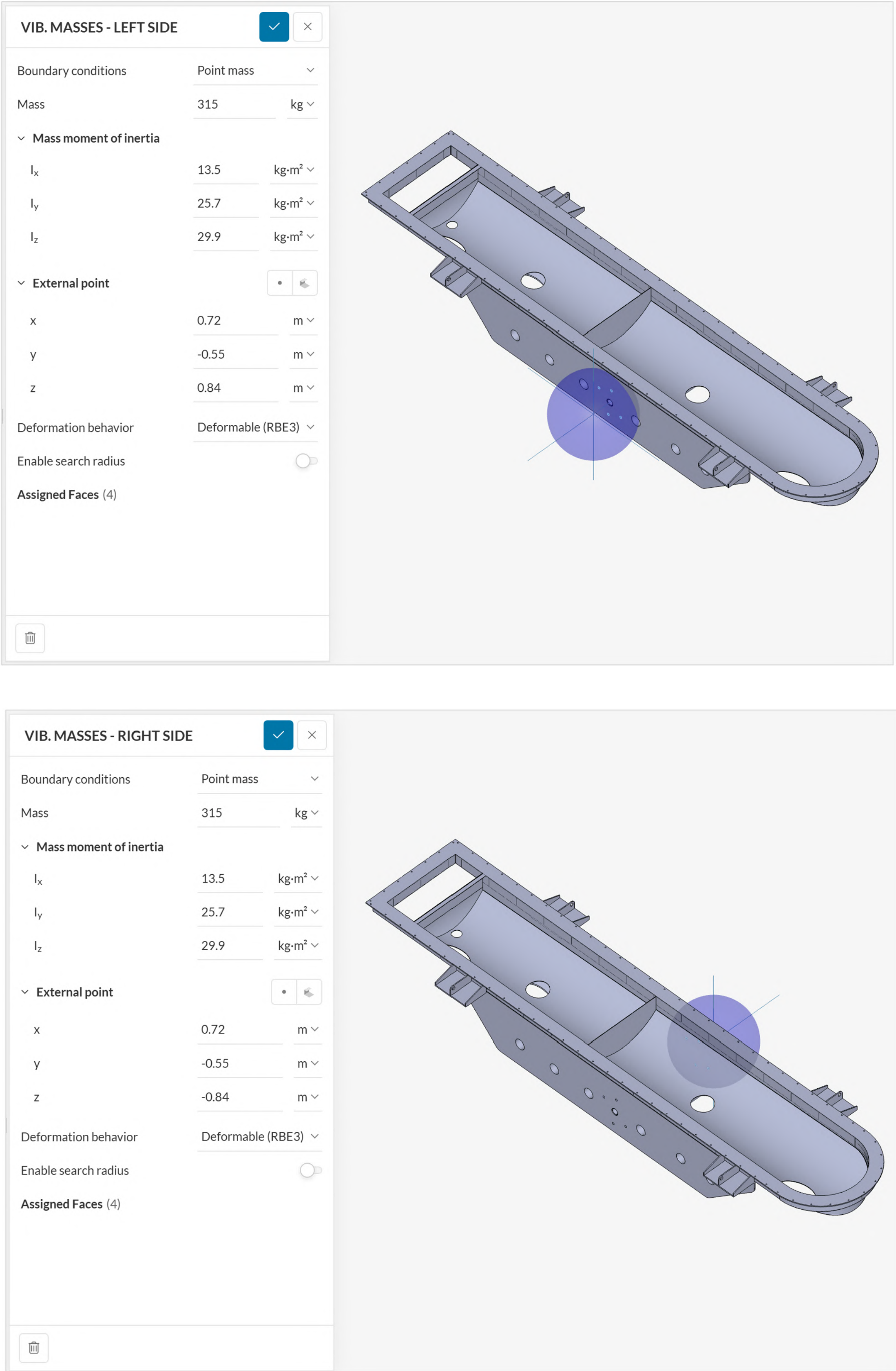

Figure 4.16: *Remote masses setup for motovibrators.*
Source: author's elaboration using SimScale

The modal analysis extracts the natural frequencies within the range from 0 Hz to 40 Hz. The analysis selects the upper limit on the basis of the experimental modal characterization, which identified the second natural frequency at approximately 32 Hz. This range allows the model to capture the two relevant structural modes while avoiding the unnecessary computational effort associated with higher-frequency modes. The setup intentionally sets the lower bound to 0 Hz to include the six rigid-body modes associated with the adopted free-free boundary conditions.

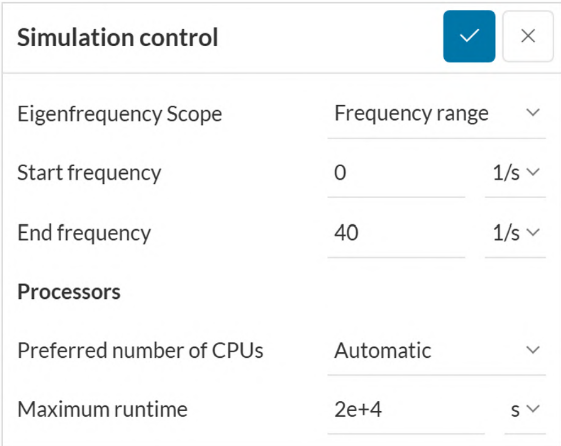

Figure 4.17: *Simulation control setup.*
Source: author's elaboration using SimScale

4.5 ”*Version 1*”: Modeling and Validation

4.5.1 Objectives of the modeling

The development of the numerical model for ”Version 1” takes the validated ”Version 0” model as its starting point. As anticipated in the previous chapter, the upper tank does not undergo any structural modification between the two configurations. Consequently, the equivalent representation developed for the non-modeled assembly, consisting of ten remote masses distributed into five longitudinal and two transverse sections, is kept unchanged.

As for the ”Version 0” configuration, the main objective of the present modeling activity is to reproduce the dynamic response observed during the experimental bump test performed on the ”Version 1” machine. In particular, the Finite Elements model aims to reproduce the first natural frequency identified experimentally, approximately equal to 11.5 Hz.

To achieve this objective, the boundary conditions adopted in the simulation must

be consistent with the experimental setup. Besides the structural modifications, the only significant difference with respect to the first experimental campaign is the presence of approximately 1 ton of acid crystals inside the vibrating trough during the measurements. Unlike the previous model, which represented the machine without the processed material, this numerical model must explicitly account for the inertial and dynamic contribution of the processed material.
Considering the morphological characteristics of the material, its physical properties and its mechanical interaction with the vibrating structure, its equivalent representation constitutes the main modeling challenge of this work. The analysis proposes reasonable, physically motivated hypotheses and progressively verifies their reliability. In particular, the development process employs One, Two and Three-Degrees of Freedom analytical models to investigate the influence of each representation. Classical mechanics of vibration theory provides the physical interpretation of each modeling assumption before the numerical modal analyses verify its effect.

4.5.2 Equivalent representation of processed product

During operation, the organic natural acid crystals enter the dryer as a wet powder and progressively lose moisture along the machine. Therefore, the analysis treats the product as a granular medium composed of particles or particle aggregates.
During the vibratory motion, repeated detachment, impact, and friction occur between the particles and the machine plates. A complete representation of this behavior would require a non-linear dynamic model, including contact interaction and possibly time-dependent redistribution of the material inside the trough. Since such an approach would significantly increase the complexity of the numerical model, the analysis represents the product through an equivalent linear model. The objective of the proposed representation is not to reproduce the detailed motion of the individual particles, which lies beyond the scope of the present modal analysis, but rather to capture the global inertial interaction between the processed material and the vibrating structure. This objective leads to two modeling assumptions.
First, the model connects the remote masses representing the product to the Finite Element model through a deformable interpolation. This choice reflects the morphology of the processed material, whose particles can undergo relative motion instead of behaving as a rigid body.
Second, the model does not assign an inertia tensor to the product masses. An inertia tensor is meaningful only for a rigid body, in which the relative position of all particles remains fixed and a single angular velocity completely describes the

rotational motion. In the present case, however, the processed material consists of particles that can move relative to one another, making the definition of a unique inertia tensor physically inappropriate.

4.5.3 Development of product modeling

The equivalent representation of the processed material follows the same methodology adopted for the upper tank. The model investigates different assumptions, each based on a different interpretation of the mechanical interaction between the product and the vibrating structure. The numerical results obtained from each hypothesis guide the subsequent modeling choices, ultimately leading to the representation that best reproduces the experimental modal response.

Hypothesis 1 - Addition of product mass to upper tank remote masses

As concluded observing the physical behavior of the product, *RBE3* scheme and no inertia tensor are modeling requirements.
Since ten distributed remote masses already represent the upper tank, the model introduces the processed material by increasing each remote mass by 100 kg, corresponding to one-tenth of the total product mass. Consequently, each remote mass represents both the structural contribution of the upper tank and the associated fraction of processed material, whereas the assigned inertia tensor represents the upper trough only.

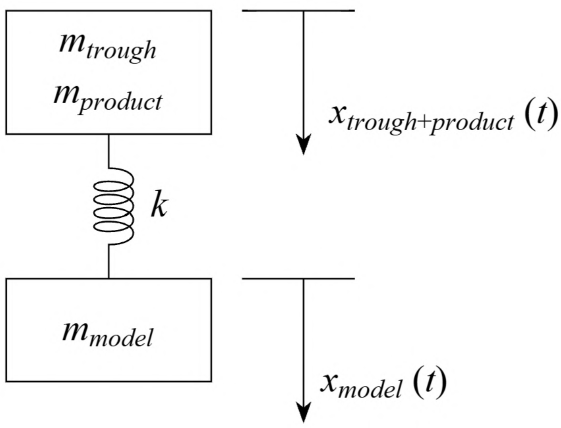

Figure 4.18: *Two-Degrees of Freedom simplified system according to "Hypothesis 1"*

This representation implicitly assumes that the product and the upper tank move together without relative motion. In other words, the two subsystems remain per-

manently kinematically coupled. From a mechanical perspective, this assumption corresponds to a simplified two-degree-of-freedom system in which the equivalent product mass is directly attached to the upper trough, as shown in Fig. 4.18.
This kinematic constraint artificially increases the global stiffness of the system and therefore overestimates the first natural frequency. The modal analysis confirms this prediction: the numerical model predicts a first natural frequency of approximately 13.5 Hz, which remains significantly higher than the experimental value of 11.5 Hz measured during the bump test.

Hypothesis 2 - Partial uncoupling between product and structure

The discrepancy observed in the previous hypothesis suggests that a fully coupled system cannot represent the interaction between the processed product and the vibrating assembly. During operation, the granular material continuously detaches from and impacts the vibrating trough, so that only a portion of the total mass effectively follows the structural motion at any given instant. This behavior introduces a partial dynamic decoupling between the product and the machine, implying that the effective participating mass is lower than the total physical mass.
To account for this behavior while preserving a linear formulation, an independent equivalent mass connected to the upper tank through an equivalent elastic stiffness models the product.
The resulting simplified representation corresponds to a Three-Degrees-of-Freedom system. The Finite Element model, the equivalent upper trough, and the processed product interact through two distinct elastic interfaces, as shown in the following figure.

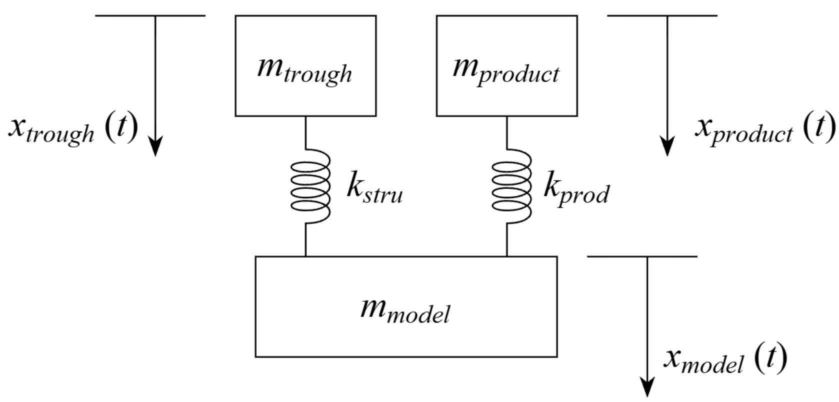

Figure 4.19: *Three-Degrees of Freedom simplified system according to "Hypothesis 2"*

The simplified Three-Degrees of Freedom system shown in Fig. 4.19 provides a conceptual framework for its development. In particular, it highlights that the model must represent the processed material as an independent inertial system interacting with the vibrating structure through an equivalent elastic interface. Accordingly, the Finite Element model schematizes the product by means of multiple remote masses connected to the structure through an equivalent stiffness.
Following the conceptual model developed for "Version 0", the analysis discretizes the total product mass into ten independent remote masses while preserving the same subdivision into five longitudinal and two transverse sections. Implementing the equivalent elastic interaction requires an equivalent stiffness between each product remote mass and the Finite Element model. Since the adopted *RBE3* interpolation does not allow the model to define the connection stiffness explicitly, the model introduces intermediate elastic elements with calibratable stiffness. The model therefore connects the product remote masses to these elements instead of connecting them directly to the geometry through the *RBE3* interpolation.
The addition into the model of ten cylindrical elements exploits the control of k_{prod}: they have diameter D of 4 mm, length L of 200 mm and the adjustment of the Young's Modulus E_{prod} of the assigned material allows the calibration of the stiffness through the formulation

$$k_{set} = \frac{E_{prod} A}{L} \tag{4.1}$$

where A is the cross-section area calculated as $\pi D^2/4$.
The introduction of the equivalent stiffness raises the problem of defining an appropriate value for k_{prod}. Rather than selecting this parameter empirically, a preliminary analytical estimation identifies its expected order of magnitude and provide a physically justified starting point for the subsequent numerical calibration. Appendix C derives this estimate through an equivalent simplified dynamic model, which provides an approximate stiffness value required to reproduce the experimentally observed dynamics.
The analytical estimation reported in Appendix C yields an equivalent Young's modulus of approximately 43 GPa for the cylindrical elements. This value originates from a simplified three-degree-of-freedom model, in which lumped masses and ideal elastic springs represent the structural components. As a result, the analytical model predicts a stiffness that should exceed the stiffness required by the complete Finite Element model. Consequently, the Young's modulus adopted for the numerical model should be lower, while remaining of the same order of magnitude, because

the Finite Element model already captures part of the structural compliance.
Nevertheless, the obtained result provides a physically meaningful order of magnitude. The estimated modulus is lower than the Young's Modulus of structural steel, consistently with the partial dynamic uncoupling between the processed product and the vibrating structure.
The analytical solution provides a physically based initial estimate, while the calibration against the experimental modal response determines the final value. The calibration leads to a Young's Modulus equal to

$$E_{prod} = 23\,GPa$$

which allows the FE model to reproduce the measured first natural frequency of 11.5 Hz. The difference with respect to the analytical estimate is consistent with the additional distributed flexibility, intrinsic in the complete Finite Element model.
This value represents the final parameter employed in all simulations of "Version 1" model.

4.5.4 Final model setup

The equivalent representation of the processed product completes the definition of the final computational model of "Version 1". The geometric model, the mesh generation strategy, structural material properties, and the equivalent representations of the upper trough and motovibrators remain unchanged with respect to "Version 0". Therefore, this section focuses exclusively on the implementation of the equivalent product model.
The present section describes the implementation of the equivalent product model within the Finite Element simulation. As discussed in the previous section, ten cylindrical elements connect the processed product to the vibrating structure and act as axial springs through their axial stiffness. This representation reproduces the mechanical interaction between the processed product and the supporting structure rather than merely accounting for the product mass. At the same time, it avoids the geometric complexity of an explicit product model and keeps the computational effort low.
Since the processed product lies on the holed plate inside the upper trough, the equivalent cylindrical elements connect to the structural region corresponding to the discharge plate, namely the interface between the upper and lower troughs.
Fig. 4.20 summarizes the material properties assigned in SimScale to the equivalent

cylindrical elements. The adopted Young's Modulus adopted for the material is 23 GPa, whereas the density remains intentionally low to minimize the inertial contribution of the elements. A zero density would better reflect their physical function, but the software does not provide this option.

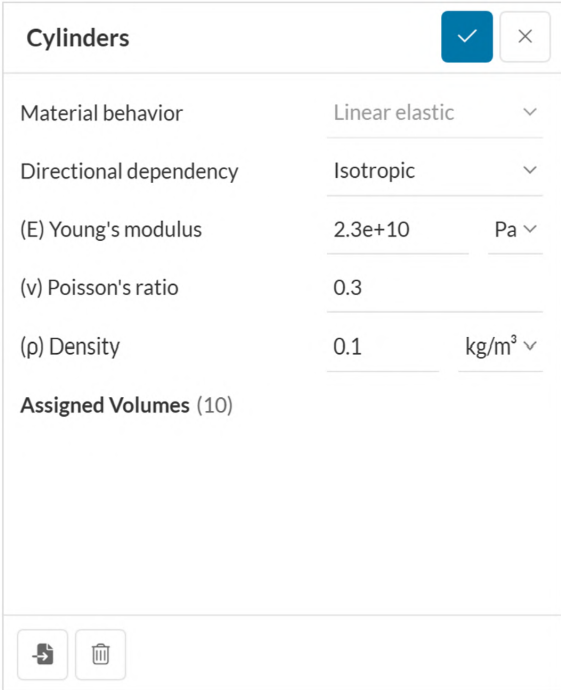

Figure 4.20: *Material properties assigned to cylindrical elements.*
Source: author's elaboration using SimScale

As already discussed, ten independent remote masses account for the total product mass, each connected to the corresponding cylindrical element through a deformable *RBE3* interpolation. The following figure illustrates the adopted implementation.

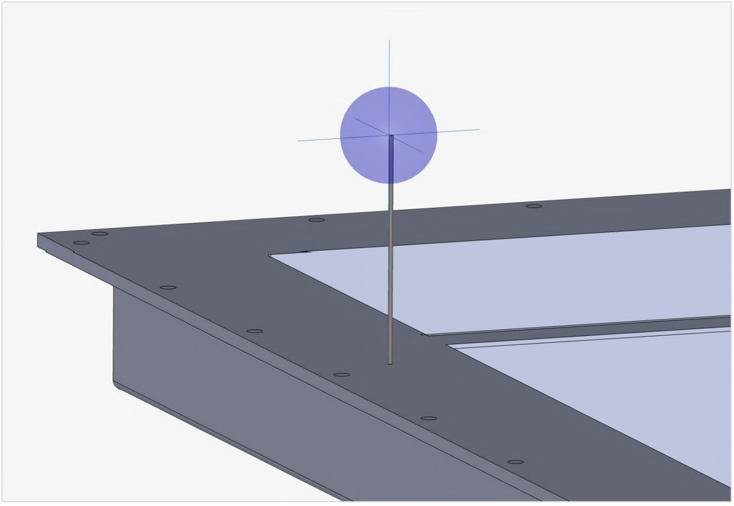

Figure 4.21: *Focus on cylindrical springs and remote mass application. Source: author's elaboration using SimScale*

The resulting arrangement and implementation of the ten equivalent masses related to processed product is shown in following figures.

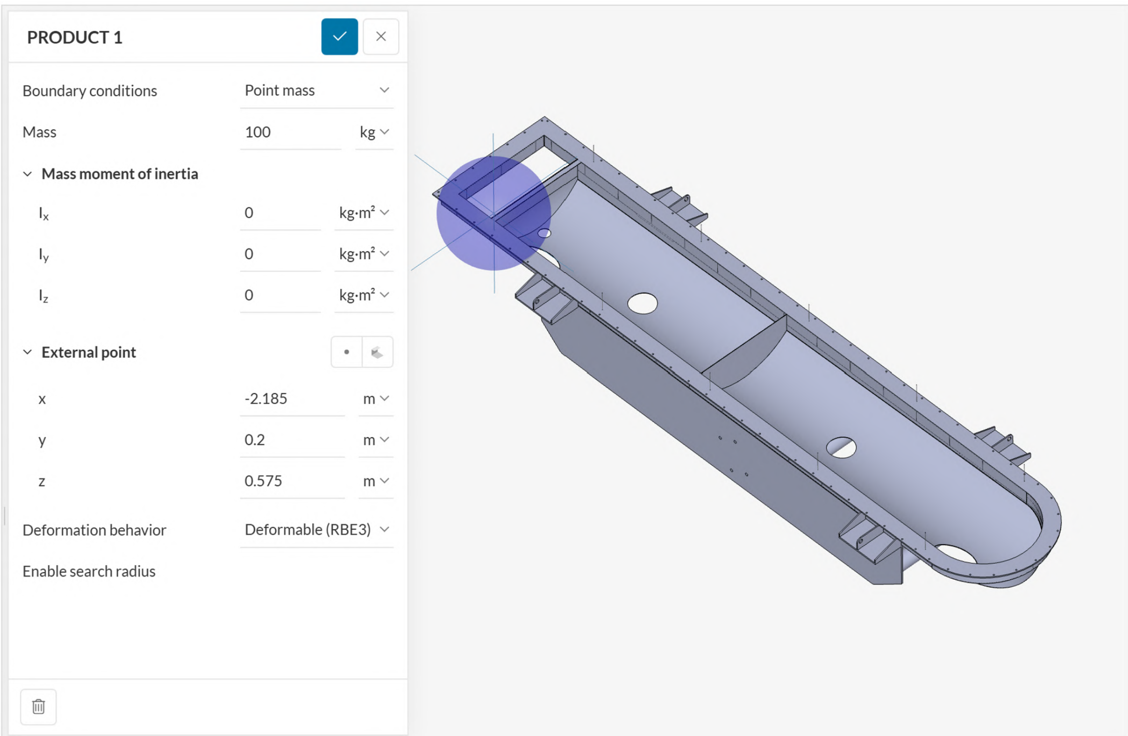

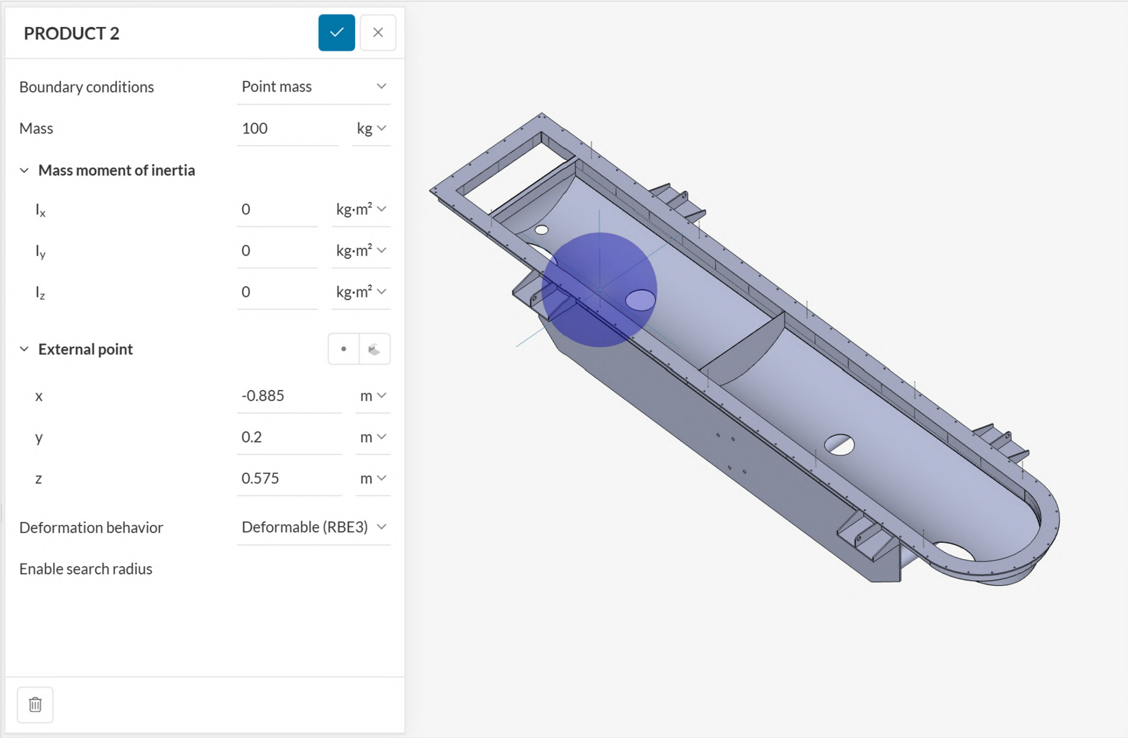
PRODUCT 2
Boundary conditions
Point mass
Mass
100
kg
Mass moment of inertia
Ix
0
kg·m²
Iy
0
kg·m²
Iz
0
kg·m²
External point
x
-0.885
m
y
0.2
m
z
0.575
m
Deformation behavior
Deformable (RBE3)
Enable search radius

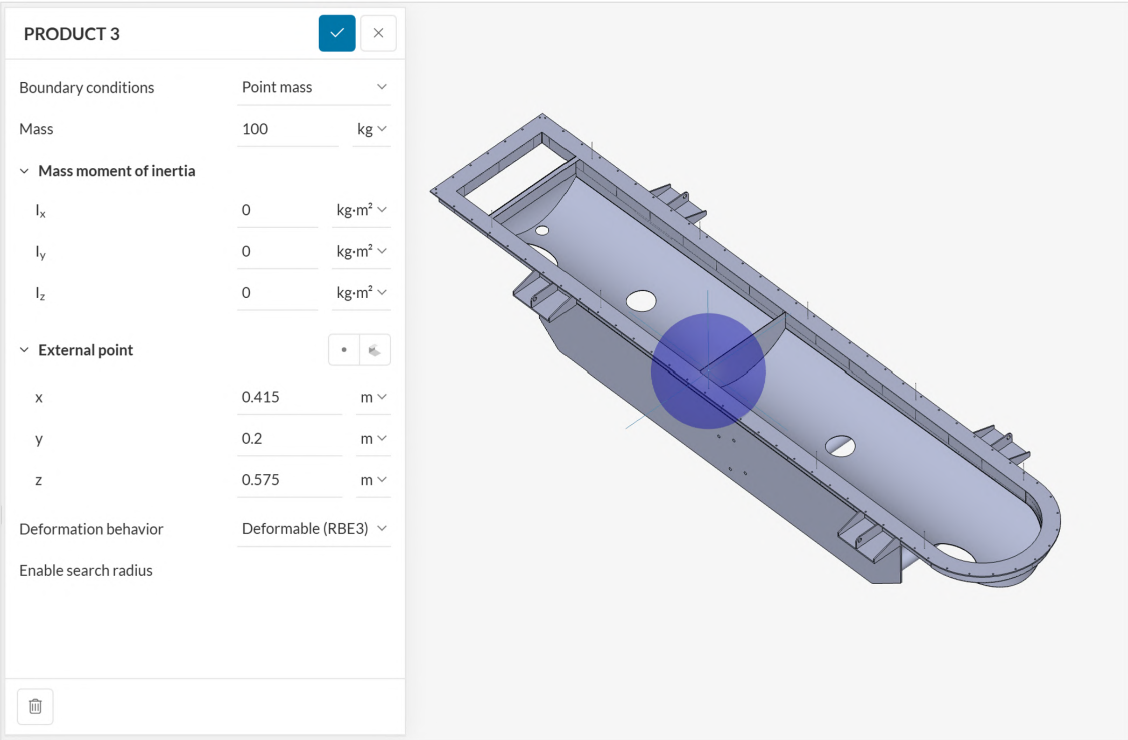
PRODUCT 3
Boundary conditions
Point mass
Mass
100
kg
Mass moment of inertia
Ix
0
kg·m²
Iy
0
kg·m²
Iz
0
kg·m²
External point
x
0.415
m
y
0.2
m
z
0.575
m
Deformation behavior
Deformable (RBE3)
Enable search radius

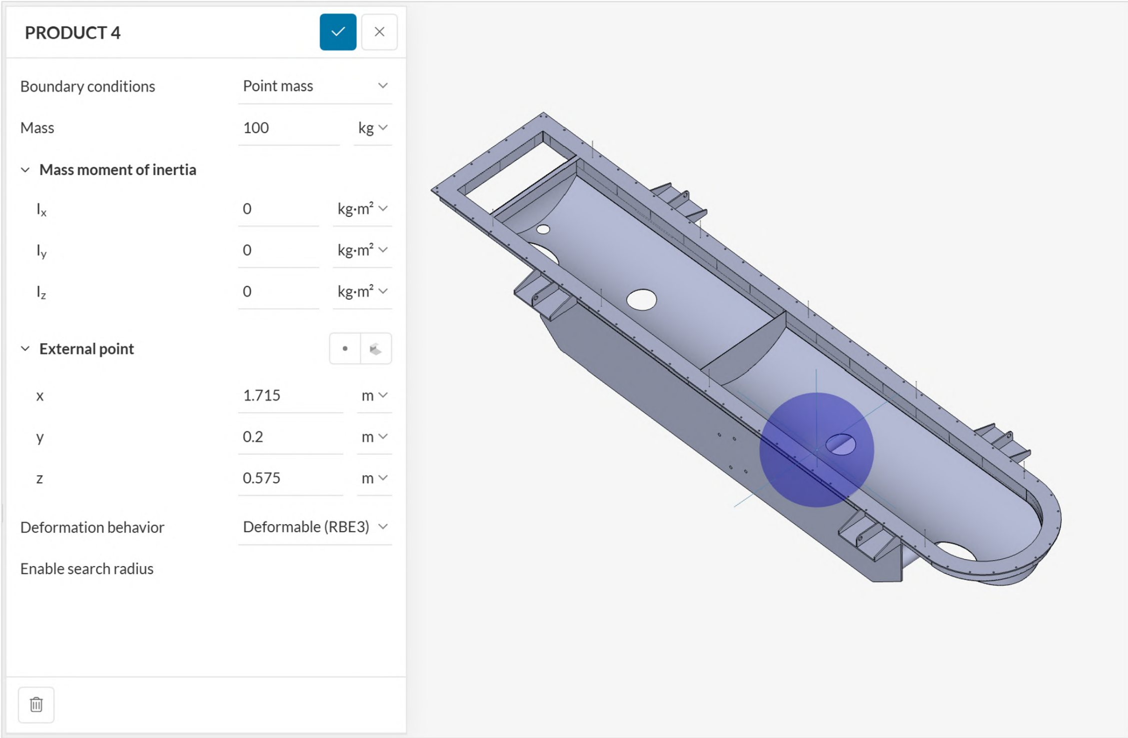
PRODUCT 4
Boundary conditions
Point mass
Mass
100
kg
Mass moment of inertia
I_x
0
kg·m²
I_y
0
kg·m²
I_z
0
kg·m²
External point
x
1.715
m
y
0.2
m
z
0.575
m
Deformation behavior
Deformable (RBE3)
Enable search radius

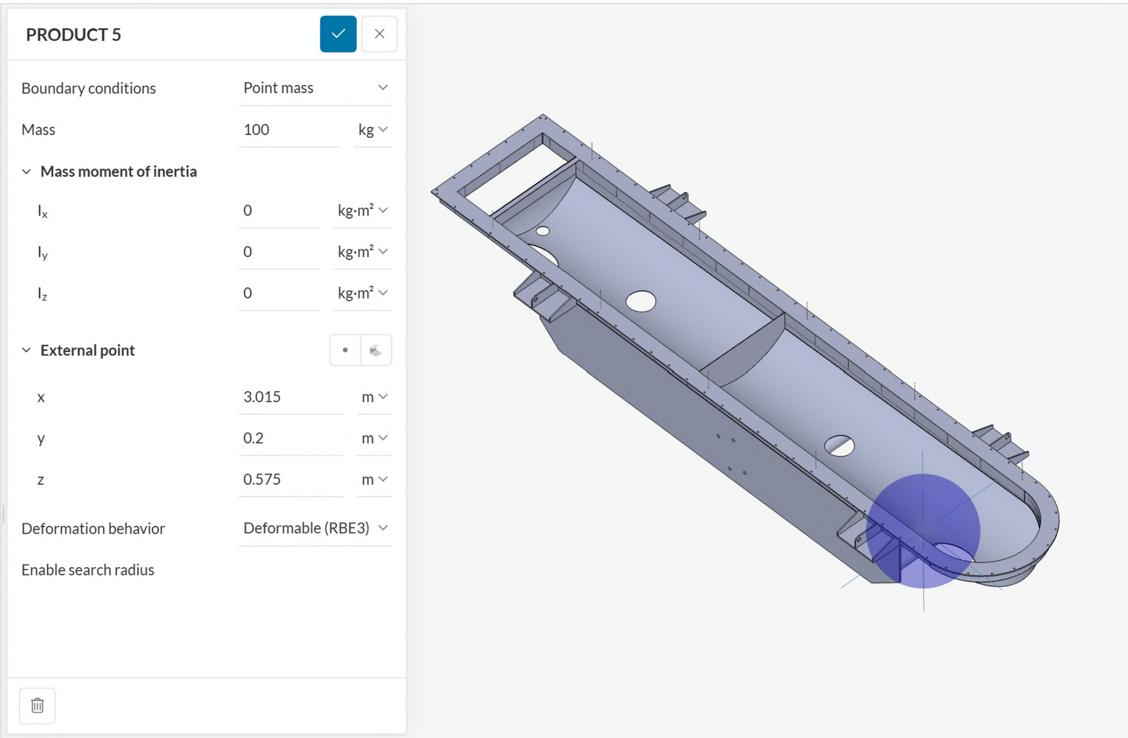
PRODUCT 5
Boundary conditions
Point mass
Mass
100
kg
Mass moment of inertia
I_x
0
kg·m²
I_y
0
kg·m²
I_z
0
kg·m²
External point
x
3.015
m
y
0.2
m
z
0.575
m
Deformation behavior
Deformable (RBE3)
Enable search radius

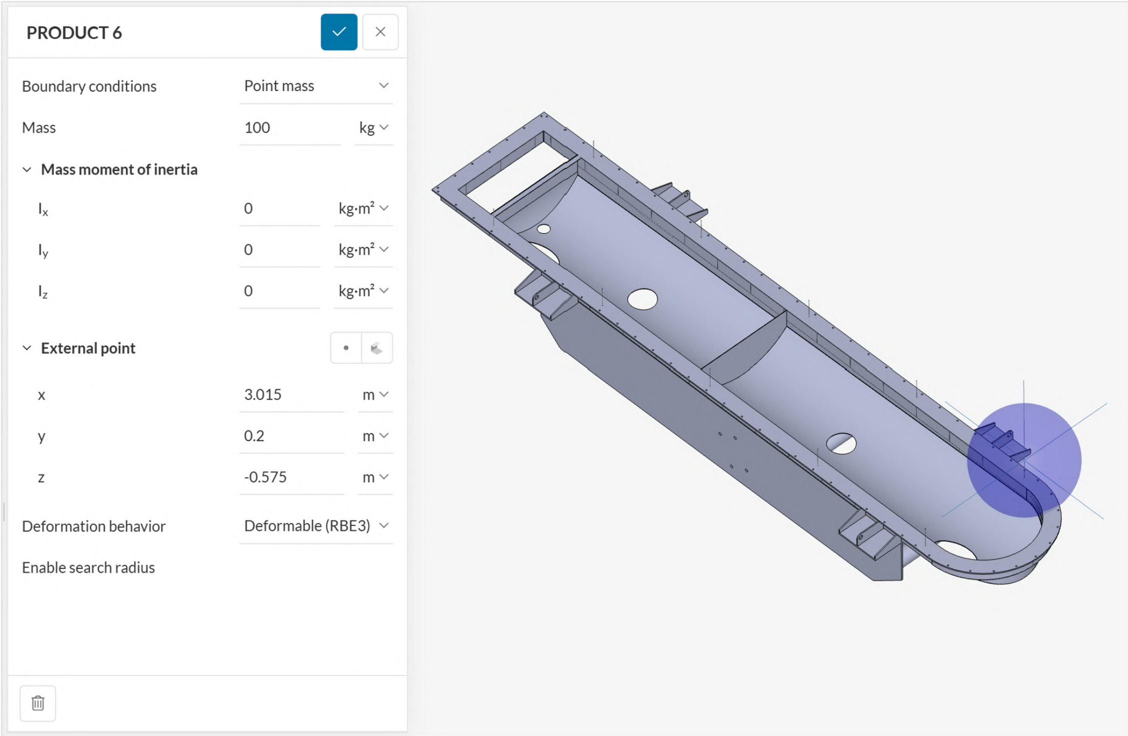
PRODUCT 6
Boundary conditions
Point mass
Mass
100
kg
Mass moment of inertia
Ix
0
kg·m²
Iy
0
kg·m²
Iz
0
kg·m²
External point
x
3.015
m
y
0.2
m
z
-0.575
m
Deformation behavior
Deformable (RBE3)
Enable search radius

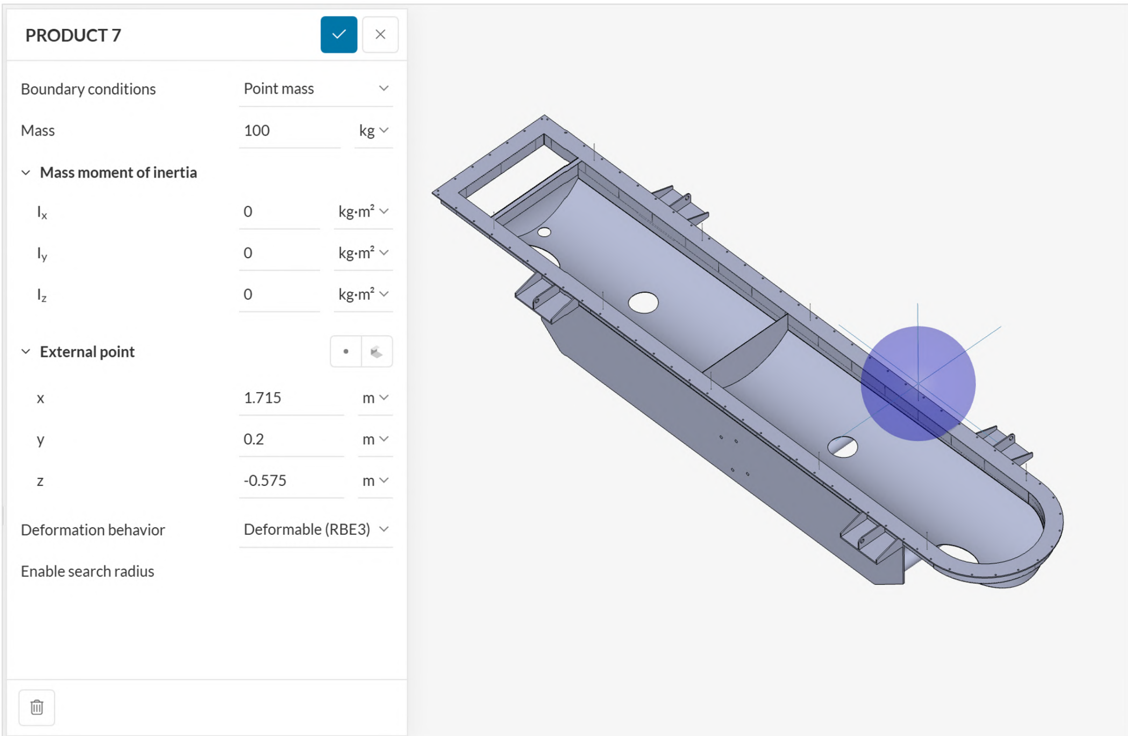
PRODUCT 7
Boundary conditions
Point mass
Mass
100
kg
Mass moment of inertia
Ix
0
kg·m²
Iy
0
kg·m²
Iz
0
kg·m²
External point
x
1.715
m
y
0.2
m
z
-0.575
m
Deformation behavior
Deformable (RBE3)
Enable search radius

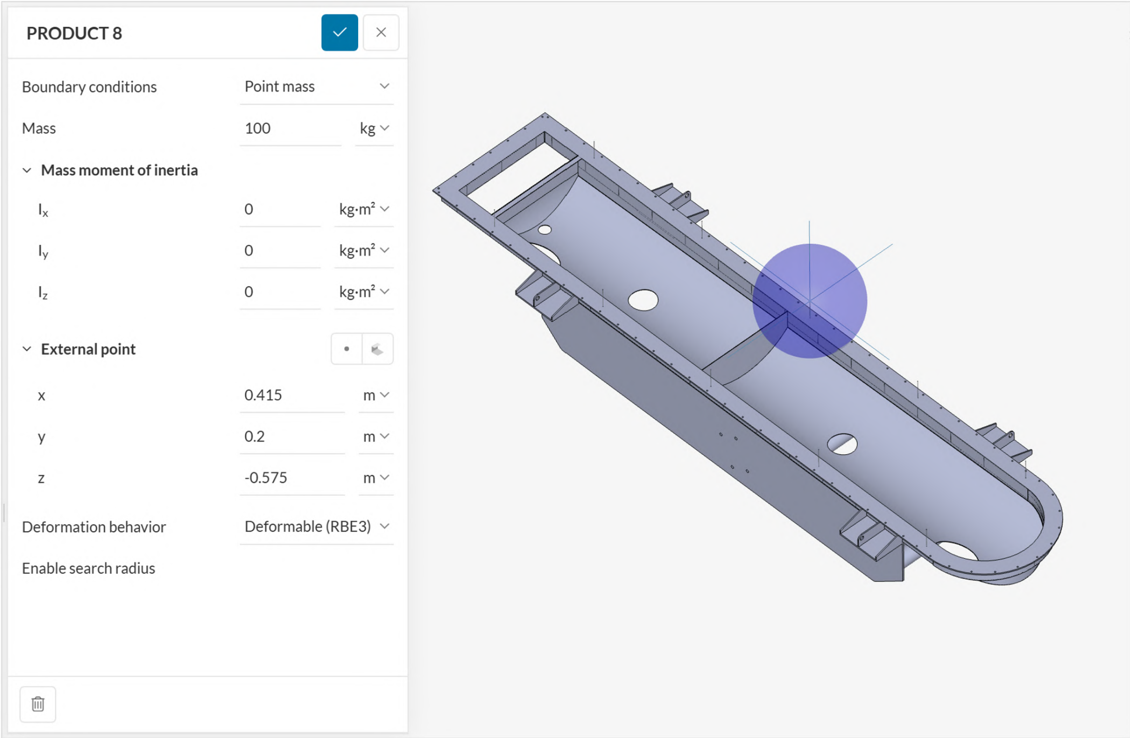
PRODUCT 8
Boundary conditions
Point mass
Mass
100
kg
Mass moment of inertia
I_x
0
kg·m²
I_y
0
kg·m²
I_z
0
kg·m²
External point
x
0.415
m
y
0.2
m
z
-0.575
m
Deformation behavior
Deformable (RBE3)
Enable search radius

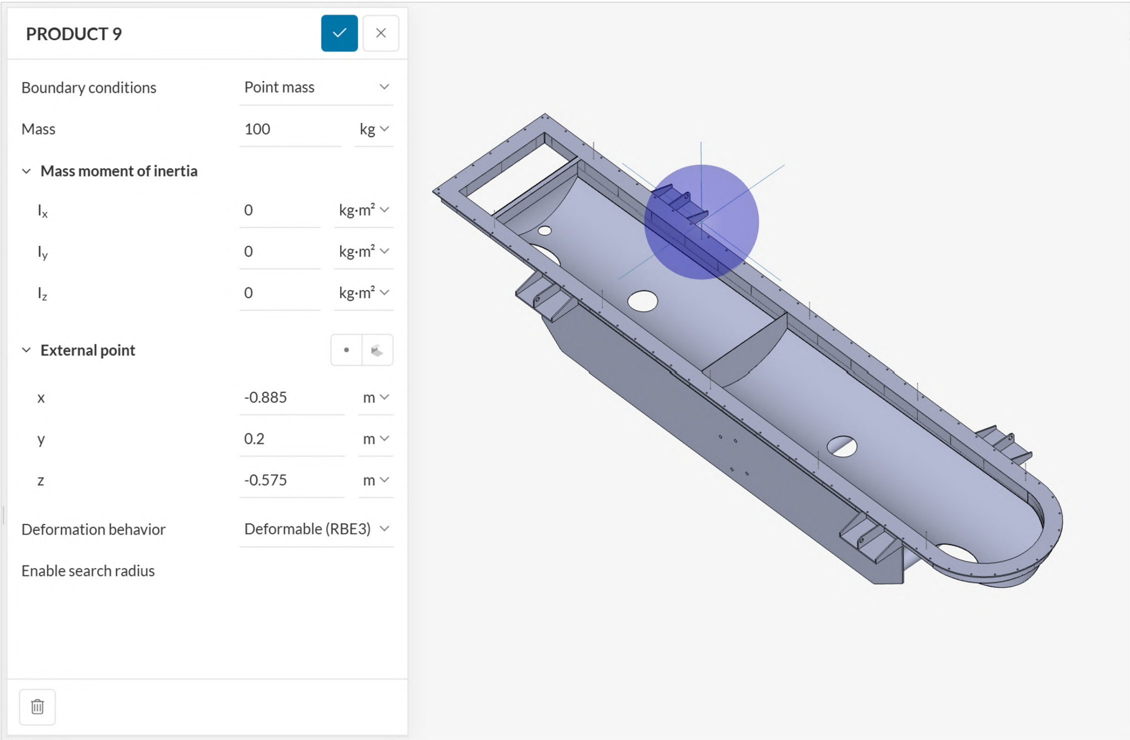
PRODUCT 9
Boundary conditions
Point mass
Mass
100
kg
Mass moment of inertia
I_x
0
kg·m²
I_y
0
kg·m²
I_z
0
kg·m²
External point
x
-0.885
m
y
0.2
m
z
-0.575
m
Deformation behavior
Deformable (RBE3)
Enable search radius

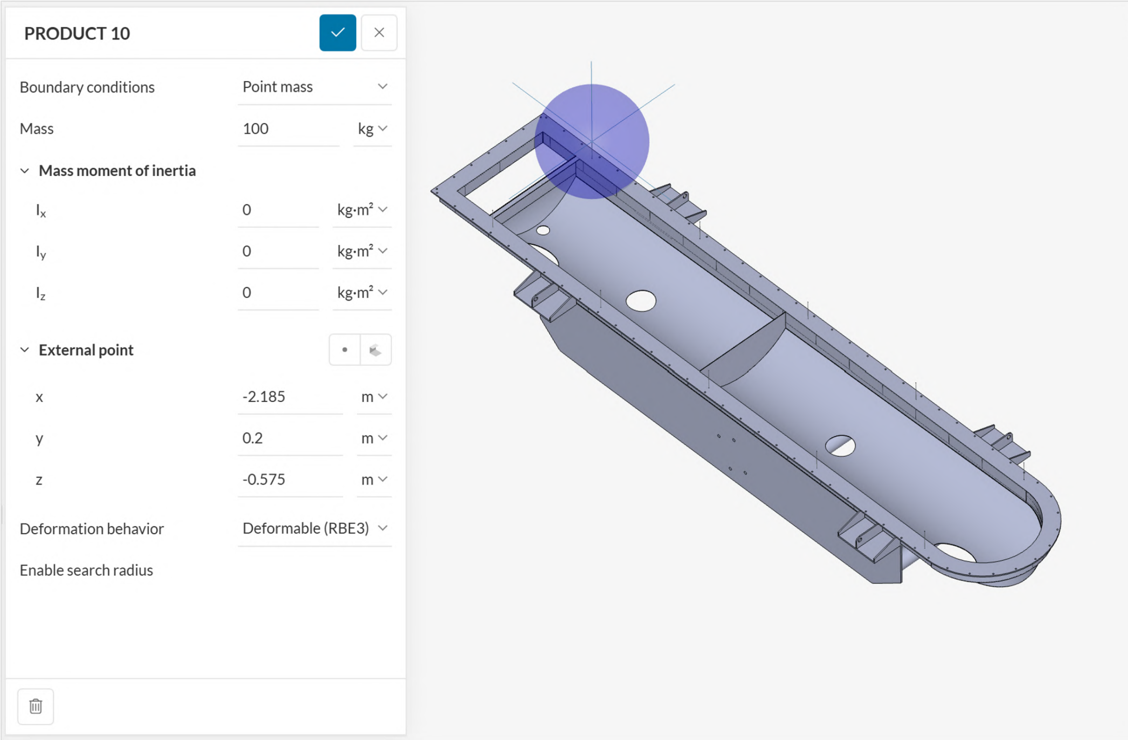

Figure 4.22: *Remote masses setup for product representation.*
Source: author's elaboration using SimScale

The previous sections fully define the numerical model. The adopted modeling strategy provides a physically consistent representation of the dynamic interaction between the processed material and the vibrating structure while preserving the computational efficiency of a linear formulation. The following chapter presents the numerical results and assesses the capability of the proposed model to reproduce the experimentally observed dynamic behavior.

4.6 Remarks on Model Validity

This chapter develops and validates the Finite Elements models against the available experimental measurements, providing a reliable representation of the structural dynamics of both investigated machine configurations. Despite the adopted simplifications, the agreement with the experimental natural frequencies demonstrates that the models successfully reproduce the dominant structural phenomena governing the machine response.
The validated model provides a suitable tool for interpreting the observed phenomena and for evaluating the influence of future structural modifications on the global

dynamic response of the vibrating dryer. Nevertheless, the validity of some equivalent modeling assumptions remains restricted to the specific structural configuration for which the analysis identified and calibrated them.

4.6.1 Validity of the equivalent product representation

The equivalent stiffness adopted to represent the interaction between the processed product and the supporting structure does not correspond to an intrinsic material property of the product. Instead, the calibration procedure described in the previous sections identifies it as an equivalent parameter that reproduces the experimentally observed dynamic response of the "Version 1" machine.
Appendix C derives the initial analytical estimate of the equivalent product stiffness from the structural stiffness identified for "Version 0". Although "Version 1" exhibits a slightly higher first natural frequency, indicating a moderate increase in structural stiffness, both configurations retain substantially the same global torsional behavior. Consequently, the structural stiffness identified for "Version 0" provides a reasonable engineering approximation for the identification procedure.
The identified equivalent stiffness k_{prod} therefore depends on the structural stiffness k_{stru} adopted in the model. Any significant modification of the structural layout, particularly those intended to increase the torsional stiffness of the machine, changes k_{stru} and consequently alters the dynamic interaction between the structure and the processed material. As a result, the product equivalent stiffness k_{prod} also changes. Therefore, the equivalent product stiffness identified for the current configuration cannot be directly transferred to a "Version 1" structure.
These considerations limit the validity of the equivalent product model to the structural configuration for which the calibration procedure identified it. Because the stiffness of the equivalent product depends inherently on the stiffness of the supporting structure, substantial structural modifications invalidate the adopted representation. For this reason, the following chapter evaluates the proposed design solutions under empty-machine conditions, where the numerical model remains independent of the equivalent product representation and therefore provides a consistent basis for comparing different structural configurations.

Chapter 5

Results of FE Analysis

This chapter presents the results of the Finite Element modal analyses performed on the "Version 0" and "Version 1" machine configurations. In particular, it employs the numerical models developed in Chapter 4 to investigate the dynamics of the supporting structure and to interpret the resonance phenomena identified experimentally during the impact hammer testing campaign.
First, the analysis investigates the modal response of the complete system under elastic support conditions to verify the behavior of the vibration isolation system and to assess the separation between the rigid-body modes and the operating excitation frequency. Subsequently, the comparison with the experimentally identified natural frequencies validates the FE models of "Version 0" and "Version 1", providing confidence in their ability to reproduce the actual dynamic response of the machine.
Once the validation confirms their accuracy, the analysis uses the numerical models to investigate the corresponding mode shapes under free-free boundary conditions and to identify the intrinsic deformation mechanisms. The analysis focuses particularly on the first flexible mode, whose flexural–torsional nature provides a physical interpretation of the fatigue damage observed in the supporting structure.
Finally, the analysis assesses the effectiveness of the implemented structural modification by comparing the "Version 0" and "Version 1" configurations under equivalent mass conditions. This comparison makes it possible to distinguish the contribution of the structural reinforcement from the influence of the processed material. In addition, it evaluates whether the adopted intervention shifts the first natural frequency outside the critical operating range.
The results presented in this chapter establish the basis for the re-design strategies, whose objective is to increase the torsional stiffness of the supporting frame and mitigate the resonance phenomenon.

5.1 Modal Analysis with Elastic Supports

The modal analyses presented in this section adopt the spring-bed boundary conditions described in Section 5.2.2, where the vibrations isolators support the vibrating assembly. Under these conditions, the six rigid-body degrees of freedom of the structure exhibit non-zero natural frequencies.

Table 5.1: *Rigid-body modes - spring-bed boundary conditions – "Version 0"*

Mode	**Frequency [Hz]**	**DoF**
1	2.9	T_Z
2	2.9	T_X
3	3.7	R_Y
4	4.4	T_Y
5	4.5	R_X
6	5.3	R_Z

Table 5.2: *Rigid-body modes - spring-bed boundary conditions – "Version 1"*

Mode	**Frequency [Hz]**	**DoF**
1	2.8	T_Z
2	2.8	T_X
3	3.5	R_Y
4	3.7	T_Y
5	4.0	R_X
6	4.3	R_Z

Tab. 5.1 and Tab. 5.2 summarize the frequencies and the corresponding dominant rigid-body motion identified for the two machine configurations. The notation adopted to describe each mode is consistent with the reference introduced in Fig. 4.4: the prefix T denotes a translational degree of freedom, while R denotes a rotational degree of freedom, and the subscript identifies the corresponding direction or axis of motion.

The rigid-body modes obtained for both machine configurations are generally consistent with the frequency interval predicted by the simplified analytical design procedure presented in Chapter 2, corresponding to a vibration isolation efficiency of approximately 80–90%.
Some rigid-body modes exhibit natural frequencies slightly below the theoretical lower bound. As a result, the excitation-to-natural-frequency ratio becomes even larger, and the degree of uncoupling exceeds 90%.
Conversely, the highest rigid-body mode identified for "Version 0" occurs at 5.3 Hz, only marginally above the theoretical upper limit of 5.1 Hz. This difference is negligible, so the result remains fully consistent with the expected dynamic behavior of the isolation system.
The numerical results confirm that the vibration isolators provide the intended dynamic decoupling between the vibrating assembly and the supporting frame. Since all rigid-body modes remain well separated from the operating excitation frequency of 12.5 Hz, the analysis excludes resonance associated with rigid-body motion for both machine configurations. The experimental evidence indicates that the observed resonance originates from the flexible deformation of the structure. The following sections investigate its modal characteristics.

5.2 Modal Analysis of "*Version 0*"

5.2.1 Model validation

The comparison of the natural frequencies obtained from the modal analysis with those experimentally identified during the impact hammer testing campaign presented in Section 3.2.3 validates the simulation, developed to reproduce "Version 0" machine, as shown in the following table.

Table 5.3: *"Version 0" - Validation comparing experimental and FE analysis natural frequencies and the corresponding relative error*

Mode	**Experimental [Hz]**	**FE Analysis [Hz]**	**Relative error [%]**
First natural frequency	12.5	12.4	0.8
Second natural frequency	32.0	32.5	1.6

The comparison shows an excellent agreement between experimental measurements and results from Finite Element Analysis. In particular, the relative error is lower than 2% for both the first and the second natural frequencies, demonstrating that the adopted modeling assumptions provide a sufficiently accurate representation of the actual dynamic behavior of the machine.
The numerical model specifically aims to reproduce the first natural frequency because this mode governs the resonance phenomenon. Therefore, the ability of the model to reproduce the second natural frequency, despite not using it as a reference during the model development, directly demonstrates the robustness of the adopted modeling strategy.
On this basis, the analysis considers the FE model sufficiently reliable to investigate the corresponding mode shapes, thereby providing information that the experimental campaign alone could not supply.

5.2.2 First natural frequency

Following the validation procedure, the analysis investigates the modal shape associated with the first flexible natural frequency using the validated numerical model.
This result is fundamental because it finally allows the assessment of the deformation pattern related to resonance conditions, enabling a physical interpretation of the dynamic behavior of the structure.
Fig. 5.1 shows the first deformable mode of the "Version 0" machine configuration. The modal shape is characterized by coupled bending–torsional deformation of the supporting structure. The top view in Fig. 5.1 barely shows the flexural deformation, whereas a significant rotation about the longitudinal axis is clearly visible. This behavior indicates that torsional compliance dominates the dynamic response of the machine. This behavior is consistent with the structural layout discussed in Chapter 2, where the supporting structure exhibits an open cross-sectional configuration characterized by limited torsional stiffness.

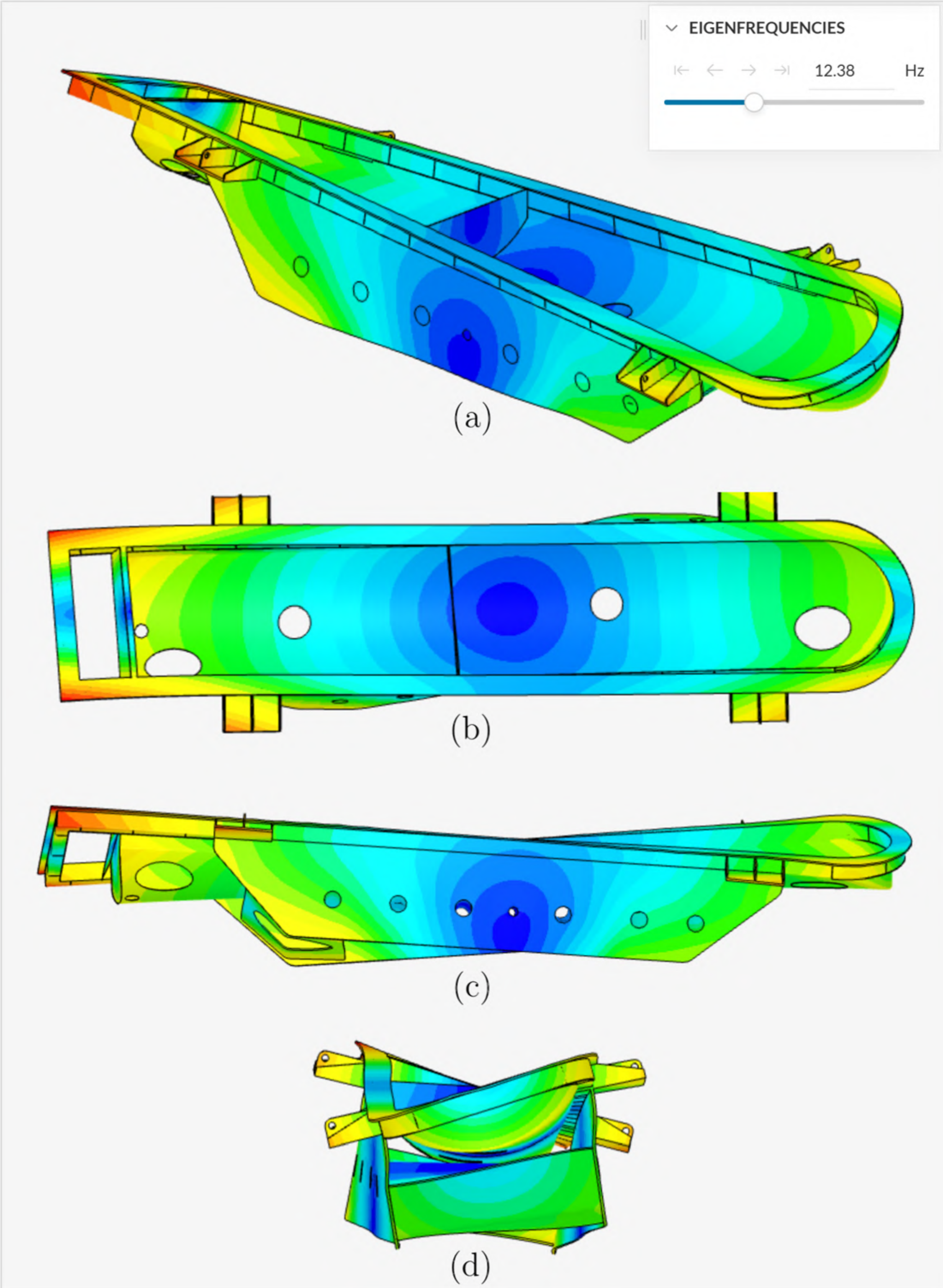

Figure 5.1: *"Version 0" - First mode shape: (a) three-dimensional view, (b) top-view, (c) frontal view, (d) lateral view.*
Source: author's elaboration using SimScale

Although the present work focuses exclusively on modal analysis and does not include stress or fatigue calculations, the identified mode shape provides a coherent interpretation of the observed structural damage. In particular, the global torsional component of the mode suggests that the transverse tubular members located closer to the center of the structure may undergo a more pronounced torsional deformation about their own longitudinal axis, whereas the outer members tend to follow the global motion of the side plates with a more rigid-body-like behavior: this kinematic behavior is consistent with the circumferential crack patterns experimentally observed. The identification of this modal shape therefore represents the main contribution of the numerical model, providing information not obtainable through the experimental campaign and allowing a deeper understanding of the structural dynamics of the machine.

From an engineering perspective, this result fundamentally changes the interpretation of the structural problem. The resonance does not arise from insufficient global bending stiffness, as initially assumed during the industrial re-design. Instead, this modal shape identifies the limited torsional stiffness of the supporting frame as the governing mechanism. This understanding defines the design target to prioritize the increase of torsional torsional rigidity rather than simply reinforcing individual members.

5.2.3 Second natural frequency

The Finite Element Analysis identifies the second mode shape at a natural frequency of 32.5 Hz, showing excellent agreement with the second resonance peak observed during the impact hammer testing campaign. As discussed in the previous section, the accurate prediction of this frequency provides an independent validation of the developed numerical model because the development procedure did not use it as a reference.

The corresponding modal shape, shown in Fig. 5.2, exhibits a predominantly flexural behavior, whose bending stiffness mainly governs the deformation of the structure. The adopted structural intervention aimed to increase the flexural rigidity of the supporting structure. Consequently, the second natural frequency should increase. The analysis of the "Version 1" machine configuration presented in the following section confirms this expectation by showing that the structural intervention primarily affects the bending-dominated response while leaving the first governing flexural–torsional mode substantially unchanged. This result explains why the industrial modification achieved only a limited improvement of the system dynamics and highlights the need to target the governing torsional compliance rather than increasing the global bending stiffness alone.

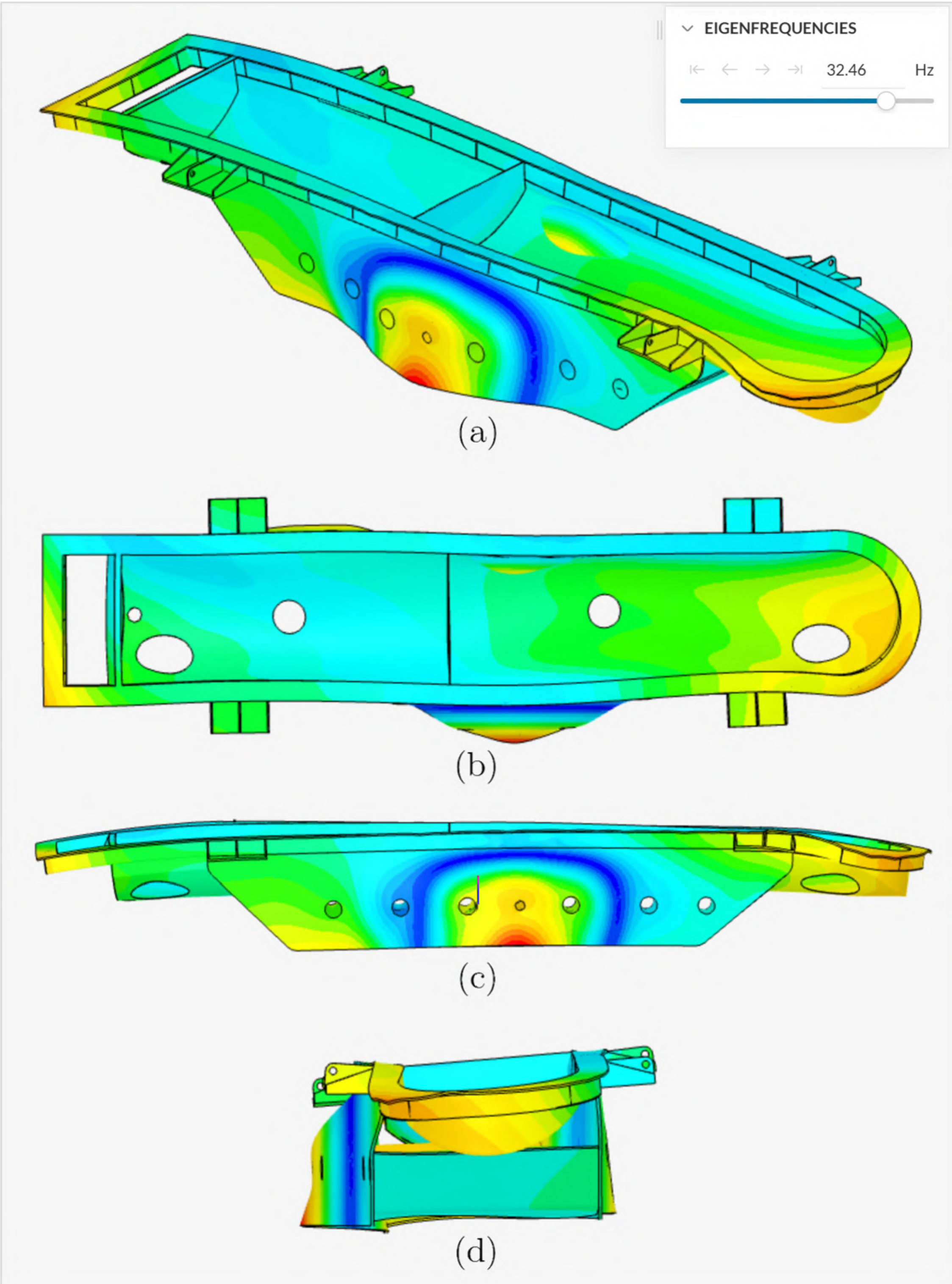

Figure 5.2: *"Version 0" - First mode shape: (a) three-dimensional view, (b) top-view, (c) frontal view, (d) lateral view.*
Source: author's elaboration using SimScale

5.3 Modal Analysis of "*Version 1*"

5.3.1 Model validation

Unlike the "Version 0" machine configuration, the development of the "Version 1" model had to account for approximately 1 ton of processed material inside the vibrating trough during the experimental campaign. As discussed in Section 4.5.3, the complex motion of the granular acid crystals, involving impacts, friction, and continuously evolving contact conditions, prevents the numerical model from representing the dynamic interaction between the structure and the processed material exactly. Consequently, the model represents the product through an equivalent formulation based on simplified engineering assumptions.
The bump test campaign presented in Section 3.2.2 provides the only experimental quantity available for validation, namely the first natural frequency. Tab. 5.4 compares this value with the corresponding Finite Element prediction.

Table 5.4: *"Version 1" - Validation comparing experimental and FE analysis first natural frequency and the corresponding relative error*

Mode	**Experimental [Hz]**	**FE Analysis [Hz]**	**Relative error [%]**
First natural frequency	11.5	11.4	0.9

Despite the uncertainty introduced by the equivalent representation of the processed material, the comparison shows an excellent agreement, with a relative error lower than 2%, and this result confirms the accuracy of the adopted modeling strategy describing the dynamic behavior of the "Version 1" machine.
Although the experimental validation of "Version 1" relies on a single natural frequency, the previously validated modeling framework developed for the "Version 0" machine configuration supports the reliability of the Finite Elements model. In particular, the model preserves the equivalent representation of the non-modeled structural components and updates only the structural geometry and the equivalent representation of the processed material.
Therefore, the agreement with the experimental measurement, together with the robustness of the previously validated modeling framework, provides sufficient confidence to use the numerical model to investigate the modal characteristics and assess the dynamic effects of the implemented structural modification.

5.3.2 First natural frequency

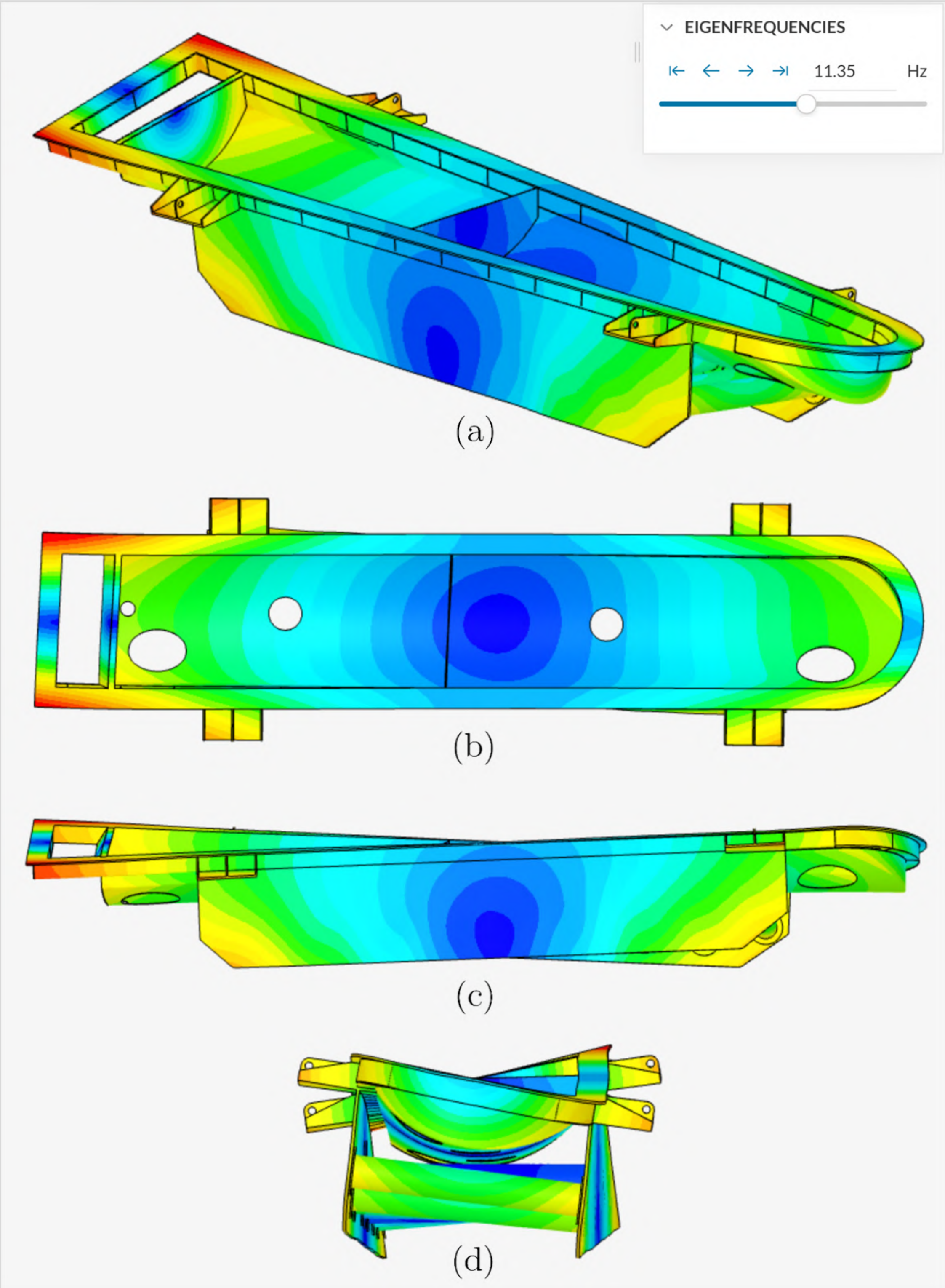

Figure 5.3: *"Version 1" - First mode shape: (a) three-dimensional view, (b) top-view, (c) frontal view, (d) lateral view.*
Source: author's elaboration using SimScale

As discussed above, the first natural frequency for the "Version 1" configuration of the machine in operating conditions, so when 1 ton of product lies on it, is 11.4 Hz according to the numerical model. Fig. 5.3 shows the corresponding modal shape.
From a qualitative point of view, the modal shape exhibits essentially the same characteristics observed for the "Version 0" machine configuration: in fact, a coupled flexural–torsional deformation still governs the dynamic response. Although the implemented stiffening intervention barely modifies the structural rigidity, the overall deformation pattern remains substantially unchanged, indicating that the torsional compliance of the supporting frame continues to govern the first flexible mode.
The modal analysis therefore provides a physical interpretation of the limited effectiveness of the implemented structural intervention. From the experimental results, the first natural frequency shifts from 12.5 Hz for "Version 0" to 11.5 Hz for "Version 1", corresponding to a variation of approximately 8%, which is an insufficient margin to move outside of the critical frequency range of 12.5 Hz $\pm$25%.
At first glance, the reduction of the first natural frequency may appear counterintuitive because reinforcing elements normally increase the structural stiffness and, consequently, the corresponding natural frequency. However, the experimental tests on the "Version 1" machine included approximately 1 ton of processed material inside the vibrating trough. This additional mass significantly increased the equivalent vibrating mass. The measured natural frequency is therefore the combined result of two competing effects: the increase in structural stiffness due to the reinforcement and the increase in equivalent mass due to the processed material.
For this reason, the comparison between the "Version 0" and "Version 1" machine configurations cannot directly assess the actual effectiveness of the structural intervention. To isolate the contribution of the implemented reinforcement, the analysis removes the equivalent contribution of the processed material from the FE model. The following section presents this study and evaluates the actual increase in structural stiffness.

5.3.3 Effectiveness of structural modification

To isolate the effect of the implemented structural reinforcement from the influence of the processed material, the analysis removes the equivalent product mass from the numerical model and then investigates the "Version 1" machine configuration.

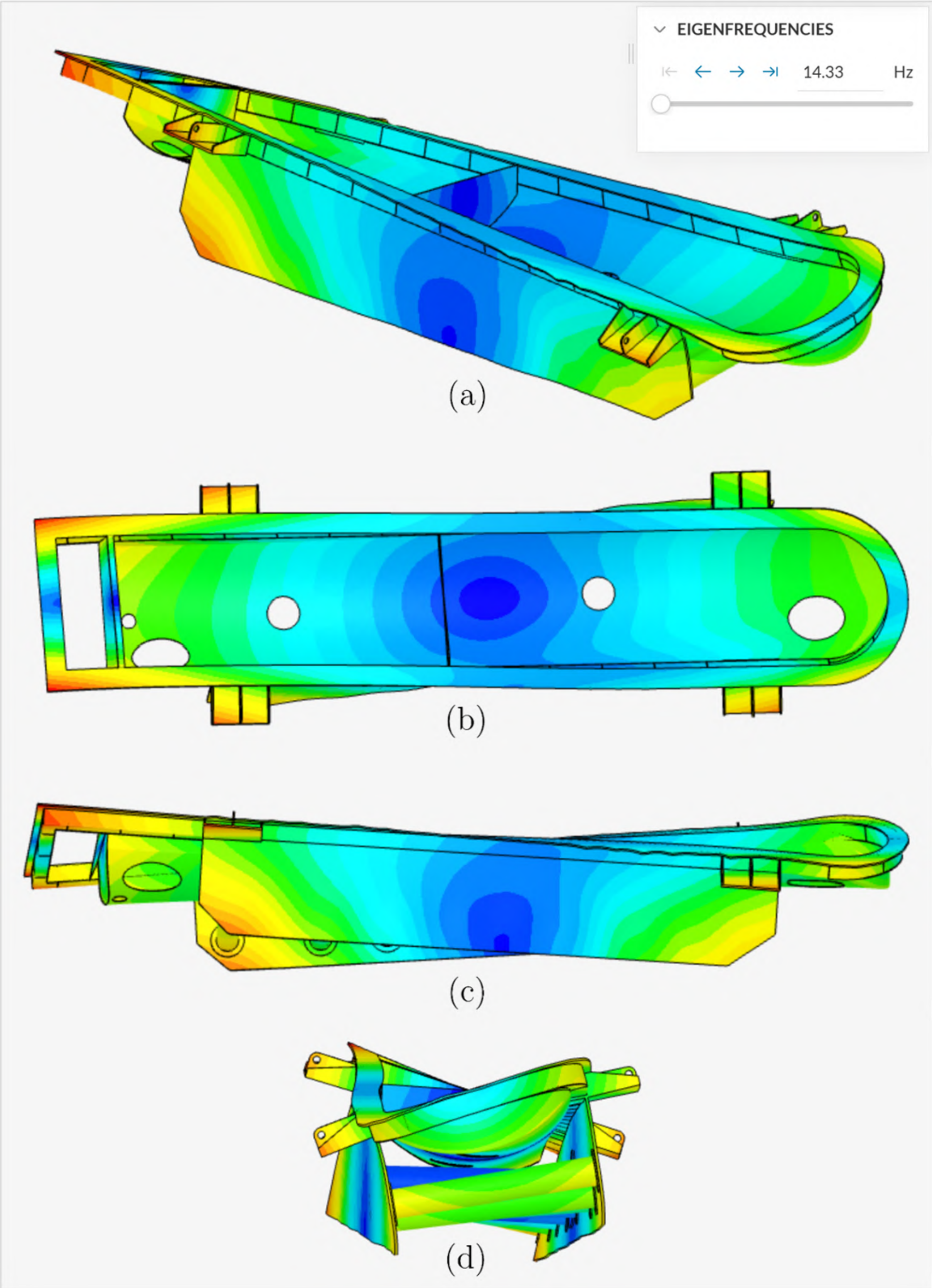

Figure 5.4: *"Version 1" in empty conditions - First mode shape:*
(a) three-dimensional view, (b) top-view, (c) frontal view, (d) lateral view.
Source: author's elaboration using SimScale

Under these conditions, the implemented structural modification increases the first flexible natural frequency from 12.5 Hz in "Version 0" to 14.3 Hz in "Version 1". This result corresponds to an overall frequency increase of approximately 15% and confirms that the reinforcement effectively increases the global stiffness of the supporting structure. The comparison with the previous analysis also highlights the significant influence of the product mass on the dynamic response of the machine. The presence of approximately 1 ton of acid crystals reduces the first natural frequency to 11.5 Hz, consistently with the well-known relationship $f_n \propto \sqrt{k/m}$. Nevertheless, since the frequency shift does not exceed $\pm 25\%$, the achieved improvement is not sufficient to completely eliminate the resonance risk.

The comparison of machine under empty-conditions demonstrates one of the main advantages of the validated numerical model. Unlike experimental testing, the model allows individual design variables to change independently while all the others remain unchanged. This capability isolates the actual contribution of the structural modification from that of the processed material, providing information that experimental measurements alone cannot access. As a result, the computational model becomes a predictive engineering tool rather than a simple validation instrument.

In conclusion, the implemented reinforcement provides only a partial improvement rather than a definitive solution. While it successfully increases the structural stiffness and shifts the first natural frequency toward higher values, it does not substantially alter the governing flexural–torsional behavior of the supporting frame nor move the first mode outside the critical resonance range.

These results indicate that future design modifications should not simply aim at increasing the overall stiffness of the structure, but should specifically target the torsional compliance responsible for the first vibration mode.

These findings indicate that increasing the torsional stiffness of the supporting frame should represent the primary objective of any future structural modification or redesign. Based on this consideration, the following chapter proposes and evaluates alternative design solutions specifically aimed at improving the torsional behavior of the structure.

Chapter 6

Proposals for Efficient Interventions

This chapter employs the validated numerical model developed in the previous chapters to investigate structural solutions that mitigate the resonance phenomena identified in the current machine configuration. The proposed interventions follow a progressive design approach. They range from simple retrofit modifications applicable to the existing "Version 1" machine installed at the industrial site at the time of writing of this thesis to a complete re-design of the supporting structure for future machine developments.

The design strategy investigates two retrofit proposals based on boxing the existing open-section structure to increase torsional stiffness while minimizing manufacturing effort. Finally, it develops a complete re-design of the supporting frame by applying the same design principles to a new structural layout specifically conceived to maximize stiffness and dynamic performance.

For each configuration, the numerical model verifies the compatibility of the vibration isolation system and assesses the resulting structural dynamic behavior through modal analysis. A subsequent comparison evaluates the effectiveness of the proposed solutions by examining their ability to shift the critical natural frequencies away from the operating excitation range while maintaining practical feasibility and structural efficiency.

6.1 Design Scope

The validated numerical model developed throughout the previous chapters represents a reliable predictive tool for investigating the dynamics of the vibrating dryer.

Before introducing any structural modification, this chapter defines the design objectives required to evaluate the effectiveness of the proposed interventions. The purpose is to establish a set of engineering criteria capable of balancing dynamic performance, structural efficiency and practical feasibility.

6.1.1 Objectives

The primary objective is to eliminate resonance conditions by shifting all structural natural frequencies outside the critical range associated with the operating excitation frequency generated by the motovibrators. Since the machine operates at a fixed excitation frequency of 12.5 Hz, the proposed modifications aim to shift every relevant structural mode beyond a safety margin of approximately $\pm 25\%$ with respect to this value. Appendix D discusses the theoretical background of this criterion, examining the concepts of dynamic amplification, damping, modeling uncertainty, and frequency separation margins. Nevertheless, maintaining an adequate separation from the excitation frequency represents a robust engineering design practice for minimizing resonance risk.

Furthermore, the proposed solutions must remain practically feasible. Every structural modification must comply with the existing machine layout and manufacturing constraints while limiting the required construction operations as much as possible. Additional stiffening elements must not interfere with surrounding equipment or process piping, and the design must preserve sufficient accessibility for assembly and maintenance activities, including flange bolting operations and access to auxiliary components. Therefore, the evaluation of each intervention considers both its structural performance and its integration within the existing industrial installation.

Another fundamental design criterion concerns structural efficiency. According to the classical relationship $f_n \propto \sqrt{k/m}$, the addition of indiscriminate mass to increase stiffness may produce only limited dynamic improvements. Therefore, the proposed interventions introduce stiffness only where it effectively contributes to the global structural response while minimizing additional mass. Limiting the amount of added material also reduces manufacturing costs.

Finally, the proposed modifications must not introduce new structural modes within the critical frequency range. In particular, natural frequencies below the operating excitation frequency do not represent an optimal solution because the motovibrators inevitably pass through lower rotational speeds during start-up and shut-down transients. Under these operating conditions, transient resonance phenomena may occur, potentially generating significant dynamic amplification and cyclic stresses.

Consequently, the design strategy shifts the critical natural frequencies above the operating range whenever possible, thereby ensuring adequate separation not only under steady-state conditions but also during transient operation.

6.1.2 Evaluation strategy

This chapter evaluates the proposed structural modifications through a consistent methodology that compares their effectiveness from both dynamic and practical perspectives.

The proposed interventions follow a progressive design philosophy. The design process starts from simple retrofit solutions requiring minimal manufacturing effort and progressively examines more extensive structural modifications to achieve increasingly larger shifts of the critical natural frequency. This strategy systematically evaluates the trade-off between dynamic effectiveness, structural efficiency, and practical feasibility.

The analyses consider all configurations under empty-machine conditions, thereby isolating the influence of the structural modifications from the equivalent product representation. As discussed in Section 4.6.1, the identification procedure defines the equivalent representation of the processed product for a specific structural stiffness of the supporting frame. Since the proposed interventions specifically modify the structural stiffness, particularly its torsional component, the analysis cannot directly extend the validated equivalent product model to the "Version 1" configurations.

Each proposed configuration first undergoes a modal analysis to verify that the vibration isolation system retains the required dynamic characteristics. In particular, the analysis examines the first six rigid-body modes associated with the elastic supports to ensure that they remain within the frequency range required for the desired vibration isolation performance, thereby avoiding modifications to the existing supports.

The comparison then quantifies the effectiveness of each structural intervention through the variation of the first structural natural frequency, which governs the resonance phenomena discussed in the previous chapters. The analysis considers this frequency shift together with the corresponding increase in structural mass. This combined evaluation quantifies the efficiency of each solution and favors interventions that produce significant dynamic improvements while requiring only limited additional material. Conversely, achieving a higher natural frequency at the expense of a disproportionate mass increase does not represent an efficient engineering solution from either a structural or an economic perspective.

6.1.3 Proposal philosophy

The modal analyses presented in the previous chapters showed that a global torsional deformation of the supporting structure governed the first structural mode. As discussed in Section 2.2, the supporting frame exhibits a predominantly open cross-section. Although this configuration provides adequate bending stiffness, it inherently offers limited torsional stiffness because open sections have a relatively low torsional constant.
The theory of thin-walled structures shows that closed sections develop significantly higher torsional stiffness than open sections with comparable dimensions and mass. Open sections resist torsional loads primarily through Saint-Venant torsion, whereas closed sections develop continuous shear flows around their perimeter. As a result, the torsional constant increases substantially, leading to a corresponding increase in torsional stiffness.
These considerations guide the design philosophy adopted for all the structural modifications proposed in this chapter, which convert the supporting structure into a boxed section.

6.2 Intervention Proposals for "*Version 1*"

6.2.1 Proposal 1 - Partial boxing

Description

The first proposed modification consists of introducing a 20 mm thick steel plate welded to the lower longitudinal beams of the supporting structure. The additional plate provides a partial closure of the "Version 0" open section, increasing the torsional stiffness of the frame while requiring only limited manufacturing operations. The reinforcing plate is approximately 2 m long. The process air pipes connected to the plenum intentionally limit its length, as shown in Fig. 6.1. Extending the plate beyond this region would interfere with both the existing piping layout and the assembly operations required for flange bolting and maintenance. Consequently, the proposed solution represents the maximum degree of section closure achievable by introducing a single reinforcing plate, while preserving the current machine architecture and ensuring full accessibility to the surrounding components.

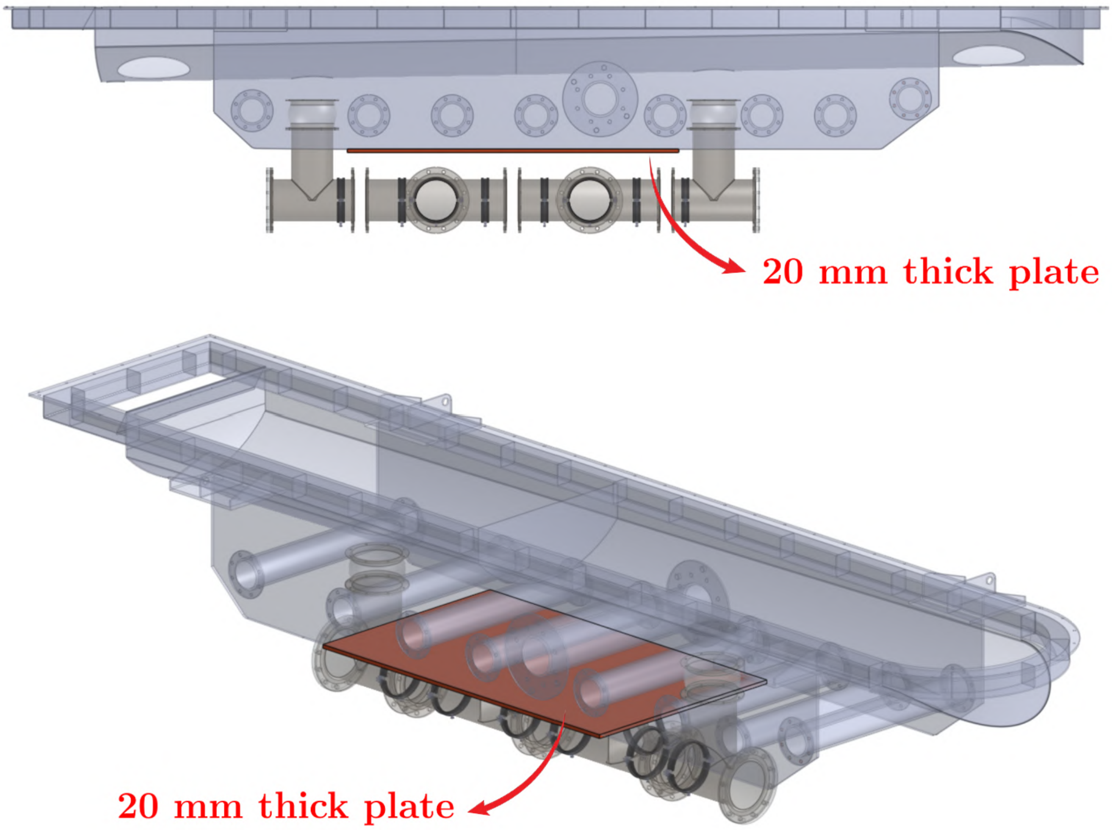

Figure 6.1: *Structure layout for "Proposal 1": partial boxing through 20 mm plate*

Vibration isolators assessment

As discussed in Section 6.1.2, the evaluation of each proposed modification begins with a verification of the vibration isolation system to confirm that its dynamic response remains substantially unchanged. The modal analysis then examines the first six rigid-body modes of the suspended assembly to ensure that they lie within the frequency range required for the desired isolation performance.

Tab. 6.1 reports the rigid-body natural frequencies obtained for the configuration under investigation. All six modes remain within, or below, the target frequency range defined in Section 2.4, which corresponds to a degree of uncoupling between 80% and 90%.Therefore, the proposed structural modification does not compromise the effectiveness of the existing suspension system.

Table 6.1: *Rigid-body modes - Proposal 1*

Mode	**Frequency [Hz]**	**DoF**
1	2.6	T_Z
2	2.7	T_X
3	3.5	R_Y
4	4.0	T_Y
5	4.2	R_X
6	5.0	R_Z

As a consequence, the proposed modification would not require any changes to the currently adopted vibration isolators.

Structural modal assessment

Tab. 6.2 reports the flexible-body natural frequencies obtained for Proposal 1. The following discussion focuses on the first structural mode because it represents the critical mode associated with the resonance phenomena identified in the previous chapters.

Table 6.2: *Proposal 1 - Flexible natural frequencies*

Mode	**Frequency [Hz]**	**Shape**
First natural frequency	**15.8**	**Torsional**
Second natural frequency	31.9	Flexural
Third natural frequency	37.5	Torsional

The closing plate significantly increases the first natural frequency, confirming the effectiveness of the adopted boxing strategy. However, the first mode retains its predominantly torsional character. Compared with the "Version 0" configuration, the additional plate markedly reduces the torsional deformation in the reinforced region, as illustrated in Fig. 6.2(b). The boxed section behaves as a considerably stiffer structural component, whereas the unboxed region continues to experience significant rotation. This result confirms the effectiveness of the local increase in torsional stiffness while also showing that the unboxed regions still govern the global structural response.

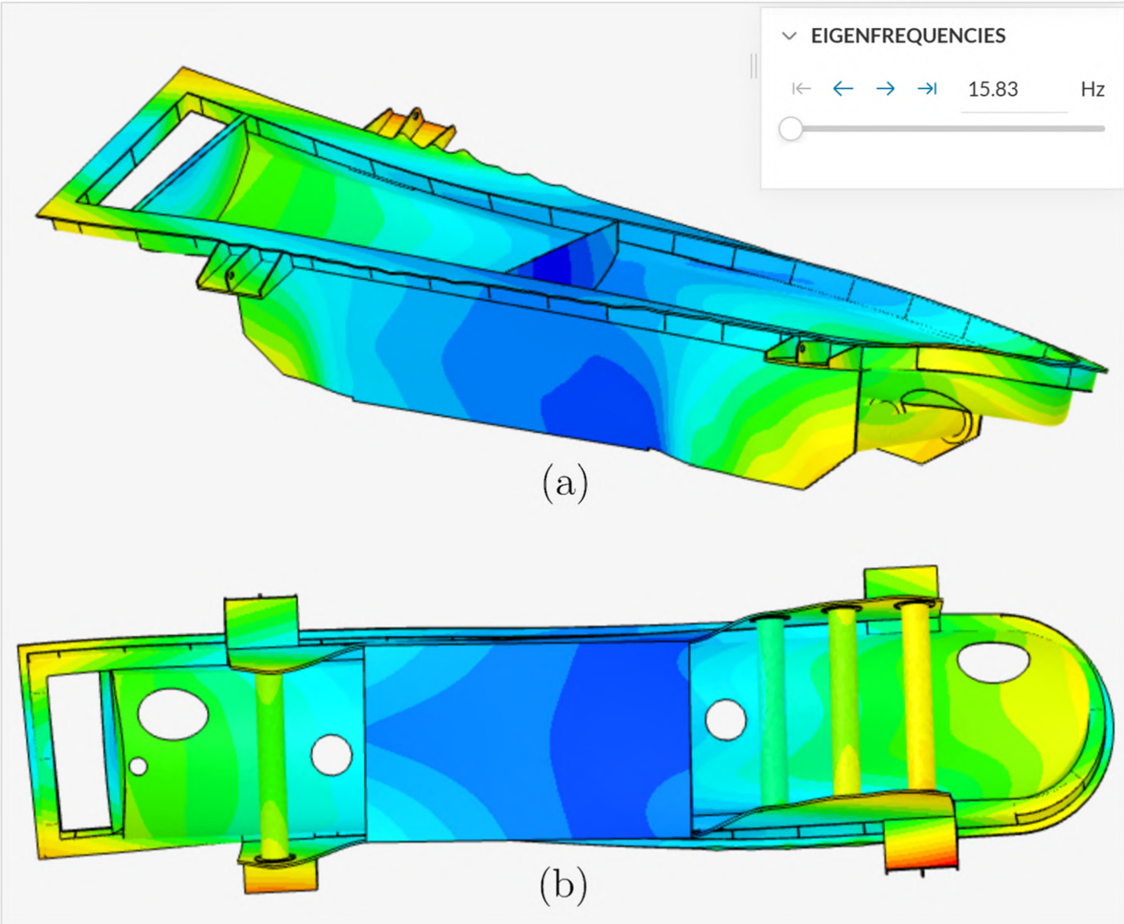

Figure 6.2: *Proposal 1 - First mode shape: (a) three-dimensional view, (b) bottom-view.*
Source: author's elaboration using SimScale

Engineering discussion

The results obtained for Proposal 1 demonstrate that even a relatively simple structural modification can produce a significant increase in the first natural frequency while requiring limited manufacturing effort and preserving the existing machine layout. The proposed intervention therefore represents an effective and practically feasible application of the boxing strategy.

Despite this improvement, two factors may still shift the first natural frequency into the critical range of 12.5 Hz ±25%. First, although the numerical model reliably represents the machine behavior, the predicted natural frequencies inevitably retain a certain degree of uncertainty. Second, the analyses presented in this chapter consider empty-machine conditions, whereas normal operation involves approximately

one ton of processed material. This additional mass should reduce the natural frequencies of the system and may shift the first mode back into the critical range.
As discussed in Section 6.1.2, the proposed configurations do not allow a reliable evaluation of the machine behavior under operating conditions with product. Therefore, although the proposed intervention successfully shifts the first natural frequency outside the critical range, the available margin does not guarantee robust separation from the excitation frequency under all operating conditions.
For this reason, the following proposal extends the boxing strategy by introducing an additional closing plate in a region not occupied by the plenum air pipes. This modification further increases the torsional stiffness of the supporting structure and provides a larger separation between the first natural frequency and the excitation frequency.
Although Proposal 1 improves the dynamic response, it primarily offers a practical retrofit solution for existing machines. The intervention requires limited structural modifications but cannot achieve the performance of a re-design specifically developed to increase torsional stiffness.

6.2.2 Proposal 2 - Extended boxing

Description

Proposal 2 directly extends the boxing strategy introduced in Proposal 1. The modal analysis of the previous configuration showed that the additional closing plate effectively increased the stiffness of the boxed region, while also revealing that the remaining open portion of the supporting frame still governed the global dynamic response of the structure.
To further increase the frame stiffness, the proposed solution introduces a second 20 mm closing plate in the portion of the structure located beyond the plenum air pipes, as shown in Fig. 6.3.
By extending the boxed region, this modification should produce a larger increase in the first natural frequency, thereby providing greater separation from the excitation frequency and reducing the uncertainty margins discussed in the previous section.

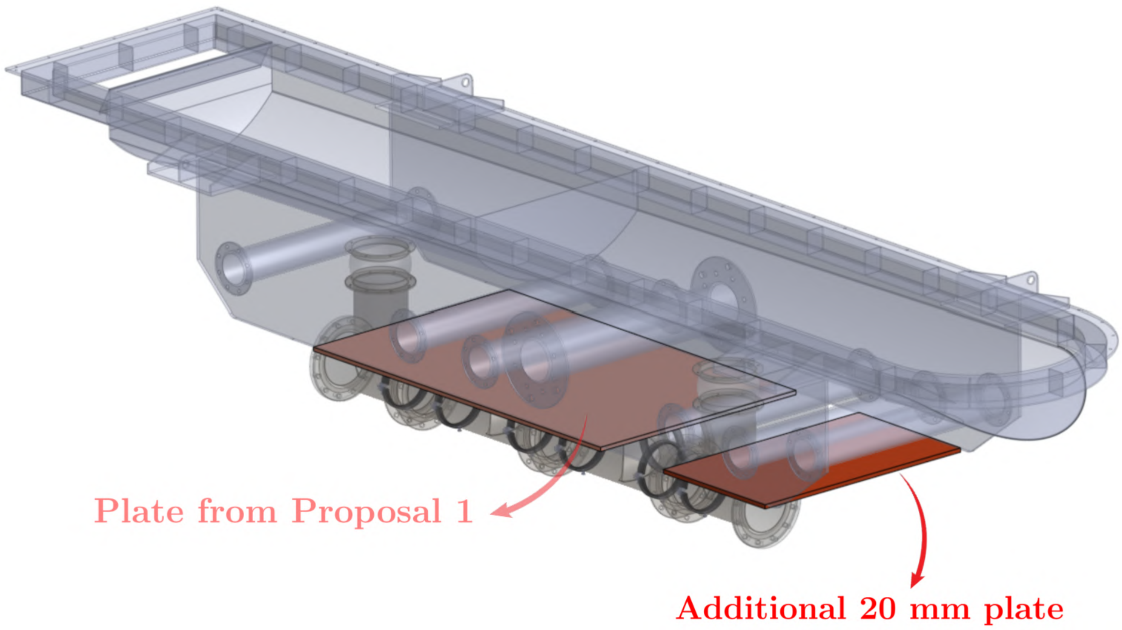

Figure 6.3: *Structure layout for "Proposal 2": extended boxing through additional 20 mm plate*

Vibration isolators assessment

Tab. 6.3 reports the rigid-body natural frequencies obtained for Proposal 2 . Similarly to Proposal 1, all six rigid-body modes remain within the frequency range required to ensure the desired degree of vibration isolation.
The additional structural modifications therefore do not significantly affect the dynamic behavior of the suspended assembly, and the existing vibration isolators continue to provide the intended level of decoupling from the supporting structure.

Table 6.3: *Rigid-body modes - Proposal 2*

Mode	**Frequency [Hz]**	**DoF**
1	2.6	T_Z
2	2.6	T_X
3	3.5	R_Y
4	3.9	T_Y
5	4.1	R_X
6	4.9	R_Z

Structural modal assessment

Tab. 6.4 reports flexible-body natural frequency. As for the previous configuration, from a dynamic standpoint, the most relevant mode is the first one, which requires a particular discussion.

Table 6.4: *Proposal 2 - Flexible natural frequencies*

Mode	Frequency [Hz]	Shape
First natural frequency	**17.7**	**Torsional**
Second natural frequency	31.5	Flexural
Third natural frequency	37.6	Torsional

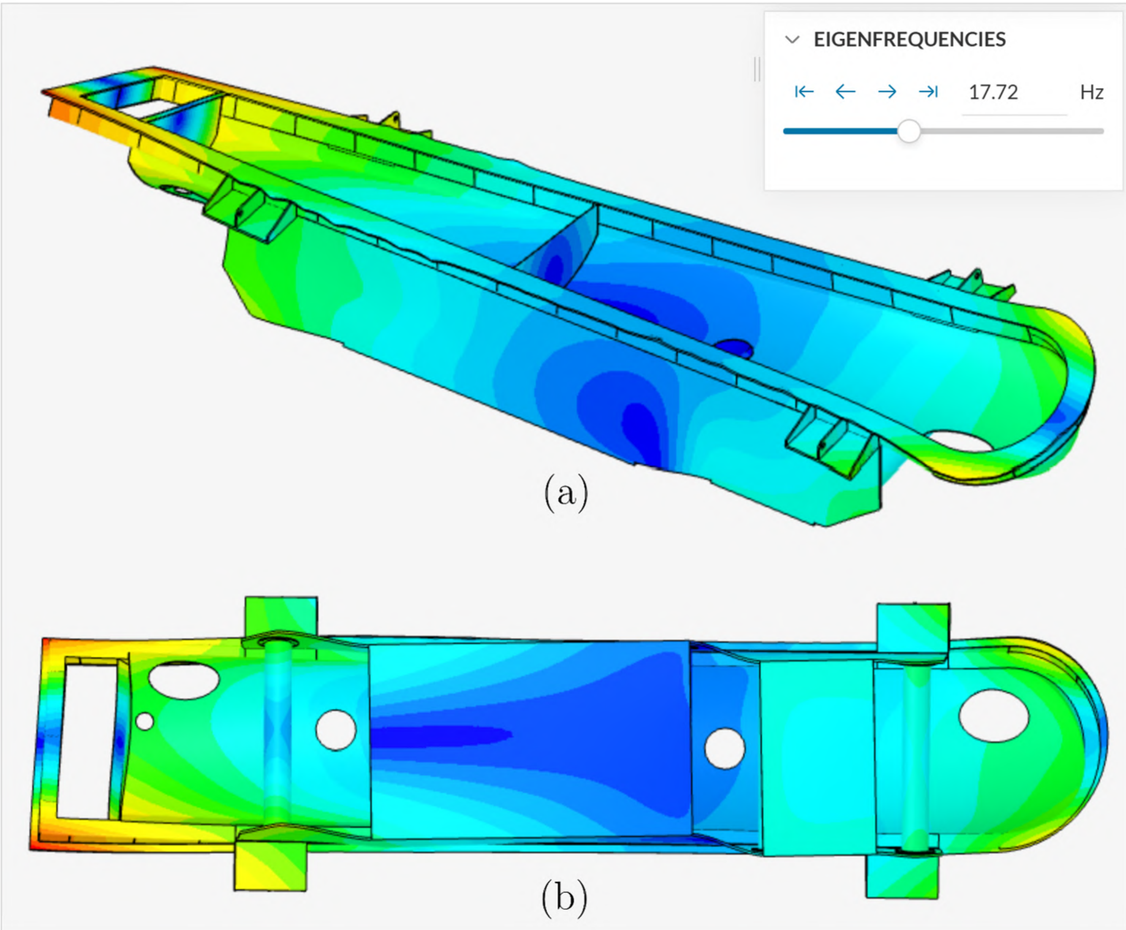

Figure 6.4: *Proposal 2 - First mode shape: (a) three-dimensional view, (b) bottom-view.*
Source: author's elaboration using SimScale

The additional closing plate further increases the first natural frequency, which rises from 15.8 Hz in Proposal 1 to 17.7 Hz. This result confirms the effectiveness of extending the boxed region and demonstrates the strong influence that the achieved degree of section closure has on structural response.
The corresponding modal shape is shown in Fig. ??. The first mode remains predominantly torsional in nature, but the deformation becomes increasingly concentrated in the portions of the structure that remain open.
The result is a substantial upward shift of the first natural frequency while preserving the existing machine layout.
It is worth noting that the second and third natural frequencies remain almost unchanged with respect to Proposal 1. This observation suggests that the proposed modification constitutes a targeted intervention aimed at increasing the torsional stiffness of the supporting frame and shifting the first natural frequency away from the critical operating range.

Engineering discussion

Extending the section closure to an additional portion of the supporting frame further increases the first natural frequency. The resulting value of 17.7 Hz provides substantially greater separation from the excitation frequency than Proposal 1. This frequency margin is sufficiently large to reasonably exclude resonance during normal operation, even after accounting for the additional mass of the processed product.
From a dynamic standpoint, however, the first mode still exhibits a global torsional deformation of the supporting structure. This observation motivates a final design concept. Rather than introducing additional local modifications to the existing machine, the proposed solution completely re-designs the supporting frame to eliminate the open-section behavior responsible for the observed deformation pattern and to achieve significantly higher stiffness in both bending and torsion.
Proposal 2 offers the best compromise between dynamic effectiveness, manufacturing complexity, and implementation cost for machines already in service. It provides a substantial increase in the first natural frequency while limiting additional mass and preserving the existing structural layout.

6.3 Structure Re-Design Proposal

6.3.1 Design Concept

Although Proposal 2 provides a satisfactory increase in the first natural frequency, the modal analyses show that the fundamental structural behavior of the machine remains essentially unchanged. The first mode still exhibits a global torsional deformation of the supporting frame, indicating that the open-section nature of the "Version 1" structure continues to govern its dynamic response. To explore the full potential of the design principles discussed throughout this chapter, the following proposal completely re-designs the supporting structure.
The proposed re-design develops a structural concept that simultaneously increases both torsional and bending stiffness while preserving the functional requirements and geometric constraints imposed by the existing machine. In particular, the design retains the layout of the vibration isolators, the geometry of the upper trough, and the arrangement of the process air pipes connected to the plenum.
The proposed solution emphasizes structural efficiency and manufacturability. The new design aims to maximize structural stiffness while minimizing the required amount of material. Furthermore, the concept assumes welded structural connections throughout, thereby avoiding the complexity, assembly effort, and local compliance associated with bolted joints. As a result, the proposed structure combines high stiffness with a relatively simple manufacturing process.
The primary objective of the proposed re-design extends beyond increasing the first natural frequency. It demonstrates how an appropriate structural concept can simultaneously achieve high stiffness, robust dynamics, and efficient material utilization while satisfying the practical constraints of the existing machine.

6.3.2 Structure Layout

The re-designed supporting structure preserves the functional interfaces of the existing machine while modifying the structural architecture responsible for its behavior. In particular, the design retains the four support plates connected to the vibration isolators and the lower plenum, since these components define the interface with the main frame anchored to the concrete foundation and with the process equipment.
Similarly, the two longitudinal plates supporting the motovibrators remain fundamental structural members. The new design preserves the 15 mm thickness adopted

in "Version 1", thereby ensuring compatibility with the existing motor arrangement and maintaining sufficient local stiffness where the excitation forces act. However, these members have a simplified geometry. Unlike Versions 1 and 2, where the plates incorporate extended tapered regions near their ends, the re-designed configuration adopts an almost rectangular profile, extending the boxed section over a larger portion of the machine length.

The primary structural modification introduces a continuous 10 mm thick closing plate welded to the lower side of the longitudinal members. Unlike Proposals 1 and 2, where the air pipes interrupted the closing plates, the re-designed structure allows the boxed section to extend over the entire available length of the frame. To preserve accessibility for assembly and maintenance of the air distribution system, the design incorporates two large openings aligned with the process air pipes.

Within the boxed section, a transverse tubular member directly connects to the two motovibrator support plates. This element has the same cross-section and performs the same structural function originally envisaged for "Version 1", but the new design integrates it completely through welded connections.

Two V-shaped braces on each side of the structure provide additional stiffness by reducing both bending and torsional compliance. The design connects the upper ends of the braces exclusively to the longitudinal side plates, without extending the connection to the lower trough. This solution simplifies the fabrication of the bracing members and avoids welding operations in the lower trough. Since the lower trough consists of thin stainless-steel plates, welding in this region would require dedicated procedures and increase manufacturing complexity.

Fig. 6.5 reports the re-designed arrangement of the structure.

The tubular profiles adopted for the bracing system correspond to the same sections originally used as transverse members in "Version 0" of the machine. Similarly, the main transverse member connecting the two motovibrator support plates uses the same profile adopted in "Version 1". This choice primarily provides the opportunity to reuse part of the material recovered from the existing structure in the event of a complete reconstruction.

Although secondary to the structural objectives of the re-design, this approach contributes to a more efficient use of materials and remains consistent with sustainability-oriented engineering principles.

Despite the substantial increase in structural efficiency, the re-designed assembly, including the upper trough, has a total mass of approximately 1985 kg. This value remains fully comparable with that of "Version 1" and demonstrates that the increase in stiffness primarily results from an improved structural layout rather than from a significant increase in material usage.

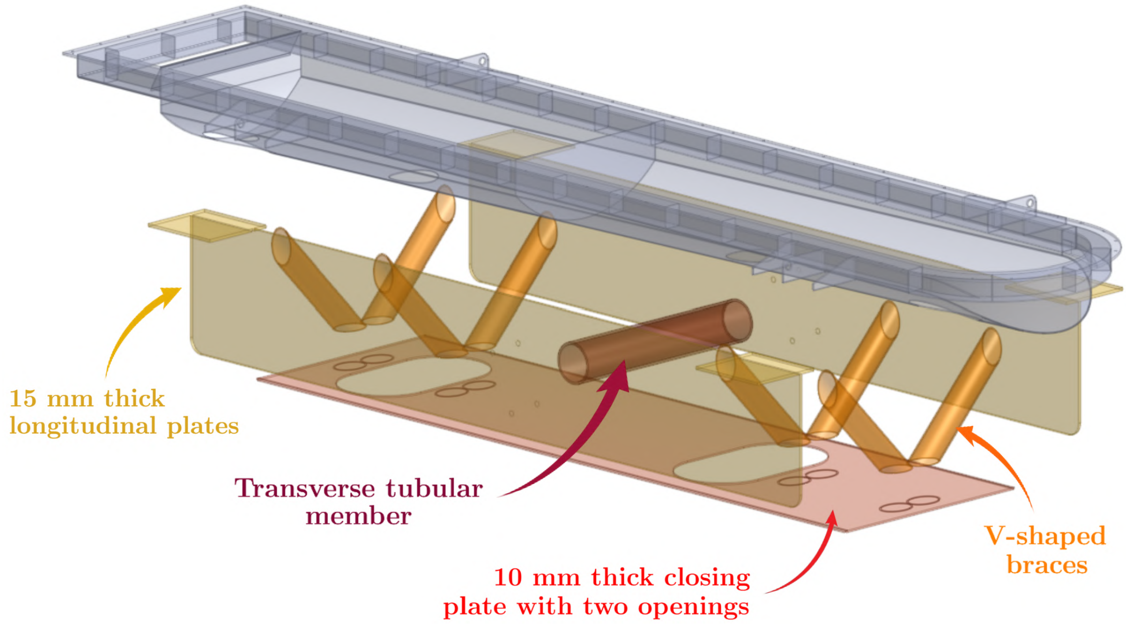

Figure 6.5: *Exploded view of the layout of the re-designed supporting structure*

6.3.3 Modal analysis results

Vibration isolators assessment

Since the re-designed structure has a total mass comparable to that of "Version 1", the rigid-body natural frequencies associated with the vibration isolation system should not vary significantly. Consequently, the dynamic behavior of the suspended assembly should remain substantially unchanged, preserving the vibration isolation performance provided by the existing support arrangement.
Tab. 6.5 reports the rigid-body natural frequencies obtained for the re-designed configuration. A comparison with the values listed in Tab. 5.2 shows only negligible differences, confirming that the re-design has a limited influence on the dynamic characteristics governed by the vibration isolators.

Table 6.5: *Rigid-body modes - Re-design Proposal*

Mode	**Frequency [Hz]**	**DoF**
1	2.8	T_Z
2	2.8	T_X
3	3.5	R_Y
4	3.7	T_Y
5	3.9	R_X
6	4.3	R_Z

As a result, the frequency range associated with the first six rigid-body modes remains fully compatible with the desired degree of vibration isolation. Therefore, the current vibration isolators adopted for "Version 1" also satisfy the requirements of the re-designed structure, without requiring any modification to their layout or stiffness characteristics.

Structural modal assessment

The first three flexible-body natural frequencies obtained for the re-designed configuration are reported in Tab. 6.6. The modal analysis limits to an upper frequency of 50 Hz, corresponding to approximately four times the excitation frequency generated by the motovibrators. This frequency range provides sufficient information to assess the dynamic behavior of the re-designed structure while limiting the computational effort required for the analysis.

Table 6.6: *Re-design Proposal - Flexible natural frequencies*

Mode	**Frequency [Hz]**	**Shape**
First natural frequency	21.1	Local Torsion
Second natural frequency	41.1	Plates Bending
Third natural frequency	45.4	Flexural-torsional

The modal analysis identifies the first natural frequency at 21.1 Hz, and Fig. 6.6 shows the corresponding mode shape. Unlike the previous configurations, where the first mode involved a global deformation of the supporting frame, the re-designed structure exhibits only a limited rotational component localized in the lower trough regions extending beyond the supporting structure. These portions remain relatively flexible because of their thin-walled construction and cantilevered geometry. Since the process layout and the functional requirements of the machine dictate their geometry, significant modifications of these components are not feasible. The resulting mode therefore represents a predominantly local deformation with only a limited contribution to the global response of the machine.

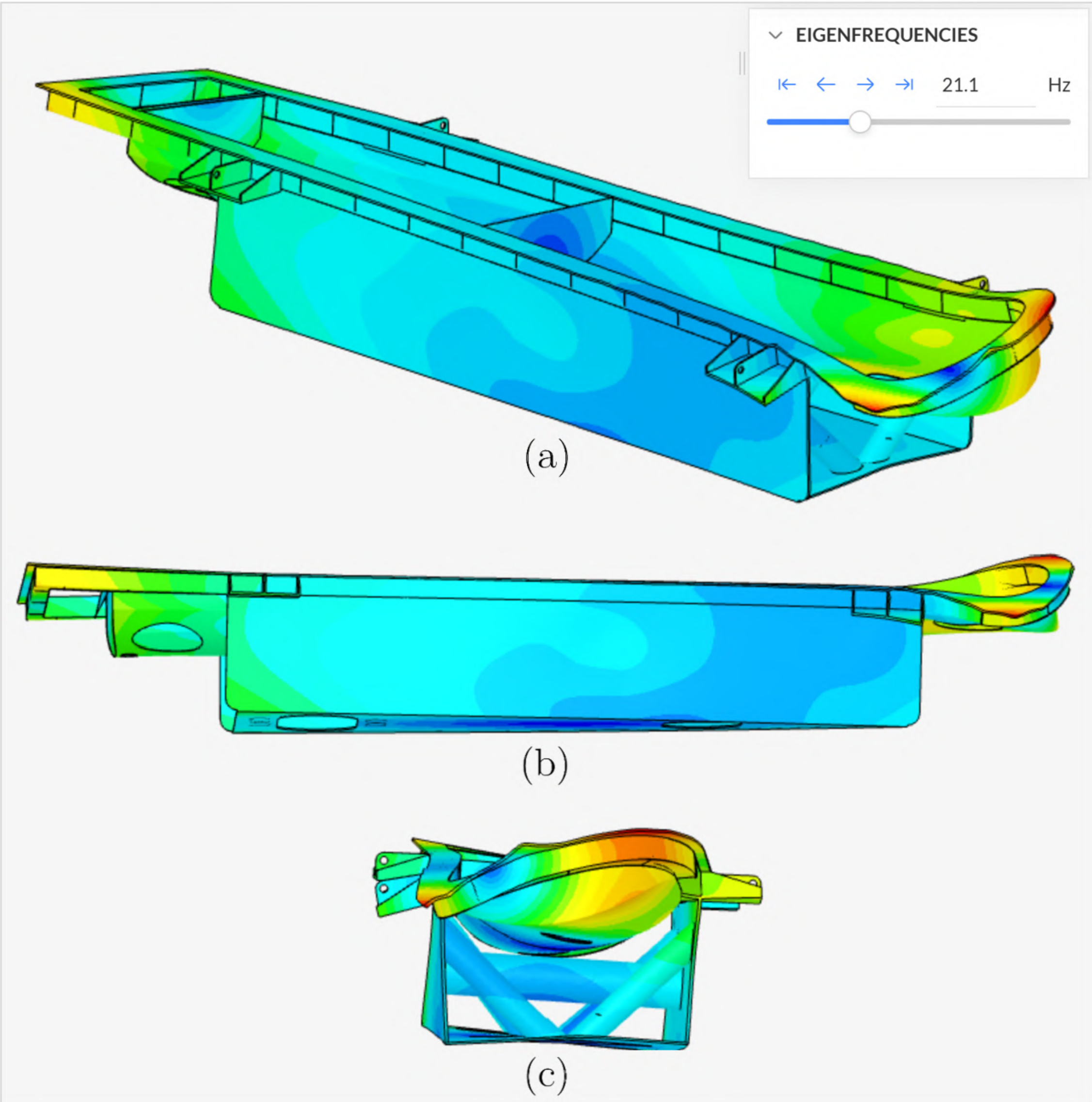

Figure 6.6: *Re-designed structure - First mode shape: (a) three-dimensional view, (b) top-view, (c) lateral view.*
Source: author's elaboration using SimScale

From a dynamic point of view, the first natural frequency is approximately 70%

higher than the excitation frequency of 12.5 Hz. Such a separation is sufficient to exclude resonance phenomena, even accounting for the frequency reduction expected under operating conditions due to the presence of approximately 1000 kg of processed product.
The second natural frequency is equal to 41.7 Hz and the associated shape matches with a bending deformation of plates in correspondence with the central transverse member. As shown in Fig. 6.7, the deformation remains localized and does not involve significant motion of the boxed structure.

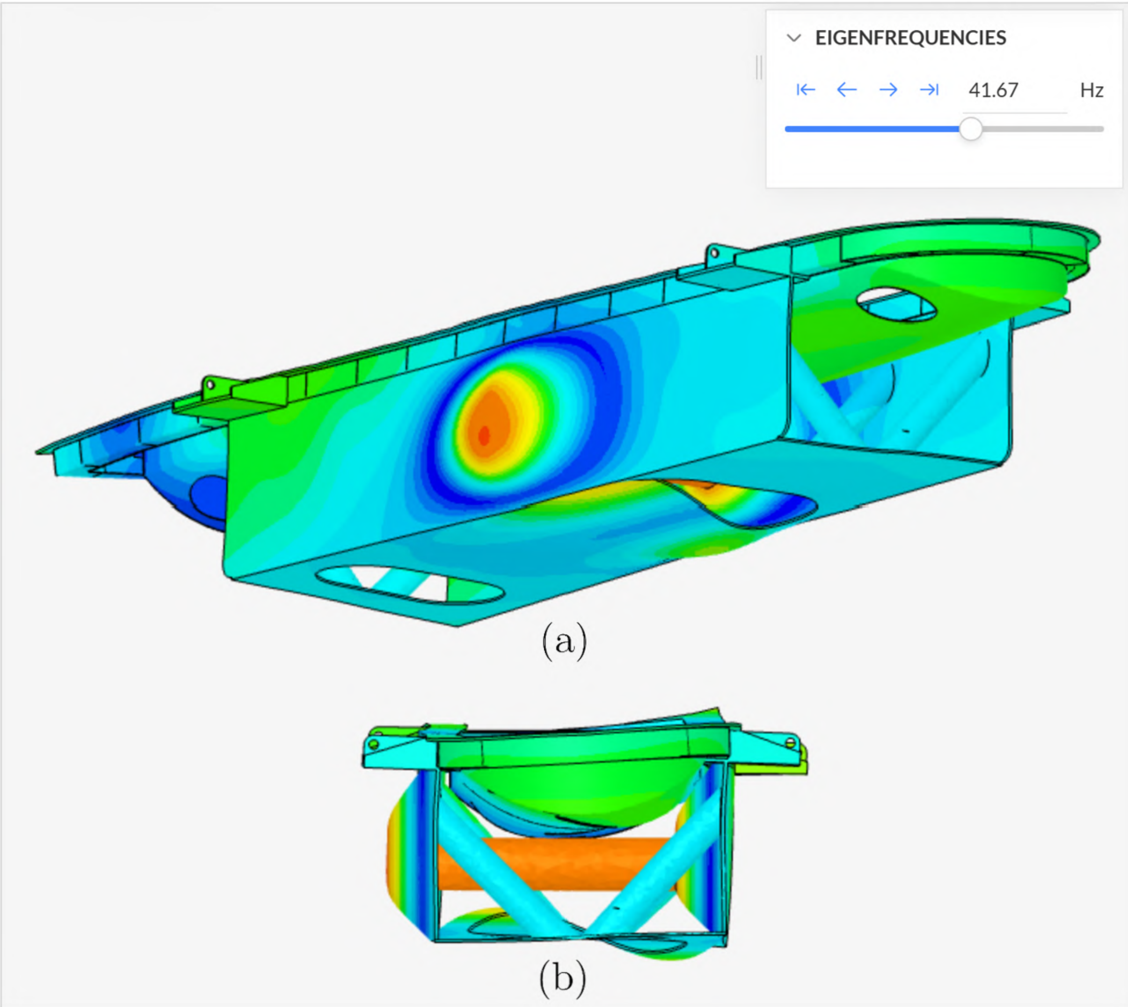

Figure 6.7: *Re-designed structure - Second mode shape: (a) three-dimensional view, (b) lateral view.*
Source: author's elaboration using SimScale

The third natural frequency is 45.4 Hz. The corresponding mode shape exhibits coupled bending–torsion behavior, although horizontal bending clearly dominates the structural response.

The deformation involves a significant portion of the supporting structure, but its natural frequency is more than three times higher than the excitation frequency generated by the motovibrators. Consequently, this mode does not represent a critical dynamic condition.
Overall, the modal analysis confirms that the re-designed structure no longer exhibits the global deformation mechanisms observed in the "Version 0" and "Version 1" machine configurations. Instead, the dominant structural modes occur at significantly higher frequencies, well above the critical excitation range. Consequently, the proposed structural concept would effectively improve the global dynamic behavior of the machine.

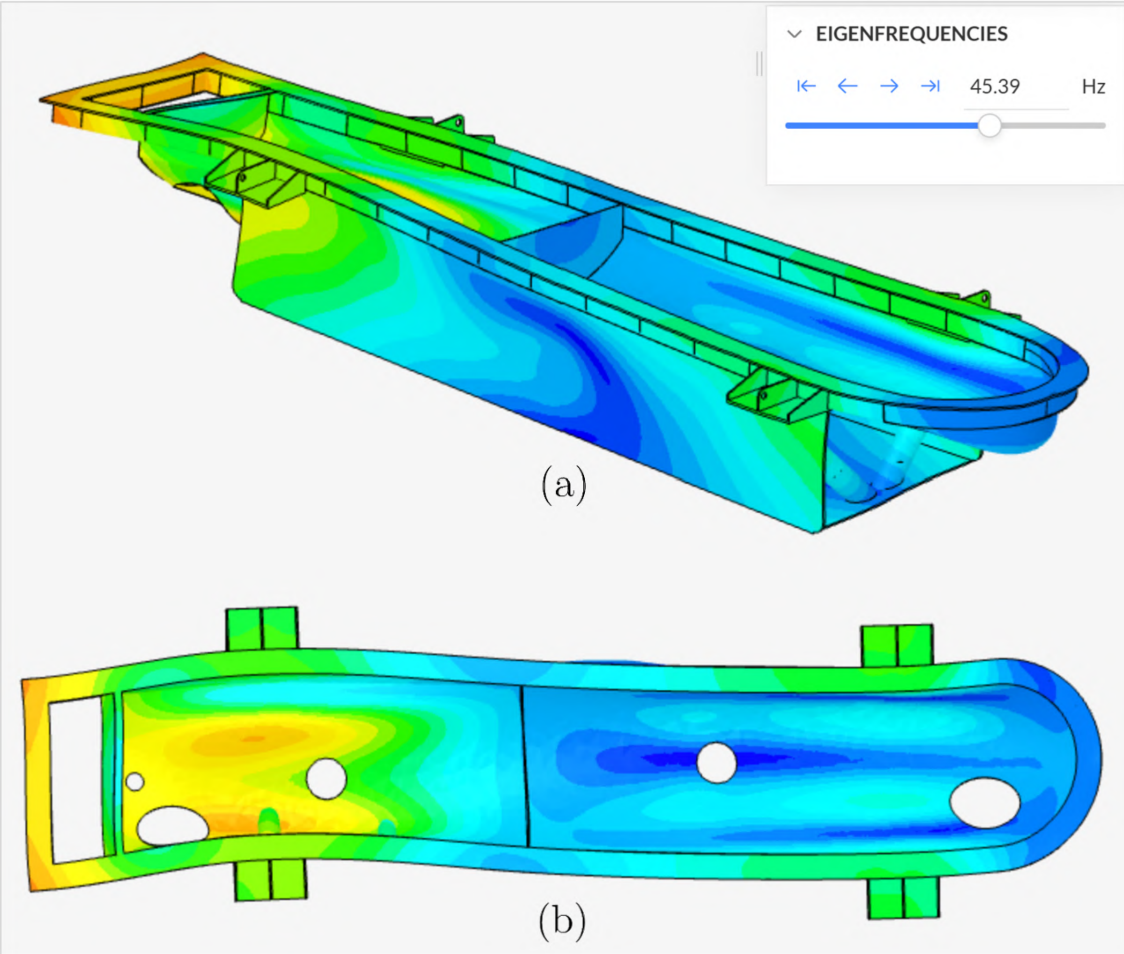

Figure 6.8: *Re-designed structure - Third mode shape: (a) three-dimensional view, (b) top view.*
Source: author's elaboration using SimScale

From a design perspective, the complete re-design demonstrates the value of understanding the governing vibration mechanism before introducing structural modifications. The modal analyses identified the regions that control the torsional stiffness of the supporting frame, allowing the re-design to increase stiffness only where it effectively influences the first vibration mode. This targeted approach improves the system dynamics while limiting the additional structural mass.

6.4 Summary of Proposed Solutions

The analyses presented in this chapter demonstrate that all the investigated interventions improve the dynamic behavior of the machine by increasing the first natural frequency and reducing the likelihood of resonance with the operating excitation generated by the motovibrators.
Proposal 1 requires only limited manufacturing effort and introduces a single closing plate. This modification increases the first natural frequency to 15.8 Hz. However, the available frequency margin remains relatively small, and the first mode continues to exhibit a global torsional deformation of the supporting structure.
Proposal 2 extends the same design philosophy by increasing the degree of section closure. The resulting first natural frequency of 17.7 Hz provides substantially greater separation from the excitation frequency, making resonance unlikely even under operating conditions. Nevertheless, the first mode retains its global torsional character, indicating that the fundamental structural behavior remains essentially unchanged.
The complete re-design addresses the problem from a different perspective by adopting a fully boxed and braced supporting frame. This solution increases the first natural frequency to 21.1 Hz while eliminating the global torsional deformation mechanism. Moreover, it achieves this improvement without a significant increase in structural mass. The total mass of the re-designed assembly remains comparable to that of the "Version 1" machine operating at the time of writing of this thesis.
Overall, the analyses presented in this chapter confirm the effectiveness of the proposed design strategies and provide technically feasible solutions for mitigating the resonance phenomena identified in the previous chapters.

Chapter 7

Conclusions

7.1 Problem Statement

The present work originated from an industrial reliability issue involving a vibrating dryer employed in the processing of organic natural acid crystals. Although the machine design aimed to operate under controlled oscillatory motion, fatigue cracks developed in the supporting structure after approximately 150 hours of operation, raising concerns about the possible occurrence of resonance phenomena.
The observed damage was particularly significant because vibration represents an essential functional requirement of the process itself. In fact, the investigated dryer relies on mechanical oscillations to ensure both product transport and drying efficiency. Consequently, the engineering challenge was not to suppress vibration, but rather to distinguish between the beneficial oscillatory motion required by the process and the excessive dynamic amplification associated with resonance conditions.
Preliminary investigations suggested that the excitation frequency generated by two rotating eccentric masses could coincide with one of the structural natural frequencies. However, the available experimental information did not provide a complete understanding of the dynamic mechanisms responsible for the observed failures or identify effective corrective actions.
Within this context, the objective of the thesis extended beyond verifying the presence of resonance. The work aimed to develop a physically representative interpretation of the machine dynamics and identify the structural features governing the critical vibration mode. It then translated this understanding into practical design solutions capable of eliminating the resonance condition while preserving the functional requirements of the equipment.

7.2 Experimental Evidence

The first indication of a resonance-related issue emerged during the experimental campaign on the "Version 0" machine configuration. Impact hammer testing revealed two dominant natural frequencies at approximately 12.5 Hz and 32 Hz, with the first resonance peak coinciding with the operating excitation frequency generated by the motovibrators. This result provided direct evidence that the machine operated under resonance conditions, explaining the excessive vibration levels and the premature development of fatigue cracks.

The forced vibration measurements further supported this interpretation. While the vibration isolation system proved effective in limiting the transmission of vibrations to the supporting frame, the dynamic response of the vibrating assembly exhibited characteristics typically associated with structural flexibility. In particular, the persistence of significant harmonic content suggested that structural flexibility, rather than the suspension system, governed the observed dynamic amplification.

Based on these findings, the objective of increasing the stiffness of the supporting frame guided a structural modification. The aim was to shift the critical natural frequency away from the operating range. Since the modal shape associated with the resonance condition was unknown, the design assumed that the flexural deformation of the frame primarily caused the observed structural weakness. Consequently, the modification targeted an increase in bending stiffness, relying on the available experimental evidence and engineering judgment rather than on a complete understanding of the deformation mechanism governing the resonance phenomenon.

A second experimental campaign then investigated the "Version 1" configuration. The measurements identified the first natural frequency at approximately 11.5 Hz. At first glance, this result could suggest that the structural intervention had been ineffective, since the resonance condition appeared to persist. However, unlike the original tests, the machine operated with approximately one ton of processed product inside the trough. This additional mass significantly altered the dynamic characteristics of the system, preventing a direct assessment of the actual contribution of the structural reinforcement based solely on the experimental observations.

The experimental investigations therefore fulfilled two fundamental objectives. First, they confirmed the existence of resonance phenomena and provided reliable reference data for identifying the critical frequencies. Second, they highlighted the limitations of an exclusively experimental approach. Although the tests clearly revealed the presence of a dynamic problem, they could neither explain the deformation mechanisms associated with the critical modes nor quantify the actual effectiveness of the implemented modification. These limitations ultimately motivated the development of a numerical model capable of reproducing the physical behavior of the machine and providing access to information unavailable from the experimental campaign alone.

7.3 Numerical Modeling Strategy

The limitations of the experimental investigations naturally motivated the development of a numerical model. While the experimental campaigns successfully identified the frequencies associated with the resonance phenomenon, they could not provide information about the corresponding mode shapes. As a result, the experimental investigation could not directly interpret the physical mechanism governing the observed dynamic behavior or evaluate alternative structural modifications before their implementation. Therefore, a numerical approach became necessary. The need was to reproduce the measured dynamic response of the machine, identify the deformation patterns associated with the critical vibration modes, and provide a predictive tool for evaluating future design solutions.
The development of the Finite Element models followed a clear objective: achieving a reliable representation of the global dynamic response of the machine while avoiding unnecessary modeling complexity. For this reason, the modeling strategy followed a stiffness hierarchy approach. The model explicitly represented only the components expected to significantly influence the structural dynamics, whereas equivalent mass representations replaced the secondary elements. This choice allowed the model to retain the physical characteristics governing the modal response while maintaining a reasonable computational cost.
While the equivalent representation of the motovibrators is relatively straightforward, the upper trough required significantly greater attention. The motovibrators behave as concentrated masses connected to the structure through highly stiff interfaces. Remote masses located at their centers of gravity represent their inertial properties. The upper trough, on the other hand, contributes a large distributed mass over the entire length of the machine. Its equivalent representation had to reproduce not only the total mass, but also its distribution and the associated inertial effects governing the global dynamic response of the structure.
An equally important aspect concerned the representation of the processed product in the "Version 1" machine configuration. The interaction between the granular acid crystals and the vibrating structure is intrinsically complex, involving impacts,

friction, and continuously evolving contact conditions. An exact description of such phenomena would require a fully nonlinear multiphysics approach, far beyond the scope of the present work. Rather than pursuing an unnecessarily sophisticated representation, the numerical model represented the product through an equivalent formulation specifically calibrated to reproduce its influence on the global modal response. Although simplified, this approach successfully captured the dominant inertial effects introduced by the approximately one ton of material contained within the machine during the experimental campaign.

The comparison with the available experimental data ultimately assessed the reliability of the adopted modeling strategy. Throughout this work, a maximum relative error of 2% defined the acceptance criterion for model validation.

For the "Version 0" machine configuration, the model reproduced the first natural frequency identified during the experimental campaign, which constituted the primary validation target. More importantly, the model also accurately predicted the second natural frequency, experimentally observed at approximately 32 Hz, despite not using it as a validation parameter. The independent agreement of two distinct vibration modes provides additional confidence in the adopted modeling assumptions.

The "Version 1" configuration showed a similarly good correlation. In this case, the equivalent stiffness representing the interaction between the processed product and the supporting structure was the only calibrated parameter. Despite the additional uncertainty associated with this simplified representation, the resulting model satisfied the validation criterion and therefore provided a sufficiently representative description of the actual system dynamics.

The resulting Finite Elements models therefore constitute more than a simple correlation with the experimental measurements. They provide a physically consistent representation of the machine dynamic behavior, sufficiently accurate to investigate the modal characteristics responsible for resonance and sufficiently robust to support the development and assessment of new structural solutions.

7.4 Interpretation of the Dynamic Behavior

The validated numerical models provided access to information unavailable from the experimental investigations alone. The modal analyses performed throughout this work enabled a physical interpretation of the machine dynamic behavior and ultimately clarified the origin of the observed structural failures.

A first important result concerns the role of the vibration isolation system. The modal analyses with elastic supports showed that all rigid-body modes lie within the frequency range required to guarantee adequate separation from the operating excitation generated by the motovibrators. This observation excludes the possibility that the experimentally observed resonance originated from the suspension system and confirms that the vibration isolators perform their intended function correctly.
The investigation of the flexible structural modes led to a substantially different conclusion. For the "Version 0" machine configuration, the first natural frequency corresponds to a coupled flexural–torsional deformation of the supporting structure. Although bending contributes to the deformation, the mode shape clearly reveals a dominant torsional response. This result is fully consistent with the structural architecture of the machine, whose supporting frame has a predominantly open cross-section and therefore relatively low torsional stiffness.
The identification of this deformation mechanism also provided a plausible interpretation of the fatigue damage observed during operation. The mode shape revealed a global rotation of the supporting structure about its longitudinal axis, indicating that the transverse tubular members underwent cyclic torsional loads. Under these conditions, the welded joints connecting the tubes to the longitudinal plates should experience alternating circumferential stresses, providing a physically consistent explanation for crack initiation and propagation.
The analyses also explained the limited effectiveness of the structural modification implemented on the machine, which followed the assumption that the main plates primarily exhibited bending flexibility. The numerical results showed that the modification effectively increased the structural stiffness. However, the resulting increase in the first natural frequency was not sufficient to move it outside the critical operating range associated with the excitation frequency. Furthermore, the first vibration mode continued to be governed by the torsional compliance of the supporting frame. This finding represents one of the most significant outcomes of the present work, as it transformed the understanding of the problem into a clearly identified torsional design issue. The interpretation of the modal behavior therefore provided both an explanation of the observed failures and a rational basis for developing targeted structural modifications. Consequently, the design effort could focus on increasing torsional stiffness, leading to more efficient and physically justified engineering solutions.

7.5 Design Implications

The numerical investigation identified the torsional stiffness of the supporting frame as the key parameter governing the first natural frequency. Consequently, all proposed structural modifications aim to increase this property as efficiently as possible.
Each proposed solution aims to move the first natural frequency outside the critical operating range without compromising the functionality of the machine. At the same time, the vibration isolation system must preserve its original performance without adversely affecting the rigid-body dynamics of the suspended assembly.
The proposed solutions followed a common design philosophy based on the progressive increase of the torsional stiffness of the supporting frame. Since the "Version 0" structure behaves predominantly as an open section, the design progressively introduces closed structural paths through the addition of boxing plates. This approach exploits the well-known increase in torsional stiffness associated with closed thin-walled sections.
Proposal 1 introduced a local reinforcement that would require limited manufacturing effort. Proposal 2 extended the same concept to achieve a larger increase in the first natural frequency and a greater separation from the critical operating range. Finally, the re-design proposal removes the geometric limitations of the current supporting frame and investigated the maximum improvement achievable while preserving the functional interfaces of the machine.
This progressive approach enabled the evaluation of different engineering solutions from both dynamic and practical perspectives. Rather than identifying a single optimal solution, the proposed configurations offered different compromises between manufacturing effort, additional structural mass, and frequency shift.

7.6 Comparison of Proposed Solutions

Tab. 7.1 summarizes the effectiveness of the proposed structural modifications. Since the proposed interventions aim to improve the machine operating at the time of writing this thesis, the comparison adopts "Version 1" as the reference configuration. This approach directly quantifies the expected benefit of each solution with respect to the existing industrial machine.
The comparison considers not only the increase in the first natural frequency but also the corresponding variation in structural mass. To evaluate this trade-off, the

table introduces an efficiency index defined as the ratio between the relative increase in the first natural frequency and the corresponding relative increase in structural mass. This parameter quantifies how effectively each intervention converts additional mass into dynamic improvement. Higher values indicate a greater increase in natural frequency for the same relative increase in structural mass, providing a consistent basis for comparing the proposed design solutions.

Table 7.1: *Comparison of the dynamic performance of the investigated machine configurations and proposed structural solutions*

Parameter		**"Version 0"**	**"Version 1"**	**Prop. 1**	**Prop. 2**	**Re-Design**
f_1	[Hz]	12.5	14.3	15.8	17.7	21.1
Δf_1 vs "V1"	[Hz]	-	-	1.5	3.4	6.8
	[%]	-	-	10.5	23.8	47.6
Δm vs "V1"	[kg]	-	-	380	515	20
	[%]	-	-	19.3	26.1	1
$\Delta f_1[\%]/\Delta m[\%]$		-	-	0.54	1.10	47.6

The comparison confirms the effectiveness of the proposed design strategy. All investigated solutions successfully move the first natural frequency further away from the excitation frequency while preserving the required vibration isolation performance. Moreover, the progressive increase in the first natural frequency demonstrates that increasing the torsional stiffness of the supporting frame effectively mitigates the resonance phenomena.

In addition, the comparison shows that material distribution governs structural efficiency more than its quantity. The re-designed structure achieves the largest increase in natural frequency with almost no mass penalty, demonstrating that an appropriate structural concept is considerably more effective than local reinforcement. This outcome also highlights the importance of understanding the governing vibration mechanism before introducing structural modifications, since only a physically informed re-design can distribute material where it provides the greatest structural benefit.

From an engineering perspective, the preferred solution depends on the available intervention scope. If the purpose is to modify the existing machine, Proposal 2 represents the most suitable solution. It increases the first natural frequency beyond the critical operating range while requiring only a limited increase in structural

mass. Furthermore, it achieves the highest efficiency among the retrofit solutions, demonstrating the most favorable balance between dynamic improvement and additional material.
Conversely, for a new manufactured machine, the re-design proposal represents the most effective structural solution. Besides providing the greatest separation between the excitation frequency and the first natural frequency, it achieves this result with only a marginal increase in structural mass. Consequently, it exhibits by far the highest efficiency index, confirming that redesigning the supporting frame is considerably more effective than simply reinforcing the existing structure.

7.7 Limitations and Future Work

Despite the good agreement achieved between the numerical models and the experimental results, some limitations remain.
The representation of the processed material relies on an equivalent linear model specifically developed to reproduce its influence on the global dynamic behavior of each machine configuration. Although this approach proved sufficiently accurate for modal validation, it cannot reproduce the complex nonlinear interaction between the granular product and the vibrating structure.
Furthermore, the modal analyses and the evaluation of the proposed structural solutions neglect damping. While this assumption does not affect the prediction of natural frequencies and mode shapes, it prevents the direct estimation of vibration amplitudes under operating conditions.
Future work could focus on developing a nonlinear model capable of representing the actual interaction between the processed material and the vibrating structure. Such an approach would provide a more realistic description of the product behavior under operating conditions. Additional investigations could also include harmonic response analyses of the proposed structural solutions in order to evaluate their forced vibration behavior. Finally, fatigue analyses could estimate the expected service life of the most promising configurations after mitigating the resonance condition.

7.8 Final Remarks

This work demonstrates that a physically consistent modeling strategy, supported by experimental evidence, can transform limited experimental observations into a comprehensive understanding of complex structural dynamics. The investigated vibrating dryer serves as the industrial case study for demonstrating the proposed methodology.

The study demonstrates that predictive Finite Element models do not require exhaustive geometric detail. Instead, they require physically consistent engineering assumptions. The proposed modeling strategy captured the dynamic contribution of non-modeled components and processed material through equivalent representations that preserved the essential structural behavior. Experimental validation confirmed the reliability of these assumptions and established the predictive capability of the simulation.

In addition, rather than reproducing measured natural frequencies alone, the FE model explained the physical mechanisms governing the machine dynamic behavior. The modal analyses identified the coupled flexural–torsional deformation responsible for resonance and showed that the limited torsional stiffness of the supporting frame governed the observed fatigue failures. This physical interpretation could not emerge from the available experimental measurements alone.

Finally, the numerical model evolved beyond a validation exercise and became an engineering decision-making tool. This thesis used the model to compare alternative structural solutions before implementation, quantify their dynamic effectiveness, and identify the most efficient design strategy. This capability reduced the need for iterative experimental modifications and provided objective support for engineering decisions.

The proposed methodology extends beyond the investigated dryer. Many industrial cases combine limited experimental data, complex structural assemblies, and practical constraints that prevent complete numerical modeling. In these situations, a physically consistent and experimentally validated modeling strategy can explain the governing dynamic mechanisms and guide structural design with confidence.

Appendix A

The correct selection of suspensions is fundamental. The dryer system, suspended on vibration isolators, can be modeled as a Single-Degree-of-Freedom system with mass m, damping c, stiffness k and harmonic excitation $F(t)$, as shown in Fig. A.1.

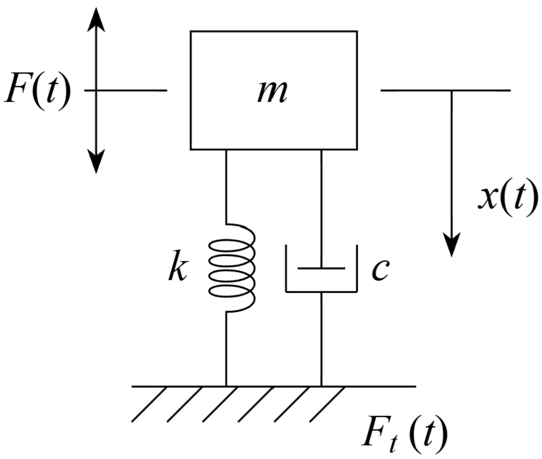

Figure A.1: *Single-Degree-of-Freedom system on rigid foundations*

In the dryer case, the motovibrators give rise to a harmonically varying force $F(t) = F_0 cos\omega t$. The equation of motion of the system is then given by

$$m\ddot{x} + c\dot{x} + kx = F_0 cos\omega t \tag{A.1}$$

Solving Eq. (A.1), the free-response dies out after the transient, while the steady-state response holds as for Eq. (A.2).

$$x(t) = Xcos(\omega t - \phi) \tag{A.2}$$

where

$$X = \frac{F_0}{\sqrt{(k - m\omega^2)^2 + \omega^2 c^2}} \tag{A.3}$$

and

$$\phi = \tan^{-1}\left(\frac{\omega c}{k - m\omega^2}\right) \tag{A.4}$$

The spring and the damper transmit the force $F_t(t)$ to the foundation, so

$$F_t(t) = c\dot{x} + kx = kXcos(\omega t - \phi) - c\omega Xsin(\omega t - \phi) \tag{A.5}$$

F_T is the magnitude of the transmitted force and its formulation is

$$\begin{aligned} F_T &= \left[(kx)^2 + (c\dot{x})^2\right]^{1/2} = X\sqrt{k^2 + \omega^2 c^2} \\ &= \frac{F_0\left(k^2 + \omega^2 c^2\right)^{1/2}}{\left[(k - m\omega^2)^2 + \omega^2 c^2\right]^{1/2}} \end{aligned} \tag{A.6}$$

Transmissibility T_f is equal to the ratio between the amplitude of the transmitted force and the exciting force, so

$$\begin{aligned} T_f = \frac{F_T}{F_0} &= \left\{\frac{k^2 + \omega^2 c^2}{(k - m\omega^2)^2 + \omega^2 c^2}\right\}^{1/2} \\ &= \left\{\frac{1 + (2\zeta r)^2}{(1 - r^2)^2 + (2\zeta r)^2}\right\}^{1/2} \end{aligned} \tag{A.7}$$

where $r = \omega/\omega_n$ is the *pulsation ratio* between the excitation frequency and the natural frequency of the suspension system. Fig. A.2 shows the variation of the transmissibility factor T_f as a function of the frequency ratio.

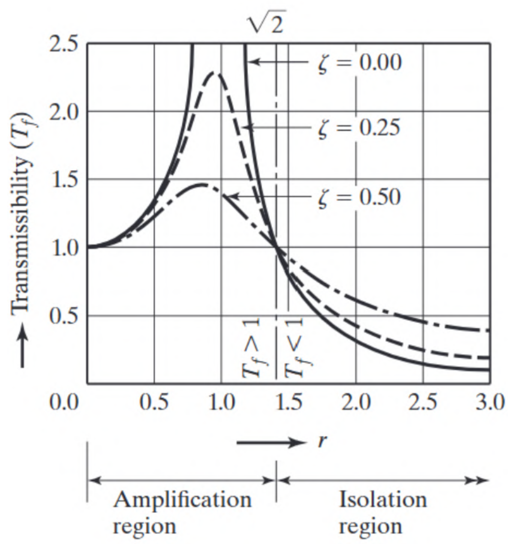

Figure A.2: *Variation of transmissibility T_f with r [1]*

In order to achieve effective vibration isolation, the dynamic force transmitted to the supporting structure must be lower than the excitation force generated by the machine. This condition is satisfied when the transmissibility factor is smaller than unity ($T_f < 1$), meaning that the isolation system attenuates the transmitted vibrations. Conversely, when $T_f > 1$, the transmitted force amplifies. As shown in Fig. A.2, the transition between the amplification region and the isolation region occurs for $r = \sqrt{2}$.
Assuming a small damping ratio ζ, Eq. (A.7) reduces to:

$$T_f = \frac{F_t}{F} \approx \frac{1}{r^2 - 1} \tag{A.8}$$

Unless otherwise stated, this appendix is based on [1].

Appendix B

In Finite Element Analysis, *Rigid Body Elements* (*RBEs*) commonly establish the connection between a remote point and a portion of the structure, whose formulation significantly influences the mechanical response of the numerical model. In particular, distinguishing between *RBE2* and *RBE3* schemes is essential, since they rely on two fundamentally different principles for transferring loads and inertial effects from the remote point to the structural nodes.

The *RBE2* formulation establishes a rigid kinematic relationship between the remote point and the associated nodes. All connected nodes move as a single rigid body, preventing any relative deformation within the selected region. As a result, the formulation introduces artificial stiffness into the numerical model. It is therefore appropriate when the attached component can reasonably be considered infinitely rigid with respect to the surrounding structure or when the model must reproduce a rigid mechanical connection. In SimScale, this formulation corresponds to the *"Rigid"* option available for Remote Displacement and Remote Mass boundary conditions [24], as shown in Fig. B.1.

Conversely, the *RBE3* formulation does not introduce additional stiffness. Instead, it employs weighted interpolation functions to distribute forces, moments, and inertial loads between the remote point and the structural nodes while preserving their relative displacements. Consequently, only the stiffness of the Finite Element domain governs the deformation of the connected region, preserving its local flexibility. This approach transfers loads without altering either the structural stiffness or the deformation pattern. According to the SimScale documentation, this formulation corresponds to the *"Deformable"* option, where an RBE3 interpolation scheme connects the remote point to the selected nodes [25], as shown in Fig. B.2.

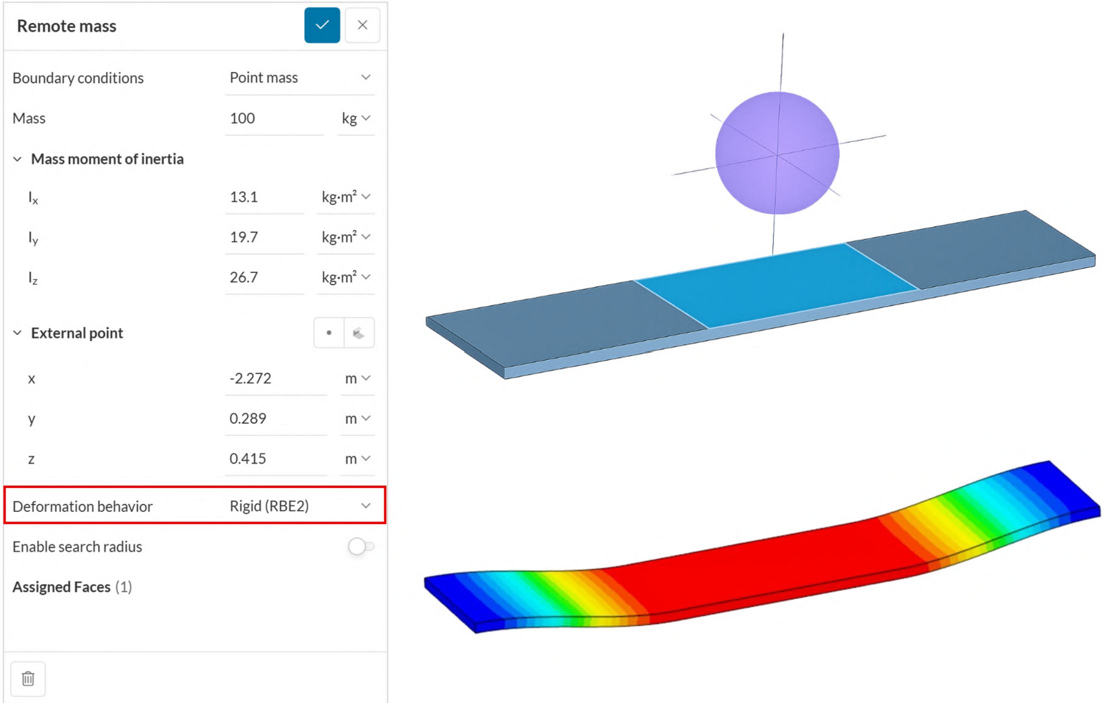

Figure B.1: *RBE2 setup and rigid behavior.*
Source: author's elaboration using SimScale

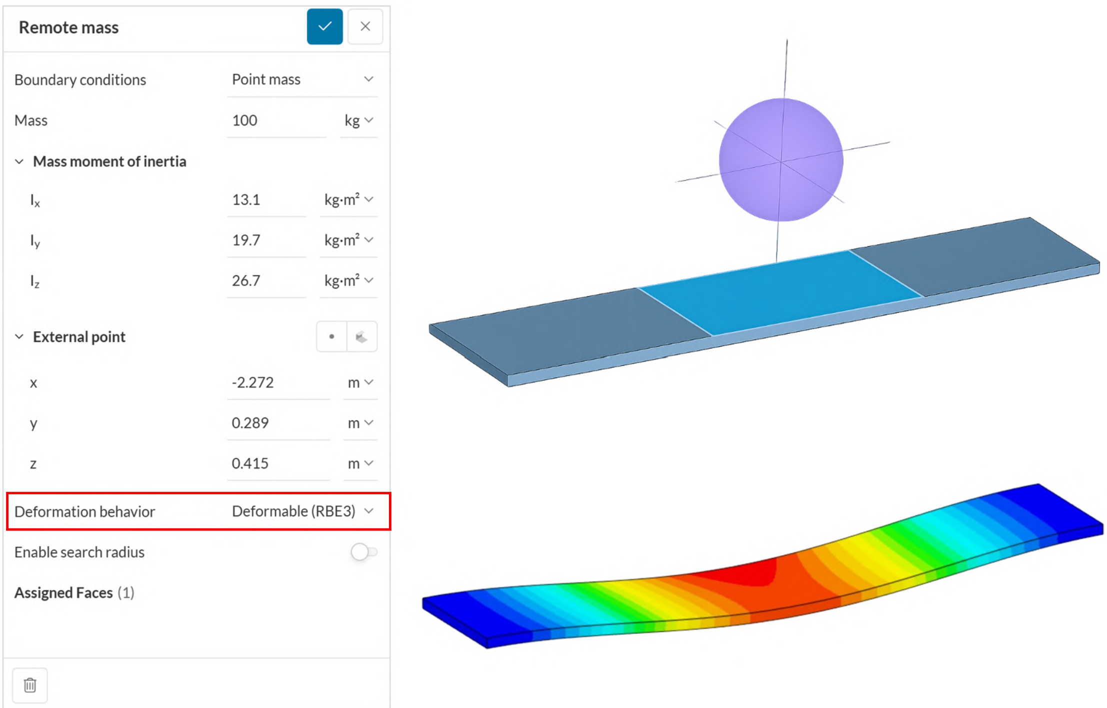

Figure B.2: *RBE3 setup and rigid behavior.*
Source: author's elaboration using SimScale

Appendix C

This section considers the simplified Three-Degrees-of-Freedom model introduced in Section 4.5.3. The associated eigenvalue problem is then solved in an inverse manner to estimate the order of magnitude of the Young's Modulus assigned to the equivalent cylindrical elements. Rather than determining the natural frequencies from known system parameters, the analysis imposes the experimentally identified first natural frequency as the target value and treats the equivalent stiffness as the unknown variable.
With reference to Fig. 4.19, the given parameters are:

- k_{prod} is the unknown parameter
- m_{model} = 1970 kg, from machine specifications
- m_{trough} = 900 kg, from machine specifications
- $m_{product}$ = 1000 kg, from experimental tests boundary conditions
- k_{stru} follows from the "Version 0" results. Starting from the Two-Degrees-of-Freedom model representing the machine configuration, the analytical solution determines the stiffness of the connection between the structural model and the upper trough, since the masses and the first natural frequency are known.

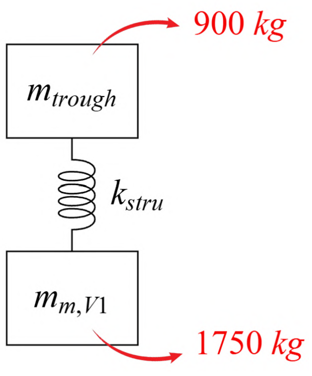

Figure C.1: *"Version 0" simplified into a Two-Degrees of Freedom scheme*

The first natural frequency is identified from both experimental tests and numerical model to be 12.5 Hz.
Therefore, the following equations hold

$$
\begin{aligned}
f_n &= \frac{1}{2\pi}\sqrt{k_{stru}\left(\frac{1}{m_{m,V1}}+\frac{1}{m_{trough}}\right)} \\
\Rightarrow \quad k_{stru} &= \frac{(2\pi f_n)^2}{\left(\frac{1}{m_{m,V1}}+\frac{1}{m_{trough}}\right)}
\end{aligned}
\tag{C.1}
$$

Eq. (C.1) determines the estimated value for the stiffness k_{stru}, and the result is hereby reported:

$$k_{stru} = 3.67 \cdot 10^6 \ N/m$$

The equation of motion

$$[M]\ddot{x} + [K]x = 0 \tag{C.2}$$

governs the free undamped dynamic system, where $[M]$ is the mass matrix, $[K]$ is the stiffness matrix and x is the vector of generalized coordinates.
Assuming harmonic vibrations, the displacement vector equation is

$$x(t) = \phi e^{i\omega t} \tag{C.3}$$

where ϕ is the modal vector and ω is the natural pulsation.
Substituting the assumed solution into the equation of motion leads to

$$([K] - \lambda[M])\,\phi = 0 \tag{C.4}$$

where λ represents the eigenvalues set associated with the modal vector ϕ and it corresponds to ω^2. A non-trivial solution ($\phi \neq 0$) exists only if the coefficient matrix is singular. Therefore, the natural frequencies of the system are obtained by solving the characteristic equation

$$\det\left([K] - \lambda[M]\right) = 0 \tag{C.5}$$

In the present work, the analysis solves this eigenvalue problem in an inverse manner. Rather than computing the natural frequencies from known system parameters, it prescribes the first natural frequency, equal to 11.5 Hz, and treats the equivalent stiffness k_{prod} associated with the processed product as the unknown variable.

In symbols, mass matrix $[M]$ is

$$[M] = \begin{bmatrix} m_{model} & 0 & 0 \\ 0 & m_{trough} & 0 \\ 0 & 0 & m_{product} \end{bmatrix}$$

while stiffness matrix $[K]$

$$[K] = \begin{bmatrix} k_{stru} + k_{prod} & -k_{stru} & -k_{prod} \\ -k_{stru} & k_{stru} & 0 \\ -k_{prod} & 0 & k_{prod} \end{bmatrix}$$

Developing the determinant given in Eq. (C.5), the resulting equation is

$$\begin{aligned} \det([K] - \lambda[M]) = \lambda\Big[& k_{prod} k_{stru}(m_{model} + m_{trough} + m_{product}) \\ & - k_{prod}\lambda(m_{model} m_{trough} + m_{product} m_{trough}) \\ & - k_{stru}\lambda(m_{model} m_{product} + m_{product} m_{trough}) \\ & + \lambda^2 m_{model} m_{trough} m_{product}\Big] = 0 \end{aligned}$$

and it represents a linear equation in the unknown parameter k_{prod}. The list above defines all the remaining quantities. The analysis computes the parameter λ from $f_1 = 11.5Hz$.
The resulting stiffness value is

$$k_{prod} = 2.70 \cdot 10^7 \ N/m$$

In the adopted representation, k_{prod} denotes the equivalent stiffness of the entire spring bed supporting the processed product. To obtain the stiffness of a single equivalent spring, the analysis divides this value by 10, since the spring bed consists of ten identical elements. This result provides the basis for evaluating the Young's Modulus of the equivalent cylindrical elements as follows:

$$E_{prod} = \frac{k_{prod}}{A} \cdot \frac{L}{A} = \frac{2.70 \cdot 10^7 \ N/m}{10} \cdot \frac{0.2\,m}{0.002^2 \pi \ m^2} = 4.30 \cdot 10^{10} \ N/m^2 = 43\,GPa$$

Appendix D

Appendix A introduced the dynamic response of a damped single-degree-of-freedom system subjected to harmonic excitation, deriving the steady-state solution and the corresponding transmissibility function. Building upon those fundamental concepts, this appendix discusses why resonance should be interpreted as a finite region of dynamic amplification rather than as a single-frequency condition, providing the engineering rationale behind the frequency separation criterion adopted throughout this work.

As demonstrated in Appendix A, the steady-state response of a damped Single-Degree-of-Freedom system subjected to harmonic excitation continuously depends on the excitation frequency through the frequency ratio $r = \omega/\omega_n$. Introducing the static displacement

$$\delta_s t = F_0/k \tag{D.1}$$

the displacement amplitude can be expressed in non-dimensional form through the magnification factor

$$M = \frac{X}{\delta_{st}} \frac{1}{\sqrt{(1-r^2)^2 + (2\zeta r)^2}} \tag{D.2}$$

where X denotes the steady-state vibration amplitude and ζ is the damping ratio. Eq. (D.2) is identical to the analytical solution derived in Appendix A, but re-written in dimensionless form to explicitly highlight the dependence of the structural response on the frequency ratio. Fig. D.1 reports the corresponding variation of the magnification factor.

Although Fig. D.1 reports a broad range of damping ratios for completeness, it should be noted that welded steel supporting structures typically exhibit damping ratios of only a few percent under operating conditions, generally in the order of 1÷5%. Consequently, the dynamic amplification experienced by such structures is significantly higher than that suggested by the curves corresponding to heavily damped systems. For lightly damped systems, the maximum magnification factor

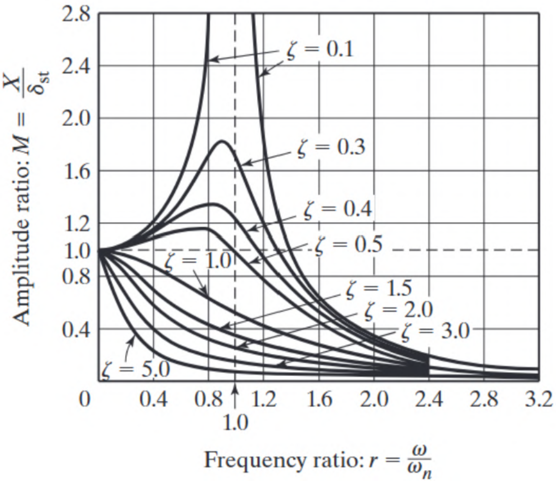

Figure D.1: *Variation of the magnification factor M with frequency ratio r for different damping ratios [1]*

becomes

$$M_{\max} \approx \frac{1}{2\zeta}, \tag{D.3}$$

which, for a representative damping ratio of ζ=2%, yields

$$M_{\max} \approx \frac{1}{2 \cdot 0.02} = 25$$

Therefore, although the figure effectively illustrates the general behavior of the magnification factor, lightly damped steel structures are considerably more sensitive to resonance phenomena.
Rather than exhibiting an abrupt increase exclusively at the resonance condition (r=1), the response evolves continuously over the entire frequency spectrum. As the excitation frequency approaches the natural frequency, the vibration amplitude progressively increases, reaches a maximum in the vicinity of resonance and then gradually decreases as the excitation frequency moves away from it. Consequently, resonance should not be interpreted as a phenomenon occurring at a single frequency. Instead, it extends over a finite frequency region characterized by elevated dynamic amplification. The continuous variation of the magnification factor clearly demonstrates this behavior. Practical engineering applications also involve unavoidable uncertainties arising from the numerical model, manufacturing tolerances, boundary conditions, material properties, damping estimation, operating conditions, and possible future structural modifications. As a result, neither the excitation frequency nor the natural frequencies represent perfectly deterministic quantities.

For these reasons, engineering design does not simply seek to avoid the exact resonance condition ($f_{exc} \neq f_n$), but rather aims to maintain an adequate frequency separation between the excitation frequency and all relevant structural modes. Such an approach provides sufficient robustness against the unavoidable uncertainties affecting both the prediction of natural frequencies and the actual operating conditions.

Accordingly, it is widely accepted engineering practice to maintain a separation margin of approximately $\pm 25\%$ with respect to the operating excitation frequency. Although this value does not represent a strict theoretical limit, it constitutes a conservative and robust design criterion that significantly reduces the likelihood of excessive dynamic amplification under real operating conditions.

Bibliography and Sitography

[1] Singiresu S. Rao. *Mechanical Vibrations*. 6th. Pearson, 2018.

[2] Singiresu S. Rao. *Vibration of Continuous Systems*. 1st. John Wiley & Sons, 2007.

[3] Daniel J. Inman. *Engineering Vibration*. 4th. Pearson, 2014.

[4] William T. Thomson and Marie Dillon Dahleh. *Theory of Vibration with Applications*. 5th. Prentice Hall, 1998.

[5] J. P. Den Hartog. *Mechanical Vibrations*. 4th. Dover Publications, 1985.

[6] Leonard Meirovitch. *Fundamentals of Vibrations*. 1st. McGraw-Hill, 2001.

[7] David J. Ewins. *Modal Testing: Theory, Practice and Application*. 2nd. Research Studies Press, 2000.

[8] Jerry H. Ginsberg. *Mechanical and Structural Vibrations: Theory and Applications*. 1st. John Wiley & Sons, 2001.

[9] Anil K. Chopra. *Dynamics of Structures: Theory and Applications to Earthquake Engineering*. 5th. Pearson, 2017.

[10] *What is Modal Analysis: The Ultimate Guide*. 2025. URL: `https://dewesoft.com/blog/what-is-modal-analysis` (visited on 03/17/2026).

[11] Dewesoft. *Modal Testing and Modal Analysis*. URL: `https://dewesoft.com/applications/modal-analysis` (visited on 03/17/2026).

[12] HBK. *Classical Modal Analysis*. URL: https://www.hbkworld.com/en/solutions/applications/vibration/structural-dynamics/modal-analysis (visited on 03/30/2026).

[13] NAFEMS. *Correlation of FE Modal Analysis with Experimental Vibration Data*. 2011. URL: https://www.nafems.org/downloads/North_America/correlation_of_fe_modal_analysis_with_experimental_vibration_data.pdf (visited on 05/09/2026).

[14] SimScale. *Simscale*. URL: https://www.simscale.com/ (visited on 06/11/2026).

[15] SimScale. *Element Technology*. 2025. URL: https://www.simscale.com/docs/simulation-setup/fea-element-technology/ (visited on 04/23/2026).

[16] SimScale. *Frequency Analysis*. 2025. URL: https://www.simscale.com/docs/analysis-types/frequency-analysis/ (visited on 03/28/2026).

[17] SimScale. *Harmonic Analysis*. 2025. URL: https://www.simscale.com/docs/analysis-types/harmonic/ (visited on 05/06/2026).

[18] SimScale. *Static Analysis*. 2025. URL: https://www.simscale.com/docs/analysis-types/static/ (visited on 05/06/2026).

[19] SimScale. *Standard Mesher*. 2026. URL: https://www.simscale.com/docs/simulation-setup/meshing/standard/ (visited on 04/23/2026).

[20] SimScale. *Hex-dominant Meshing*. 2025. URL: https://www.simscale.com/docs/simulation-setup/meshing/hex-dominant/ (visited on 04/23/2026).

[21] SimScale. *Mesh Quality*. 2025. URL: https://www.simscale.com/docs/simulation-setup/meshing/mesh-quality/ (visited on 04/23/2026).

[22] SimScale. *Second-Order Elements*. 2025. URL: https://www.simscale.com/docs/simulation-setup/fea-element-technology/ (visited on 04/24/2026).

[23] SimScale. *Remote Connections*. 2025. URL: https://www.simscale.com/docs/simulation-setup/contacts/remote-connections/ (visited on 04/29/2026).

[24] SimScale. *Point Mass*. 2025. URL: https://www.simscale.com/docs/simulation-setup/boundary-conditions/point-mass/ (visited on 04/29/2026).

[25] SimScale. *Remote Displacement*. 2025. URL: https://www.simscale.com/docs/simulation-setup/boundary-conditions/remote-displacement/ (visited on 04/29/2026).

[26] SimScale. *Contacts*. 2025. URL: https://www.simscale.com/docs/simulation-setup/contacts/ (visited on 04/12/2026).

[27] *Manuale Tecnico Antivibranti*. Dalmar. URL: https://www.bulloneriabergamasca.com/doc-pdf/DALMAR%20Antivibranti.pdf (visited on 05/20/2025).